DYNAMIC SIMULATION OF MUSCULOTENDON MECHANICS DURING HIGH SPEED RUNNING

By

Elizabeth Schmerr Chumanov

A dissertation submitted in partial fulfillment of

the requirements for the degree of

Doctor of Philosophy

(Mechanical Engineering)

at the

UNIVERSITY OF WISCONSIN-MADISON

2009

UMI Number: 3368041

INFORMATION TO USERS

The quality of this reproduction is dependent upon the quality of the copy
submitted.   Broken or indistinct print, colored or poor quality illustrations
and photographs, print bleed-through, substandard margins, and improper
alignment can adversely affect reproduction.
In the unlikely event that the author did not send a complete manuscript
and there are missing pages, these will be noted.   Also, if unauthorized
copyright material had to be removed, a note will indicate the deletion.

UMI®

A dissertation entitled

DYNAMIC SIMULATION OF MUSCULOTENDON MECHANICS DURING HIGH SPEED RUNNING

submitted to the Graduate School of the
University of Wisconsin-Madison
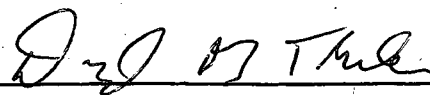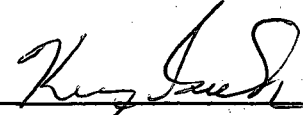in partial fulfillment of the requirements for the
degree of Doctor of Philosophy

by
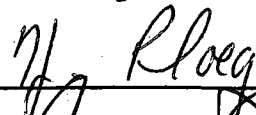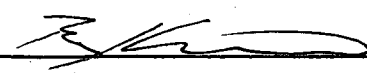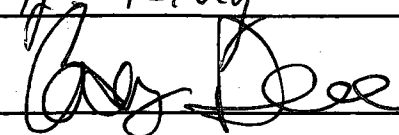
Elizabeth Schmerr Chumanov

Date of Final Oral Examination: April 29th, 2009

Month & Year Degree to be awarded: **December**   **May** 2009   **August**

****

Approval Signatures of Dissertation Committee

Signature, Dean of Graduate School

TABLE OF CONTENTS

)

CHAPTER 1: INTRODUCTION

The American College of Sports Medicine estimates that over 60 percent of the American population will incur a muscle injury in their lifetime. Acute muscle strain injuries are particularly troublesome due to their tendency to recur. These strain injuries typically occur along the musculotendinous junction (De Smet and Best 2000; Garrett 1996). In the athletic population, sports that involve high speed running such as soccer, football, baseball, track and field, etc. places athletes at a risk for a specific type of muscle injury, namely an acute hamstring strain injury and in fact the hamstrings (including the semimembranosus, semitendinosus, biceps femoris long head) are among the most commonly injured muscles for sports that require high speed maneuvers. For example, a hamstring strain incidence rate of 24% was found among a group of collegiate sprinters and jumpers over a two year period (Yamamoto 1993). Similarly, high rates of hamstring muscle injuries and associated missed playing time occur in soccer, rugby and football (Kujala et al. 1997; Seward et al. 1993). In addition, acute hamstring strain injuries are commonly associated with maximal speed sprinting activities, with on average 77% more injuries occurring during competition rather than during training (Gabbe 2005). Previous studies have shown that the single best predictor for an acute hamstring strain injury is a prior injury (Orchard and Best 2002), which highlights the shortcomings of traditional rehabilitation programs. Brockett, *et al.* (Brockett et al. 2004; Proske et al. 2004) has suggested that this injury recurrence risk is related to a change in optimal muscle length for force production that occurs after injury. Such a change may arise from the repeated performance of shortening (concentric) contraction exercises in the rehabilitative phase following injury. For this reason, some individuals are now promoting the use of lengthening (eccentric) contraction exercises in rehabilitation (Proske et al. 2004). An

alternative explanation of the change in optimal muscle length is that post-injury remodeling involves scar tissue formation that persists for some time after recovery (Kaariainen et al. 2000), thereby altering normal musculotendon mechanics. Sherry and Best (Sherry and Best 2004) have also shown that a rehabilitation program focused on early movement and neuromuscular control dramatically reduces hamstring re-injury rates compared with a traditional rehabilitation approach of strengthening and stretching. Their rehabilitation program included exercises that emphasized neuromuscular control, particularly of the pelvis and trunk muscles. While the clinical outcome is promising, it remains unclear which neuromuscular factors are responsible for the reduced re-injury risk. The goal of this thesis research is to improve the understanding of hamstring musculotendon mechanics during high speed running, so as to contribute to a scientific basis for evaluating and developing appropriate strategies for rehabilitation and injury prevention.

Imaging studies. Radiological analyses have found that the biceps femoris long head is the most injured of the three biarticular hamstring muscles (Koulouris and Connell 2003). It has been speculated that the more distal insertion and the relatively short fiber length of the biceps femoris may place it at a greater risk for injury (Wood 1987). However, it is not clear how the anatomical differences translate into injury potential during dynamic movement. Simple, two dimensional analyses often miss important differences in moment arms between the hamstring muscle. At the knee, the semimembranosus and the semitendinosus generate internal rotation moments, while the biceps femoris long head generates an external moment. The difference in moment arms at the knee can explain

why there is a greater peak musculotendon stretch in the biceps femoris long head during sprinting than either the semitendinosus or semimenbranosus (Thelen 2005). Using a model that represents full three dimensional motion is essential to identifying these subtle, yet potentially important, differences in dynamic muscle mechanics and function.

Animal models. Muscle injury is often associated with eccentric (lengthening) contractions (Lieber 1992). This is generally believed to be due to the large muscle forces that arise during a lengthening contraction, compared to the forces developed by an actively shortening muscle. Animal models of muscle injury have shown that peak muscle stretch (i.e. mechanical strain) and negative work (the product of force and strain) are good predictors of muscle injury (Brooks and Faulkner 2001; Lieber and Friden 1993; Lieber and Friden 2002). However, many animal studies use a single maximal stretch to induce injury, which may be beyond the physiological limits during normal motion. If a more physiological range of motion is used, a muscle must be subjected to repeated stretch-shortening cycles in order for injury to result (Butterfield and Herzog 2005). This latter scenario is likely more related to hamstring strain injury mechanisms, since the hamstrings exhibit a stretch-shortening cycle during the sprinting gait cycle (Thelen 2005; Thelen 2006) with injury often occurring after repeated strides.

In vivo muscle function and mechanics. Examining dynamic muscle function is challenging because of the lack of techniques to measure musculotendon mechanics and loading *in vivo*. The development of dynamic imaging techniques, such as cine phase contrast magnetic resonance imaging (Asakawa et al. 2003) and ultrasound elastography

(Loram et al. 2006), make empirical approaches more plausible. However, it is not feasible with current imaging techniques to measure *in vivo* muscle mechanics during whole body movement such as sprinting. Therefore it is necessary to use dynamic musculoskeletal modeling to bridge the gap between animal models of muscle injury, and injuries arising during dynamic human movement. Modeling approaches provide estimates of quantities such as muscle stretch, force and negative work that cannot otherwise be obtained. In addition, using a forward dynamic simulation approach facilitates investigations of the influence of perturbations on muscle function and mechanics, which is important to assess injury risk.

Muscle injury mechanisms during sprinting. The point in the sprinting gait cycle when the hamstrings are actually injured remains an area of debate (Orchard 2002). It is known that the hamstrings are active (Jonhagen et al. 1996; Swanson and Caldwell 2000; Wood 1987) and undergoing a stretch-shortening cycle (Thelen 2005) during the latter half of swing and early stance phase of sprinting. In addition, during the late swing phase of sprinting the hip is highly flexed and the pelvis is rotated anterior, which places the hamstring in a lengthened state. This lengthened state is likely to put the hamstrings at risk for injury; however, it was previously shown that the peak musculotendon stretch does not change when going from 80 percent to maximum sprinting speed (Thelen 2005; van Don 1998; Wood 1987). Joint level analyses reveal that there is both a large hip extension moment and knee flexion moment during swing and presumably the hamstrings act to absorb the energy as the leg swings forward (Kuitunen et al. 2002). Because of the strong relationship between muscle stretch and injury potential seen in

animal models of muscle injury (Brooks and Faulkner 2001; Lieber and Friden 1993; Lieber and Friden 2002), it is plausible that the hamstrings are at greatest risk for a lengthening contraction injury during swing phase (Heiderscheit et al. 2005; Schache et al. 2009; Thelen 2006; van Don 1998; Walker et al. 1988). However, other researchers have suggested that injury may be associated with the contact loads seen during early stance (Mann and Sprague 1980; Orchard 2002), though little is known about hamstring mechanics during stance. A recent study suggested that the hamstrings may be susceptible to injury due to a lengthening contraction during late stance (Yu et al. 2008). From joint level analyses, it is not possible to describe how individual muscles are acting. Thus, it is advantageous to use a musculoskeletal modeling approach to estimate quantities such as muscle force and negative work to fully understand the underlying mechanics of the system for both swing and stance phase.

Forward dynamic simulations. Forward dynamic simulation is emerging as a powerful tool to investigate musculotendon mechanics and function during movement (Delp et al. 2007). Using experiments alone to understand dynamic movement dynamics has two fundamental limitations. First, important variables, including the forces generated by muscles, are not generally measurable in experiments. Second, it is difficult to establish cause-effect relationships in complex dynamic systems from experimental data alone. Forward dynamic approaches allow investigators to directly characterize the musculotendon mechanics that give rise to dynamic human movement, and to predict how movement would change as a result of a perturbation to muscle coordination or properties of the musculoskeletal system (Delp et al. 2007). The development of a

computationally efficient algorithms for generating simulations of subject-specific movement, termed computed muscle control (CMC) (Thelen and Anderson 2006; Thelen et al. 2003), has greatly extended the benefits and use of simulations to address clinical problems. The CMC algorithm solves for a set of muscle excitations that, when input to a forward dynamic model of the musculoskeletal system, replicates movement observed in the laboratory. Complex three-dimensional models can be used which account for the interactions between the musculotendon mechanics, the geometry of the system, and the whole-body dynamics The main advantage that a forward dynamic model has over an inverse dynamic model is the ability to make changes to the system since the equations of motion are integrated forward. For example, changes in the muscle excitation and force trajectories can be introduced in the model and then used to predict how other muscles react to this change and how the resulting movement has been altered. This is a powerful approach to investigate the potential mechanisms of injury, and to predict how changes in muscle coordination influence injury risk.

The focus of this study is to use modeling along with measured kinematics and kinetics to characterize and contrast hamstring mechanics during the swing and stance phases of sprinting, so as to gain further insights into injury mechanisms.

Aim 1. Investigate how hamstring musculotendon mechanics during swing phase vary with treadmill sprinting speed. To do this, muscle-actuated forward dynamic simulations were generated that closely replicated the swing phase kinematics of 19 athletes running at 80-100% of maximum speed on a treadmill. The simulations were then used to estimate hamstring musculotendon, muscle, and tendon stretch, force and work for the swing phase of the gait cycle. The hypothesis tested was that sprinting

speed increases the magnitude of loading and negative work required of the muscle fibers, while musculotendon stretch remains consistent across a range of speeds.

Aim 2. Investigate how individual muscles, particularly those surrounding the pelvis and back (i.e. the "core"), could influence hamstring stretch during sprinting. To do this, muscle actuated simulations of sprinting were generated, then small perturbations to individual muscle force trajectories (~1N) were introduced and the movement was re-simulated. The hypothesis tested was that core muscles would have a larger influence on hamstring stretch than other muscles of the lower limb, which would suggest that rehabilitation programs that include core strengthening exercises could potentially be beneficial for reducing re-injury risk.

Aim 3. Develop a least squares forward dynamics methodology for computing joint mechanics during sprinting on an un-instrumented treadmill. To do this, the center of pressure (COP) and the vertical ground reaction forces was measured from pressure sensitive insoles during treadmill sprinting of eight athletes. A least-squares forward dynamic approach was then implemented to estimate the unmeasured anterio-posterior and medio-lateral ground reactions. In addition, verification of the COP and vertical ground reactions along with the calculated components was performed against force platform data.

Aim 4. Systematically compare biomechanical demands between stance and swing phase of the sprinting gait cycle to better understand potential injury mechanisms. To do this, 11 subjects sprinted on a fully instrumented high-speed treadmill. Muscle-actuated forward dynamic simulations were then generated of sagittal hip and knee motion at speeds ranging from 80 to 100% of maximum. Simulations were used to

estimate hamstring musculotendon, muscle, and tendon stretch, force, and work throughout the entire gait cycle. The hypotheses tested were that hamstring musculotendon stretch, force and negative work are all greater during the swing phase of sprinting than during stance phase.

CHAPTER 2

Hamstring Muscle Kinematics during Treadmill Sprinting

[1]Darryl G. Thelen, [1]Elizabeth S. Chumanov, [1]Dina M. Hoerth, [1]Thomas M. Best,
[2]Stephen C. Swanson, , [3]Li Li, , [3]Michael Young, [1]Bryan C. Heiderscheit

[1]University of Wisconsin-Madison, Madison, WI
[2]The Orthopedic Specialty Hospital, Murray, UT
[3]Lousiana State University, Baton Rouge, LA

Abstract

Introduction/Purpose: The objective of this study was to characterize hamstring muscle kinematics during sprinting, so as to provide scientific data to better understand injury mechanisms and differences in injury rates between muscles. *Methods:* We conducted three-dimensional motion analyses of 14 athletes performing treadmill sprinting at speeds ranging from 80% to 100% of maximum. Scaled musculoskeletal models were used to estimate hamstring muscle-tendon lengths throughout the sprinting gait cycle for each speed. We tested our hypotheses that the biceps femoris (BF) long head would be stretched a greater amount, relative to its length in an upright posture, than the semitendinosus (ST) and semimembranosus (SM) muscles We also tested the hypothesis that increasing from submaximal to maximal sprinting speed would both increase the magnitude and delay the occurrence of peak muscle-tendon lengths in the gait cycle. *Results:* Maximum hamstring lengths occurred during the late swing phase of sprinting and were an average of 7.4% (SM), 8.1% (ST), and 9.5% (BF) greater than the respective muscle-tendon lengths in an upright configuration. Peak lengths were significantly larger in the BF than the ST and SM ($p<0.01$), occurred significantly later in the gait cycle at the maximal speed ($p<0.01$), but did not increase significantly with speed. Differences in the hip extension and knee flexion moment arms between the biarticular hamstrings account for the intermuscle variations in the peak lengths that were estimated. *Conclusions:* We conclude that intermuscle differences in hamstring moment arms about the hip and knee may be a factor contributing to the greater propensity for hamstring strain injuires to occur in the BF muscle.

Introduction

Hamstring muscle strains are one of the most frequent injuries in sports that involve sprinting. For example, a hamstring strain incidence rate of 24% was found among a group of collegiate sprinters and jumpers over a two year period (Yamamoto 1993). Similarly, high rates of hamstring muscle injuries and associated missed playing time occur in soccer, rugby and football (Kujala et al. 1997; Seward et al. 1993). Radiologic analyses of athletes postinjury indicate that a large majority of all acute hamstring strains involve the biceps femoris, whereas the semitendinosus and semimembranosus muscles are less often injured (De Smet and Best 2000; Garrett et al. 1989; Koulouris and Connell 2003).

Despite the frequency of hamstring muscle injuries during sprinting, it remains unclear when in the gait cycle the muscle is injured or why the biceps femoris is more susceptible to injury. Late swing (Wood 1987) and early stance (Mann and Sprague 1980) phases of sprinting have been suggested as potentially injurious phases of the gait cycle. During late swing, the hip is flexed and the knee is extending. The hamstring muscles are active at this stage (Kuitunen et al. 2002; Mero and Komi 1987) while lengthening, which could induce an eccentric contraction injury (Garrett 1996; Whiting and Zernicke 1998). Alternatively, hamstring muscles remain active into stance when they are presumably shortening which could induce a concentric contraction injury (Mann and Sprague 1980). As for the differences in injury rates between muscles, investigators have speculated that the biceps femoris muscle's unique dual innervation, lateral distal insertion and/or relatively shorter fiber lengths could contribute to a greater susceptibility to injury (Garrett et al. 1989; Wood 1987).

Part of the current ambiguity surrounding hamstring muscle injuries may result from difficulties in inferring the action of biarticular hamstring muscles from joint level analyses of sprinting (Chapman and Caldwell 1983; Jacobs and Vvan Ingen Schenau 1992; Mann 1981; Mann and Sprague 1980; Swanson and Caldwell 2000; Wood 1987) and anatomical descriptions of muscles. A quantitative assessment of when the hamstring muscles are actively shortening, lengthening, or acting isometrically during sprinting may be important for understanding the biomechanical mechanisms of hamstring injuries. Such information could in turn provide a scientific basis for evaluating alternative treatment strategies (Sherry and Best 2004) and methods of injury prevention

The objective of this study was to characterize hamstring muscle kinematics during treadmill sprinting. Specifically, we used three-dimensional motion analyses of sprinting along with scaled musculoskeletal models to estimate hamstring muscle-tendon lengths throughout the gait cycle. We tested our primary hypothesis that the biceps femoris would be stretched a greater amount than the semitendinosus and semimembranosus muscles. We also tested our secondary hypothesis that increasing from submaximal to maximal sprinting speed would both increase the magnitude and delay the occurrence of peak hamstring muscle lengths in the gait cycle. To provide additional characterization of hamstring muscle kinematics, peak velocities and joint angles were also analyzed.

Methods

Subjects: A total of 14 athletes, 16-31 yr old, volunteered to participate in this study. All athletes were competent sprinting on high-speed treadmills, having completed a minimum of 6 previous treadmill training sessions of 45-60 min. Experimental testing was conducted at The Orthopedic Specialty Hospital in Murray, Utah. The protocol was approved by the Institutional Review Boards of both the testing institution and UW-Madison. Each subject provided informed consent in accordance with institutional policy.

Within 10 days before the test session, each athlete completed a speed testing protocol to establish maximum treadmill sprinting speed. The protocol consisted of five to six trials of sprinting at increasing speeds until the athlete was unable to maintain the treadmill speed for a minimum of 4 seconds. The athlete was allowed a full recovery between trials (heart rate < 110 bpm).

Protocol: Each test session started with the subject running at an easy speed on a high-speed treadmill, until they were acclimated to running with the passive markers attached and were adequately warmed up to sprint. Motion analysis data were then recorded during treadmill sprinting at 80, 85, 90, and 95% of the subject's maximum speed from the previous speed testing session. These trials were performed in a fixed, increasing speed order because it was not ethical or feasible to require athletes to attempt a maximum sprint on their first trial. If the subject was able to sprint at a maximal speed that was greater than what had been established previously, additional trials at speeds corresponding to 80-95% of the new maximum were performed in descending order. This

occurred with 6 of the 14 subjects. A minimum of 3 min of rest was allotted between trials to offset effects of fatigue.

Motion Analysis: An optical, motion capture system (Motion Analysis Corporation, Santa Rosa, CA) to track the three-dimensional positions of 47 reflective markers placed on palpable anatomical landmarks. An initial recording of marker positions during quiet upright stance was performed to establish joint centers, body segment coordinate systems and segment lengths. Kinematic data were recorded at 200 Hz.

Musculoskeletal Model: A three-dimensional, 14 segment, 29 degree-of-freedom musculoskeletal model was used to compute joint angles and hamstring muscle-tendon lengths during sprinting (Figure 1.2a). Six degrees of freedom described the position and orientation of the pelvis relative to the ground. Each hip was represented as a ball-and-socket joint with three degrees of freedom. A one degree-of-freedom knee was used to account for tibiofemoral and patellofemoral translations and non-sagittal joint rotations as a function of knee angle (Walker et al. 1988). The talocrural-subtalar joint was represented as a universal joint and the metatarsal joint as a revolute, with the orientation of lower extremity joint axes set to anatomically determined values(Delp et al. 1990). The musculoskeletal model was scaled to individual subjects using the segment lengths computed during the initial calibration trial. Both the bone and hamstring muscle geometries were based on cadaveric imaging and modeling studies conducted by Arnold et al. (Arnold et al. 2000) (Figure 1.2).

A nonlinear optimization algorithm (SIMM Motion Module, Motion Analysis Corporation) was used to compute the joint angles from the experimental kinematic data collected during the sprinting trials. At each time step, joint angles were computed that minimized the sum of squared differences between virtual markers on the model and experimental marker kinematics. Lengths of the biceps femoris (BF), semitendinosus (ST) and semimembranosus (SM) muscle-tendons were computed from the joint angles by determining the distance from muscle origin to insertion, accounting for the wrapping of the muscles about the hip and knee joints. Muscle-tendon velocities were computed by numerically differentiating the muscle length data with respect to time. Muscle-tendon lengths and velocities were normalized to the respective muscle-tendon length in an upright posture that is, with all lower extremity joint angles set to zero.

(a)

(b) Hip Extension Moment Arm (m) vs Hip Flexion Angle (deg)

Exp — Model
□ ST — ■ ST
△ BF — ▲ BF
○ SM — ● SM

(c) Knee Flexion Moment Arm (m) vs Knee Flexion Angle (deg)

Exp — Model
□ ST — ■ ST
○ SM — ● SM
△ BF — ▲ BF
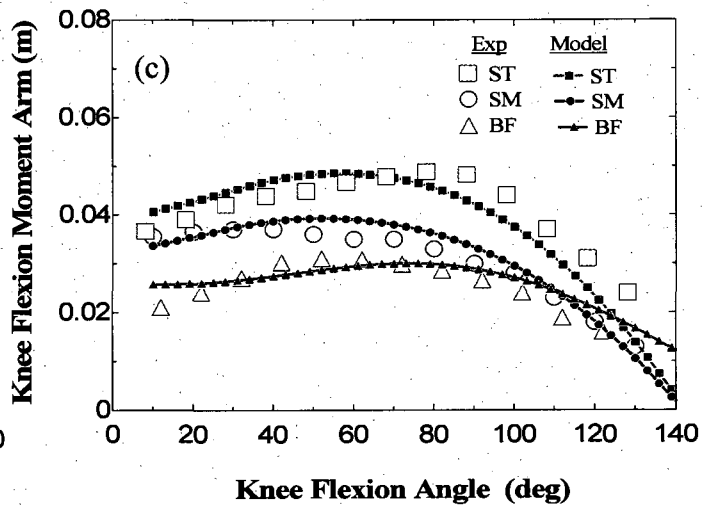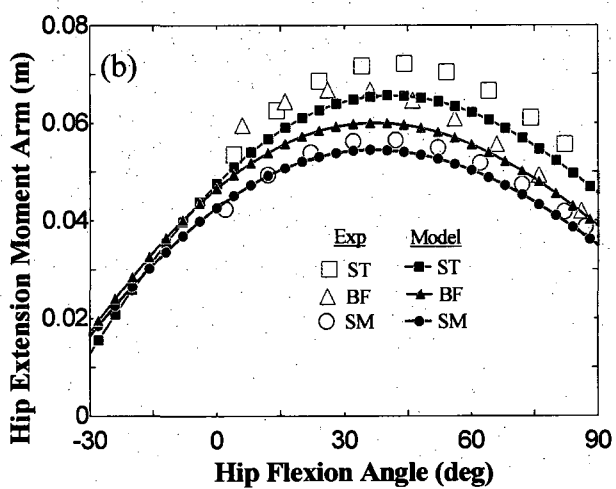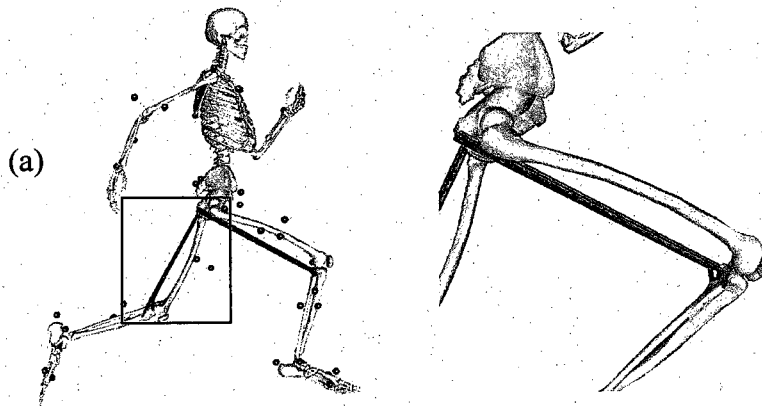
Figure 1.2. (a) Joint angles were computed by optimally fitting a scaled, 29 degree-of-freedom linked-segment model to measured marker kinematics. Biarticular hamstring muscles were represented by a series of line segments between origin and insertion, with wrapping surfaces used to represent wrapping about structures near the knee (Delp et al. 1990). (b) Semitendinosus (ST) and biceps femoris (BF) have larger hip extension moment arms than the semimembranosus (SM). This difference causes the ST and BF muscles to lengthen more than the SM as a result of hip flexion during sprinting. (c) BF has the smallest knee flexion moment arm of the bi-articular hamstring muscles. Consequently knee flexion during sprinting shortens the BF less than the SM and ST muscles. Model predictions of hip extension and knee flexion moment arms are compared to the experimental data of Arnold et al. (2000) and Buford et al. (1997), respectively.

The occurrence of foot contact times was identified using the toe marker kinematics. A distinct oscillation in the vertical position of this marker was present at landing and was detected by determining when the vertical velocity of the toe marker exceeded a threshold value. The time (percentage of the gait cycle) and magnitude of both the minimum and maximum muscle-tendon lengths and velocities were determined from three gait cycles for both the right and left legs. The hip and knee flexion angles at the time of peak muscle-tendon lengths were also computed. Repeated measures analysis of variance was used to determine the effect of muscle and speed on the magnitude and timing of maximum muscle-tendon lengths and muscle-tendon velocities. Repeated measures analysis of variance was also used to determine the effects of muscle and speed on muscle-tendon length excursions, and to assess the effect of speed on peak hip flexion and knee extension angles. Tukey's test was used for post-hoc analysis of significant main effects. All statistical analyses were completed with Systat (SPSS Inc., Chicago, IL) with a significance level of 0.01 used for all comparisons.

Results

Maximal sprinting speeds for the subjects averaged 9.4 m/s for the males and 8.1 m/s for the females (Table 1.2). The hamstring muscle-tendons were shortening at foot contact and continued to shorten throughout the stance phase of sprinting (Figure 2.2). Hamstring muscle-tendon lengthening started at ~45% of the gait cycle, which was during swing just before the knee was reversing direction and starting to extend. Muscle-

knee flexion to knee extension during the swing phase of sprinting. Peak lengthening velocities increased significantly with speed for each of the muscles ($p < 0.01$). Lengthening velocities were greater in the ST than the BF and SM ($p < 0.01$).

Maximum hip flexion did not vary with speed, reaching approximately 70° at each of the speeds. The knee was significantly ($p < 0.01$) more flexed, by 8°, during late swing at the maximum speed than at the slowest (80% max) speed (Table 4.2).
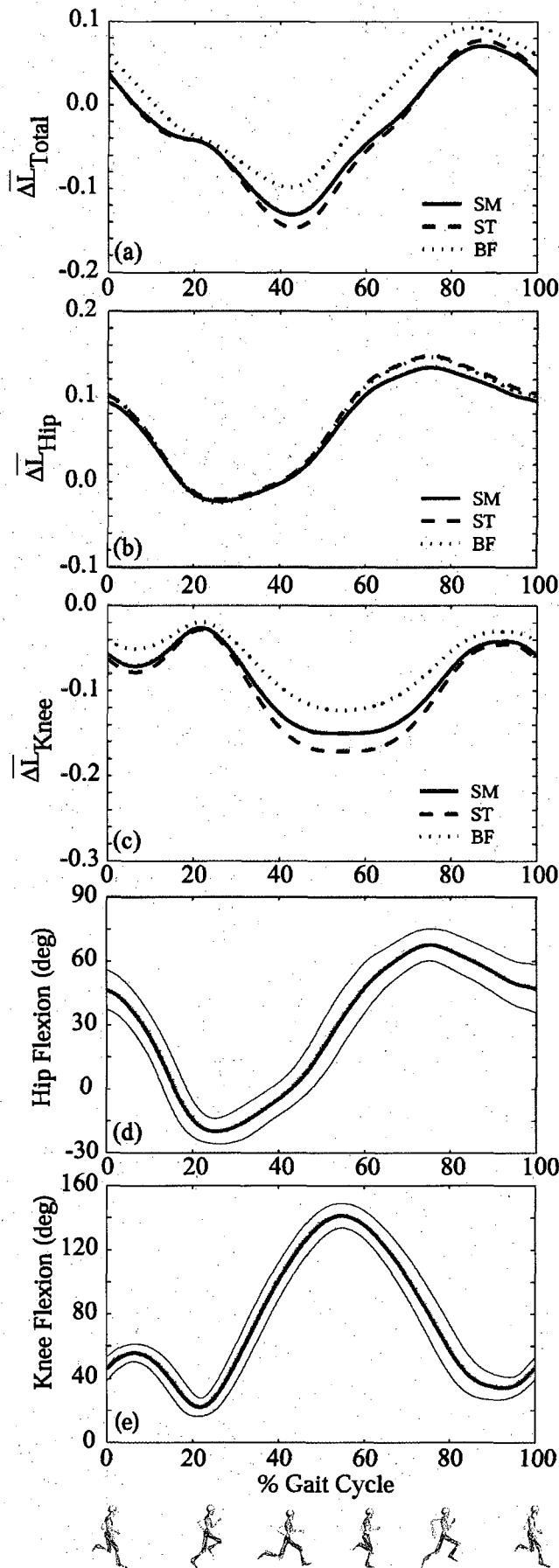
Figure 2.2. a) The net change in length ($\Delta\overline{L}$) of the hamstring muscles during the sprinting gait cycle, relative to the respective muscle-tendon lengths in an upright configuration. Peak lengths of the hamstring muscles occurred at ~92% of the gait. b) Much of the lengthening of the hamstring muscles was attributable to hip flexion (d) during the swing phase of sprinting. c) Knee flexion (e) during late swing acted to reduce the net change in muscle lengths. However because the biceps femoris (BF) has a smaller knee flexion moment arm, it undergoes the least amount of shortening with knee flexion. These effects at the hip and knee contributed to a larger net lengthening of BF, compared to the semitendinosus (ST) and semimembranosus (SM) muscles.

Table 2.2. Mean (SD) peak muscle-tendon lengths ($\overline{L}_{max}$) normalized to lengths in an upright posture, over the sprinting gait cycle. Peak lengths were significantly larger in the biceps femoris than the semimembranosus and semitendinosus muscles (p<0.01) and were reached significantly later (t_{max}) in the gait cycle (GC) at the fastest speed (p<0.01). Although the peak muscle-tendon lengths were invariant with speed, the corresponding posture of the limb did vary. This was evident in the hip and knee flexion angles which, at the time of peak muscle-tendon length, both significantly varied with speed (p < 0.01).

Muscle	Speed (% max)	$\overline{L}_{max}$ [1,3]	t_{max} [1,2] (%GC)	$\theta_{hip}^{1,2}$		$\theta_{knee}^{1,2}$	
Biceps Femoris	80	1.098 (0.026)	86.9 (4.2)	62.7	(8.3)	43.9	(12.6)
	85	1.096 (0.028)	87.1 (4.5)	63.1	(6.8)	44.3	(11.6)
	90	1.097 (0.027)	87.4 (3.8)	63.3	(7.1)	44.8	(10.2)
	95	1.094 (0.027)	88.3 (3.5)	62.6	(5.8)	45.4	(9.9)
	100	1.098 (0.028)	89.6 (3.7)	64.6	(6.7)	45.4	(8.7)
Semimembranosus	80	1.077 (0.015)	89.9 (2.9)	56.6	(7.5)	31.4	(6.6)
	85	1.075 (0.019)	90.4 (3.1)	57.2	(7.0)	32.1	(5.7)
	90	1.075 (0.015)	90.0 (2.7)	58.8	(7.4)	35.4	(5.2)
	95	1.072 (0.015)	90.8 (2.4)	58.8	(6.4)	37.1	(5.6)
	100	1.075 (0.016)	92.0 (2.7)	61.4	(8.0)	38.4	(5.3)
Semitendinosus	80	1.084 (0.017)	89.7 (2.9)	56.9	(7.5)	31.8	(6.6)
	85	1.082 (0.020)	90.1 (3.1)	57.5	(6.9)	32.7	(5.8)
	90	1.082 (0.017)	90.0 (2.7)	58.9	(7.4)	35.6	(5.3)
	95	1.078 (0.016)	90.7 (2.4)	58.9	(6.4)	37.4	(5.6)
	100	1.082 (0.018)	92.0 (2.7)	61.5	(8.0)	38.7	(5.3)

[1]significant muscle effects (p<0.01), [2]significant speed effects (p<0.01), [3]significant muscle by speed interactions (p<0.01)

Table 3.2. Mean (SD) maximum and mimimum muscle-tendon velocities, normalized to lengths in an upright posture, during the sprinting gait cycle. The magnitude of both maximum $(\overline{V}_{max})$ and minimum $(\overline{V}_{min})$ velocities increased significantly with running speed. Peak lengthening velocities were significantly larger in the semitendinosus than the biceps femoris and semimembranosus muscles. The time of occurrence of peak lengthening (t_{max}) and shortening (t_{min}) velocities within the gait cycle (GC) did not vary with speed or between muscles.

Muscle	Speed (% max)	$\overline{V}_{max}$[1,2,3] $(\overline{L}_0/s)$	t_{max} (%GC)	$\overline{V}_{min}$[1,2] $(\overline{L}_0/s)$	t_{min} (%GC)
Biceps Femoris	80	1.63 (0.25)	59.0 (7.1)	-1.21 (0.22)	18.9 (18.3)
	85	1.69 (0.28)	59.0 (7.3)	-1.28 (0.20)	21.5 (17.2)
	90	1.70 (0.26)	59.0 (8.0)	-1.33 (0.22)	17.7 (14.9)
	95	1.74 (0.29)	58.6 (7.4)	-1.40 (0.23)	16.3 (17.4)
	100	1.77 (0.27)	60.5 (10.7)	-1.47 (0.24)	16.8 (15.5)
Semimembranosus	80	1.54 (0.24)	59.9 (7.1)	-1.27 (0.21)	26.4 (16.7)
	85	1.59 (0.26)	60.3 (7.2)	-1.33 (0.20)	27.1 (16.2)
	90	1.63 (0.24)	60.4 (7.9)	-1.36 (0.21)	22.0 (14.2)
	95	1.66 (0.28)	59.8 (7.3)	-1.42 (0.23)	22.4 (16.3)
	100	1.71 (0.26)	63.7 (10.2)	-1.49 (0.23)	21.4 (14.7)
Semitendinosus	80	1.74 (0.31)	60.8 (7.1)	-1.45 (0.28)	27.7 (16.8)
	85	1.79 (0.33)	60.9 (7.2)	-1.53 (0.28)	28.5 (16.3)
	90	1.83 (0.32)	60.8 (7.9)	-1.55 (0.29)	24.3 (14.4)
	95	1.87 (0.35)	61.1 (7.5)	-1.62 (0.31)	25.7 (16.7)
	100	1.93 (0.34)	64.8 (10.3)	-1.70 (0.32)	24.2 (15.0)

[1]significant muscle effects (p<0.01), [2]significant speed effects (p<0.01), [3]significant muscle by speed interactions (p<0.01).
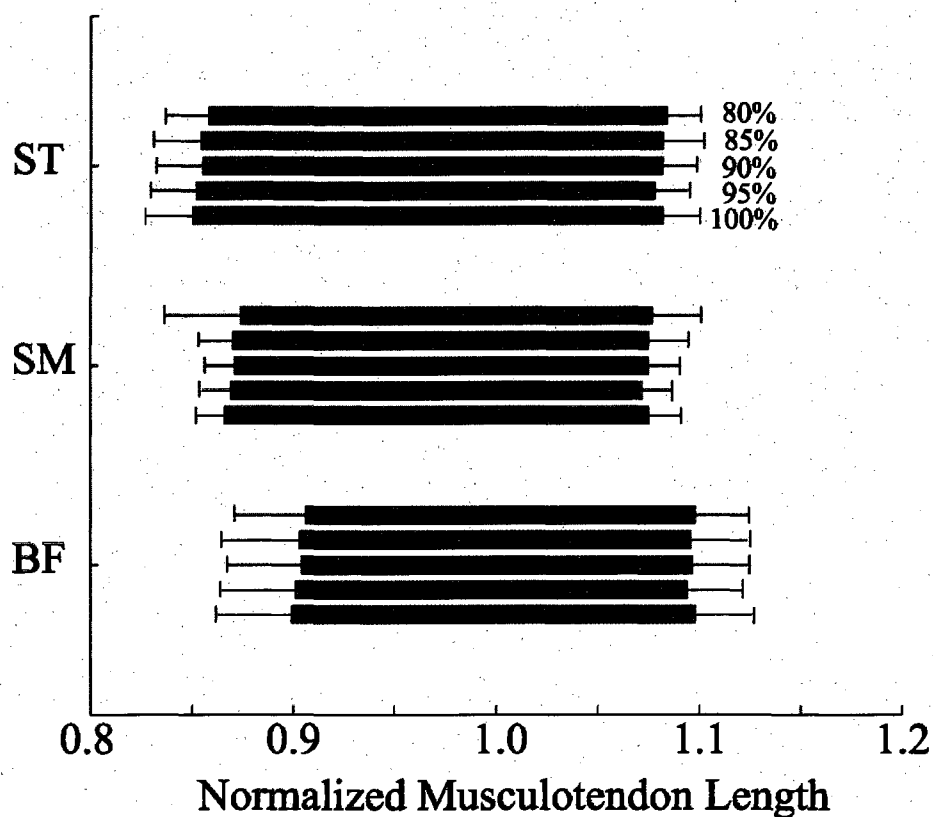
Figure 3.2. Range of normalized muscle-tendon lengths through which the hamstring muscles act during sprinting. The largest excursion is seen in the semitendinosus (ST), which is attributable to the ST having a larger knee flexion moment arm and hence greater shortening with knee flexion. Relative to respective upright lengths, the biceps femoris (BF) is stretched more than the ST and semimembranosus (SM) muscles at all speeds.

Table 4.2. Maximum hip flexion (θ_{hip}) and minimum knee flexion (θ_{knee}) angles over the sprinting gait cycle. Maximum hip flexion did not vary with speed, but was reached (t_{hip}) significantly later in the gait cycle at high speeds. The knee was more flexed at the higher speeds, with peak knee extension being reached (t_{knee}) slightly closer to heel contact as speed was increased.

Speed (% of max)	$\theta_{hip,\max}$ (°)	$t_{hip,\max}$ (% of GC)	$\theta_{Knee,\min}$ (°)	$t_{knee,\min}$ (% of GC)
80	71.5(9.4)	78.0(1.8)	24.7(4.7)	95.5(2.1)
85	71.4(8.1)	78.4(2.2)	25.8(4.9)	95.8(1.9)
90	70.8(7.8)	79.0(2.2)	28.9(4.3)	96.4(2.0)
95	69.5(5.9)	80.0(1.7)	31.0(4.8)	96.9(2.1)
100	70.3(5.9)	81.6(3.3)	32.5(5.2)	96.7(2.3)

Discussion

We used experimental joint kinematics along with a musculoskeletal model to estimate hamstring lengths during sprinting, thus providing an indication of overall stretch in the muscle-tendon unit. We found that the hamstring muscle-tendons undergo lengthening from approximately 45-90% of the sprinting gait cycle, with peak lengths occurring while in flight phase before foot contact. Previous estimates of hamstring kinematics during sprinting have also concluded that peak muscle-tendon lengths occur during late swing (Simonsen et al. 1985; Wood 1987). EMG analysis indicates that the hamstring muscles are active during the last ~20% of the gait cycle (Kuitunen et al. 2002; Wood 1987). Taken together, this means the hamstring muscles are likely undergoing an active lengthening contraction during late swing.

We estimated that muscle-tendon stretch, relative to muscle-tendon length in an upright posture, during sprinting is greater for the biceps femoris than the semimembranosus and semitendinosus. This difference is a direct result of slight variations in hip extension and knee flexion moment arms between the individual hamstring muscles. Peak hamstring muscle lengths during sprinting occur during late swing when the hip is highly flexed (~55-65°) and the knee is slightly flexed (~30-45°) (Table 2.2). Experimental studies have found that the semitendinosus and biceps femoris have a slightly larger hip extension moment arm than the semimembranosus (Arnold et al. 2000). Thus, hip flexion causes relatively greater lengthening of these two muscles. Conversely, knee flexion causes a reduction in the overall length of the biarticular hamstrings. At the knee, the biceps femoris has a smaller flexion moment arm than the

semitendinosus and semimembranosus (Buford et al. 1997), and a corresponding smaller reduction in overall length. The net result of these combined effects is for sprinting to require greater stretch of the biceps femoris than of the semimembranosus and semitendinosus (Figure 2.2).

Intermuscle differences in hamstring muscle injury rates have been observed among sprinters. The long head of the biceps femoris is the most commonly injured (De Smet and Best 2000; Garrett et al. 1989; Koulouris and Connell 2003). For example, imaging analysis of 170 athletes post-injury found that 80% of hamstring muscle strain injuries involved the biceps femoris (Koulouris and Connell 2003). These observations are consistent with our estimate that the BF incurs the largest overall stretch during sprinting. Thus it is possible that slight differences in muscle moment arms, particularly at the knee, may contribute to the differences in injury rates among the hamstring muscles. This potential factor has not been previously proposed, with other researchers focusing on differences in fiber lengths, pennation, and innervation (Garrett 1996; Wood 1987). Further research is warranted to better understand how these various factors actually combine to cause differences in injury rates.

Surprisingly we did not estimate significant changes in peak hamstring lengths as running speed was increased from 80% to 100% of maximum. However, we did find that the posture of the limb, at the time of peak hamstring lengths were reached, varied significantly with speed. Both the hip and knee flexion angles were greater at faster sprinting speeds (Table 2.2). Therefore, the increase in hamstring muscle-tendon due to a more flexed hip was offset by the decrease in length due to a more flexed knee at fast

sprinting speeds. This result suggests that hamstring extensibility may be a limiting factor dictating postures seen during the late swing phase of running. It is also interesting to note that the pattern of muscle-tendon lengths occurring during sprinting (Figure 2.2) are qualitatively similar to that seen in walking (Delp et al. 1996). However, the stretch magnitude during sprinting, from 7 to 10% beyond upright lengths, exceed the 5% hamstring stretch that occurs during walking (Delp et al. 1996).

We did find a delayed occurrence of peak hamstring lengths within the gait cycle and an increased muscle-tendon lengthening velocity at the maximum sprinting speed. It has been suggested that increasing from submaximal to maximal speed may be accomplished by delaying the reduction of swing leg energy within the gait cycle, with eccentric knee moment capacity being a potential limiting factor (Chapman and Caldwell 1983). Similarly, post hoc analysis of our data indicated that increasing from 95 to 100% of sprinting speed involved a delay in when the peak hamstring muscle-tendon lengths occurred in the gait cycle. Give that there were no significant changes in the timing of peak lengths at speeds below 95%, the delay seen at the the highest speed may well result from reaching a limiting neuromuscular factor at a maximum running speed.

There are some limitations of our study that are important to consider when interpreting the results. Our estimates of hamstring muscle-tendon kinematics are based on generic musculoskeletal models that do not account for individual differences in muscle origins and insertions, or the effects of loads on joint kinematics. Accounting for these factors would likely alter the absolute magnitudes of the muscle-tendon lengths, but is unlikely to impact either the timing or intermuscle differences of peak muscle-tendon

lengths. This is because the timing of peak lengths depends primarily on the simultaneous occurrence of near maximal hip flexion and knee extension, rather than on the geometry. Dynamic joint and muscle loading could alter the instantaneous joint axes and/or muscle paths. However the anthropometric relationship among the muscles would still be retained meaning the relative differences in lengths and velocities between muscles would likely remain similar.

Our subjects were running on a treadmill rather than overground, as treadmill running allowed us to capture multiple trials that improved the strength of our statistical comparisons. Nigg et al. (1995) found biomechanical differences between treadmill and overground running to be highly subject dependent, such that it is difficult to infer how hamstring muscle kinematics may differ between the two conditions. Frishberg (1983) found that at foot contact, sprinters tended to have a more upright leg but less upright thigh when sprinting overground compared to on a treadmill. This could indicate the athletes were running with greater hip and knee flexion during terminal swing. Because hip flexion lengthens the hamstrings and knee flexion shortens the hamstrings, these two factors could potentially combine to produce similar muscle-tendon kinematics as seen in treadmill sprinting.

Animal models have demonstrated that muscle fiber strain is a primary determinant of injury during active lengthening contractions (Best et al. 1995; Brooks and Faulkner 2001; Lieber and Friden 1993). For example, Best et al. (1995) found that acute strain injuries occurred when fiber strain reached ~60% across strain rates ranging from 4 to 100 cm/s. Therefore, although we found intermuscle differences in both the

stretch and lengthening velocity of the muscle-tendons, the peak stretch measures may be more relevant as indicators of injury potential. Based on the stretch measures, our data would support the idea that injury potential is greatest during the late swing phase of sprinting and is higher for the biceps femoris than the medial hamstrings (van Don 1998). However, it is important to recognize that muscle-tendon stretch does not equate directly to fiber strain due to the dynamic interactions between muscle contraction properties and tendon elasticity (Zajac 1989). For example, a recent experimental study demonstrated that gastrocnemius muscle fascicles remain at a relatively constant length while the muscle-tendon and tendon undergo substantial lengthening and shortening during the stance phase of walking (Fukunaga et al. 2001). It is similarly feasible that the hamstring muscle fibers undergo different motion than the muscle-tendon unit during the late swing phase of sprinting, contracting isometrically while the tendon stretches and then recoils before foot contact. Accounting for these dynamic muscle-tendon interactions is important for estimating actual fiber strain during functional movement such as sprinting. Given that the vast majority of hamstring strain injuries occur at or near a myotendinosus junction (De Smet and Best 2000), such analyses are highly relevant for furthering our understanding of injury mechanisms *in vivo*.

In summary, our results suggest that peak hamstring muscle-tendon lengths occur during late swing prior to foot contact, tend to be larger in the biceps femoris than in the semitendinosus and semimembranosus muscles, but do not vary significantly as sprinting speed is increased from sub-maximal to maximal. Combining these analyses with an assessment of hamstring muscle-tendon interactions may lend insights into the

biomechanical mechanisms of hamstring injuries, and thus provide a scientific basis for evaluating clinical treatment strategies and methods of injury prevention.

Acknowledgements

CHAPTER 3

The Effect of Speed and Influence of Individual Muscles on Hamstring Mechanics during the Swing Phase of Sprinting

[1]Elizabeth S. Chumanov, [1]Bryan C. Heiderscheit, [1]Darryl G. Thelen

[1]University of Wisconsin-Madison, Madison, WI

Abstract

The purpose of this study was to characterize the effect of speed and influence of individual muscles on hamstring stretch, loading, and work during the swing phase of sprinting. We measured three-dimensional kinematics and electromyography (EMG) activities of 19 athletes sprinting on a treadmill at speeds ranging from 80% to 100% of maximum speed. We then generated muscle-actuated forward dynamic simulations of swing and double-float phases of the sprinting gait cycle. Simulated lower extremity joint angles and model predicted excitations were similar to measured quantities. Swing phase simulations were used to characterize the effects of speed on the peak stretch, maximum force, and negative work of the biceps femoris long head (BF), the most often injured hamstring muscle. Perturbations of the double float simulations were used to assess the influence of individual muscles on BF stretch.

Peak hamstring musculotendon stretch occurred at ~90% of the gait cycle (late swing) and was independent of speed. Peak hamstring force and negative musculotendon work increased significantly with speed ($p < 0.05$). Muscles in the lumbo-pelvic region had greater influence on hamstring stretch than muscles acting about the knee and ankle. In particular, the hip flexors were found to induce substantial hamstring stretch in the opposite limb, with that influence increasing with running speed. We conclude that hamstring strain injury during sprinting may be related to the performance of large amounts of negative work over repeated strides and/or resulting from a perturbation in pelvic muscle coordination that induces excessive hamstring stretch in a single stride.

Key words: muscle strain injury, motion analysis, musculoskeletal modeling, stretch shortening cycle, forward dynamics

Introduction

Acute hamstring strain injuries are commonly linked with maximal speed running in a variety of sports such as track, football and soccer (Gabbe 2005; Woods 2004). While it is generally agreed that strain injuries are the result of exceeding the local mechanical limits of the muscle tissue, little is known on how running speed changes the mechanical demands of the hamstrings. Such information is relevant for establishing a scientific basis for injury prevention programs and rehabilitative approaches that can mitigate the high risk for re-injury (Orchard and Best 2002). For example, a recent study found that the performance of rehabilitative exercises targeting neuromuscular control of muscles in the lumbo-pelvic region (e.g. abdominal obliques, erector spinae, illiopsoas) reduced hamstring re-injury rates compared to a stretching and strengthening approach (Sherry and Best 2004). However, the complexities of multi-segmental dynamics (Zajac and Gordon 1989) make it challenging to understand how lumbo-pelvic muscles may influence hamstring mechanics, and hence injury risk.

Prior studies have shown that the biarticular hamstrings are active (Jonhagen et al. 1996; Swanson and Caldwell 2000; Wood 1987) and undergo a stretch-shortening cycle (Thelen 2005) during the second half of the swing phase of sprinting. The hamstrings do a substantial amount of negative work over this period, with the peak stretch of the hamstring musculotendon unit occurring during late swing (Thelen 2005; van Don 1998; Wood 1987). Thus, the hamstrings are likely susceptible to a lengthening contraction injury during late swing. We have previously shown that peak musculotendon stretch is invariant as speed increases from submaximal to maximal speeds (Thelen 2005). The purpose of this study was to utilize simulations of subject-specific sprinting dynamics to

test the hypothesis that sprinting speed increases the loading and negative work required of the hamstrings. We also evaluated the sensitivity of hamstring stretch to perturbations in individual muscle forces, to understand the potential influence that lumbo-pelvic muscles have on injury risk.

Methods

Subjects. 19 athletes participated in this study (Table 1.3). All subjects had experience sprinting on a treadmill. Testing was conducted at two sites: the Orthopedic Specialty Hospital in Murray, UT and the University of Wisconsin-Madison in Madison, WI. The testing protocol was approved by the Institutional Review Boards at both institutions and all subjects provided informed consent in accordance with institutional policies.

Table 1.3. Subject characteristics and maximum treadmill sprinting speed (V_{max}) of the athletes who participated in this study.

	Males mean (s.d.)	Females mean (s.d.)
Number of subjects	14	5
Age, yrs	20.9 (5.7)	19.6 (6.4)
Height, cm	179 (8)	176 (5)
Body mass, kg	78.6 (9.6)	65.7 (4.2)
V_{max} (m/s)	9.10 (0.60)	8.18 (0.77)

Experimental protocol. Whole body kinematics were recorded using 40 reflective markers placed on each subject, with 21 located on anatomical landmarks. In addition, a subset (n=5) of the subjects had electromyography (EMG) surface electrodes placed on muscles of the right lower limb: biceps femoris (BF), medial hamstrings (ST and SM), vastus lateralis, rectus femoris, and the medial gastrocnemius. After the markers and EMG electrodes were in place, each subject warmed up prior to sprinting at 80, 85, 90, 95, and 100% of his/her maximum speed, with 5 strides (3-5 seconds) collected for each trial. Subjects were given adequate rest between trials. A standing trial was also performed to establish segment lengths, joint centers and joint coordinate systems.

Data acquisition. Three-dimensional kinematics were collected at 200 Hz using an 8-camera passive marker system (Motion Analysis Corporation, Santa Rosa, CA). Kinematic data were low pass filtered using a bidirectional, 4th order Butterworth filter with a cutoff frequency of 12 Hz. Foot contact times were ascertained from a contact-induced vertical acceleration of the 5th metatarsal toe marker at foot strike. The validity of this approach has been verified with pressure sensitive foot switches on four of the subjects.

EMG activities were recorded (synchronously with kinematics at 2000Hz) using single differential, surface electrodes with an inter-electrode distance of 10 mm (DE-2.1, DelSys, Inc, Boston, MA). Each electrode pre-amplified the signal and interfaced to an amplifier unit (Bagnoli-16, DelSys, Boston, MA). The EMG signals were subsequently full-wave rectified and low pass filtered using a bidirectional, 6th order Butterworth filter with a cutoff frequency of 20 Hz.

Musculoskeletal model: The body was modeled as a 14 segment, 31 degree of freedom (DOF) articulated linkage (Figure 1.3). Anthropometric properties of the segments were scaled to each individual using the subject's height, mass and segment lengths (de Leva 1996). Each hip was modeled as a ball and socket joint with three DOF. The knee was represented as a one DOF joint, in which the tibiofemoral translations and nonsagittal rotations were constrained functions of knee flexion-extension angle (Walker et al. 1988). The ankle-subtalar complex was represented by two revolute joints aligned with anatomical axes (Delp et al. 1990). The low back was represented as a ball and socket joint at the 3rd lumbar vertebra (Anderson and Pandy 1999). For each trial, joint angles were computed at each time step using a global optimization routine to minimize the sum of squared error between the measured and model marker positions (Lu and O'Connor 1999).

Musculotendon actuators were represented as line segments connecting the origin to the insertion with wrapping about joints and other structures accounted for with wrapping surfaces (Arnold et al. 2000). The input to each musculotendon actuator was an idealized excitation level that varied between zero and one (full excitation). Muscle excitation-to-activation dynamics was
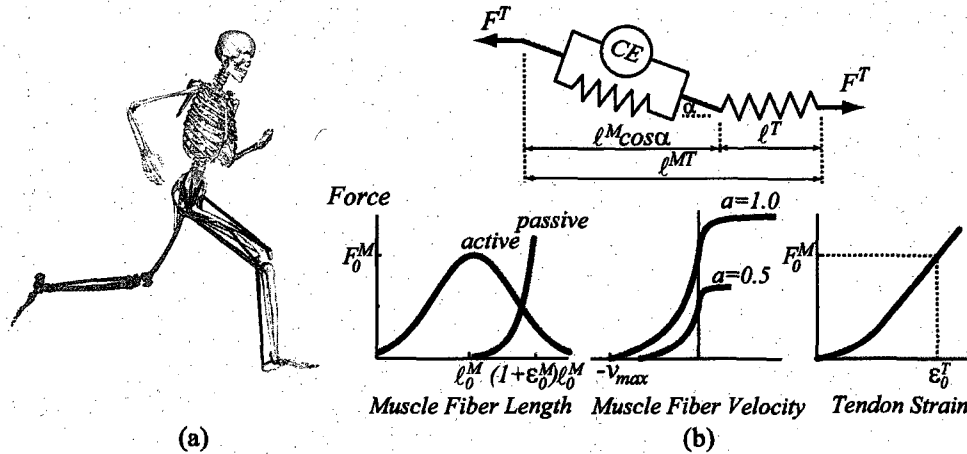
Figure 1.3. (a) A forward dynamic musculoskeletal model, shown with 58

musculotendon actuators, was used to simulate both the swing phase and double float

phases of sprinting. (b) A Hill-type model was used to characterize musculotendon

contraction dynamics. The muscle force-length-velocity properties and tendon force-

strain properties were scaled to each muscle using four parameters: ℓ_0^M - optimal fiber

length, F_0^M - maximum isometric force, ℓ_s^T - tendon slack length and α_0 - fiber pennation

angle (Zajac 1989). Parameters used for the biarticular hamstring muscles were adapted

from the literature (Delp, et al., 1990, Arnold, et al., 2000) 1) BF: $\ell_0^M = 0.109\,m$,

$\ell_s^T = 0.341\,m$, $F_0^M = 1792\,N$, $\alpha_0^M = 0\,\text{deg}$, 2) ST: $\ell_0^M = 0.201\,m$, $\ell_s^T = 0.262\,m$,

$F_0^M = 820\,N$, $\alpha_0^M = 5\,\text{deg}$, SM: $\ell_0^M = 0.08\,m$, $\ell_s^T = 0.359\,m$, $F_0^M = 2576\,N$, $\alpha_0^M = 15\,\text{deg}$.

represented using a first order differential equation that had a faster time constant during activation (10 ms) than deactivation (30 ms). A Hill-type model (Figure 1.3) of musculotendon contraction dynamics was assumed, where muscle fibers were in series with an elastic tendon (Zajac 1989). Force produced by the musculotendon actuator was applied to the segments to which it attached. The equations of motion of the musculoskeletal model were derived using SDFast (Parametric Technology Corporation, Waltham, MA) and SIMM Pipeline (Musculographics Inc., Chicago, IL).

Forward dynamic simulations: We generated muscle-actuated forward dynamic simulations of swing limb movement to characterize hamstring stretch, force and work. In *swing phase* simulations, 52 musculotendon actuators (26 actuators on each limb) were used to actuate 3 DOF on each limb (hip flexion-extension, hip adduction-abduction, knee flexion-extension). All other DOF were prescribed to follow the measured kinematic trajectories, thereby accounting for inter-segmental dynamics. Swing phase simulations were generated for 3 strides for each subject at each speed.

We also generated forward dynamic simulations of the *double float phase* of sprinting (i.e. when both feet are off the ground) to assess the influence of individual muscles on hamstring stretch. Double float phase was selected because peak hamstring musculotendon stretch occurs during this time period. In the double float simulations, 58 musculotendon actuators (26 on each limb and 6 acting about the low back) were used to actuate 21 DOF (6 DOF for the pelvis and each limb, 3 DOF about the low back), with only the upper extremity DOF prescribed to follow measured trajectories. Double float phase simulations were generated for one stride at 80 and 100% speeds for 4 subjects, whom we had a full set of kinematic, EMG and foot switch data.

For all simulations, a computed muscle control (CMC) algorithm was used to determine muscle excitation patterns that, when input into the forward dynamic model, produced joint angles that closely replicated experimental kinematics. A brief description of the CMC algorithm follows (for details, see (Thelen and Anderson 2006)). When computing the excitations, we first determined the difference between the experimental and simulated joint angles and angular velocities. These errors were fed back and combined with the experimental accelerations to compute a set of desired accelerations to ensure the experimental kinematics were tracked. We then determined a set of muscle excitations that would generate the desired accelerations, while minimizing a cost function (sum of muscle volume-weighted squared activations, (Happee 1994) to resolve muscle redundancy. Computed muscle excitations were then input into the forward dynamic model equations, which were numerically integrated to generate a set of simulated muscle excitations, activations, lengths, musculotendon forces and joint kinematics. The excitations were re-computed using this process at 0.01 sec intervals throughout the simulations.

Swing phase simulations, in which muscles actuated 3 DOF on each limb, were used to characterize the musculotendon stretch, force and power development of the biarticular hamstrings. Stretch was defined as the change in length of the musculotendon unit relative to the relaxed length in an upright posture. Relaxed lengths were estimated by setting all joint angles and muscle excitations to zero in the subject-specific scaled model. The musculotendon power generated (absorbed) was computed as the product of the force and musculotendon velocity. Negative and positive musculotendon work was computed by integrating the respective portions of the power curves. A one-way

repeated measures analysis of variance was used to determine the effects of normalized speed (80, 85, 90, 95, and 100%) on the magnitude of peak musculotendon stretch, force, and negative work. Tukey's post hoc test was used to analyze significant main effects. The statistical analyses were completed using Systat (SPSS Inc., Chicago, IL) with a significance level of 0.05.

Perturbations of the *double float phase* simulations, in which muscles actuated 21 DOF, were performed to investigate how individual muscles influence BF musculotendon stretch (Figure 2.3). We report perturbation results for the BF because it is the most frequently injured of the hamstring muscles (Connell et al. 2004), the perturbation results for the other biarticular hamstrings were similar. For each muscle in the model, the nominal force trajectory was perturbed by a fixed ratio (0.1%) throughout double float, while the excitations of all other muscles were held constant (Figure 2.3). The musculoskeletal dynamic model equations were then re-integrated to produce a perturbed set of joint and musculotendon kinematic trajectories. It is noted that perturbation-induced changes in kinematics could alter the lengths and velocities, and hence forces, of other muscles in the system, thereby reflecting the complex interactions inherent in the musculoskeletal system (Goldberg et al. 2004). The influence of an individual muscle was then defined as the change in the peak stretch of the BF scaled by the inverse of the force perturbation magnitude. Perturbations with a fixed force magnitude (1N) were also performed to assess the potential of muscles to influence biceps femoris stretch per unit force (Goldberg et al. 2004).

Excitations

R. BF

R. RF

R. VL

R. GAS

Perturbed Force Trajectory

L. PS

(a)

(b)

R. Biceps Femoris
Musculotendon Stretch

(c)
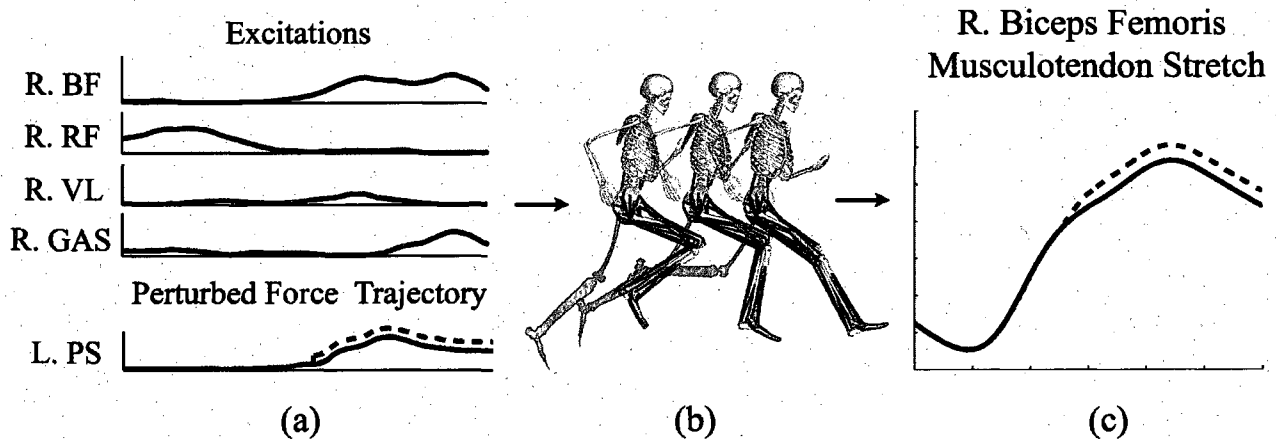
Figure 2.3. In the perturbation analyses used to assess muscle influence, we first generated forward dynamic simulations of the double float phase of sprinting in which all lower extremity and low back degrees of freedom were actuated by muscles (note that left limb muscles are not shown for clarity). (a) We then perturbed individual muscle force trajectories, one at a time, by 0.1 percent throughout the simulation while other muscle excitations were held constant (solid line is nominal trajectory, dashed line is perturbed force trajectory). (b) The movement was then re-simulated. (c) The difference in the BF nominal length (solid line) and perturbed length (dashed line) was attributed to the force perturbation. The change in peak musculotendon stretch scaled by the inverse of the perturbation magnitude to determine the absolute influence of the muscle (in mm) on BF stretch.

Results

The CMC algorithm generated simulations that closely tracked the experimental kinematics (Figure 3.3). For the swing phase simulations, RMS errors for the hip and knee angles were $1.0 \pm 0.7°$ for hip flexion-extension, $0.7 \pm 0.3°$ for hip abduction-adduction, and $2.2 \pm 1.2°$ for knee flexion-extension. For the double float simulations, the average RMS errors for the actuated 21 DOF were $3.3 \pm 4.3°$. The simulated muscle excitation patterns of the lower limb muscles were similar to measured EMG signals (Figure 4.3). Hamstring muscle excitations were initiated at ~70% of the gait cycle and remained elevated throughout the remainder of swing phase. The hamstring musculotendon units lengthened from approximately 50% to 90% of the gait cycle with peak force reached between 85 and 95% of the gait cycle (Figure 5.3).

Peak hamstring musculotendon stretch was independent of speed. However, both peak musculotendon force and negative musculotendon work increased significantly ($p<0.01$) with speed (Figure 6.3). The average net hamstring force increased from ~36 N/kg at the 80% speed to ~52 N/kg at maximal speed and the average net negative work increased from ~1.4 J/kg to ~2.61 J/kg as speed was increased (Table 2.3).

The influence of individual muscles on hamstring stretch was larger at maximal speed when compared to slower speeds (Figure 7.3). Other than the hamstrings themselves, muscles in the lumbo-pelvic region had the greatest influence (Figure 7.3) and potential influence (Figure 8.3) on hamstring stretch. These muscles included the uniarticular hip flexors (iliopsoas), the gluteus maximus, the erector spinae and the internal and external obliques. The right adductor magnus has a large potential influence (Figure 8.3) to decrease BF stretch, resulting from a large hip flexion moment arm when

hip flexion is greater than 50 degrees (Delp et al. 1990). However, the actual influence of adductor magnus is substantially less because the muscle is not active during double float. At the maximum speed, the uniarticular hip flexors induced >20 mm increase in BF stretch on the opposite limb, which was of comparable magnitude to the decrease in stretch induced by hamstrings themselves.
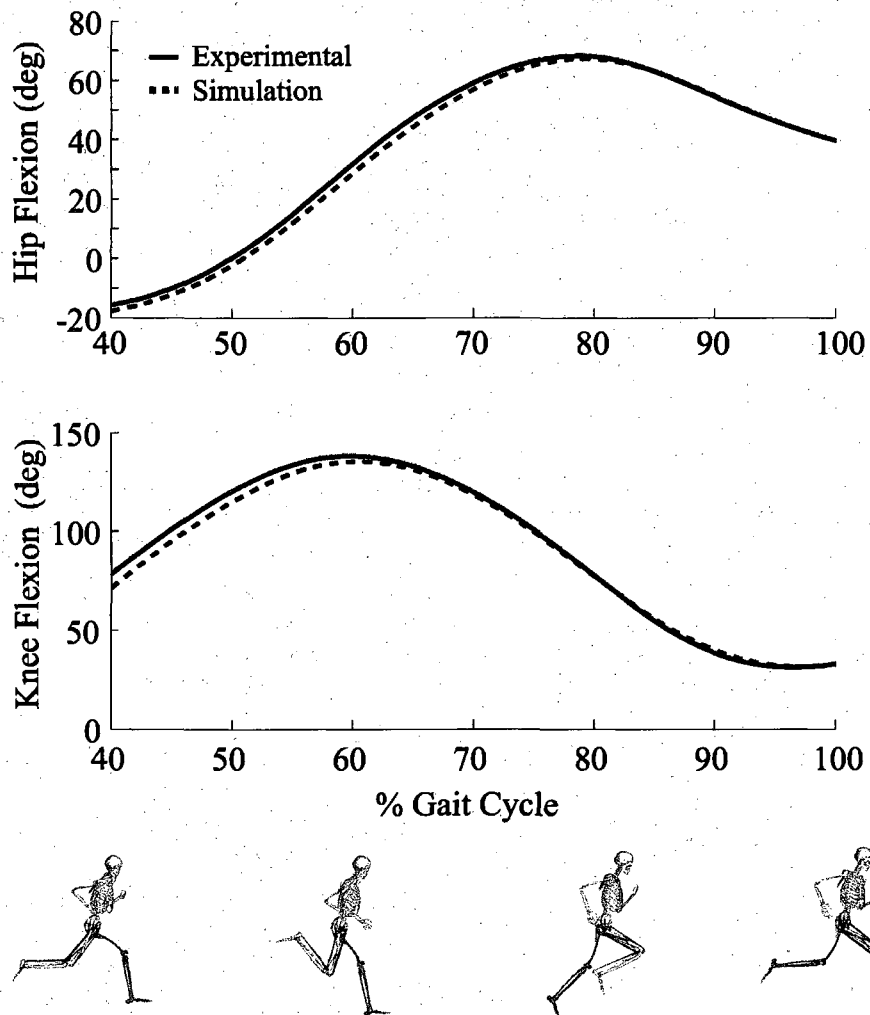
Figure 3.3. A sample swing phase simulation is shown demonstrating that the simulated hip and knee angles closely tracked the experimentally quantities.
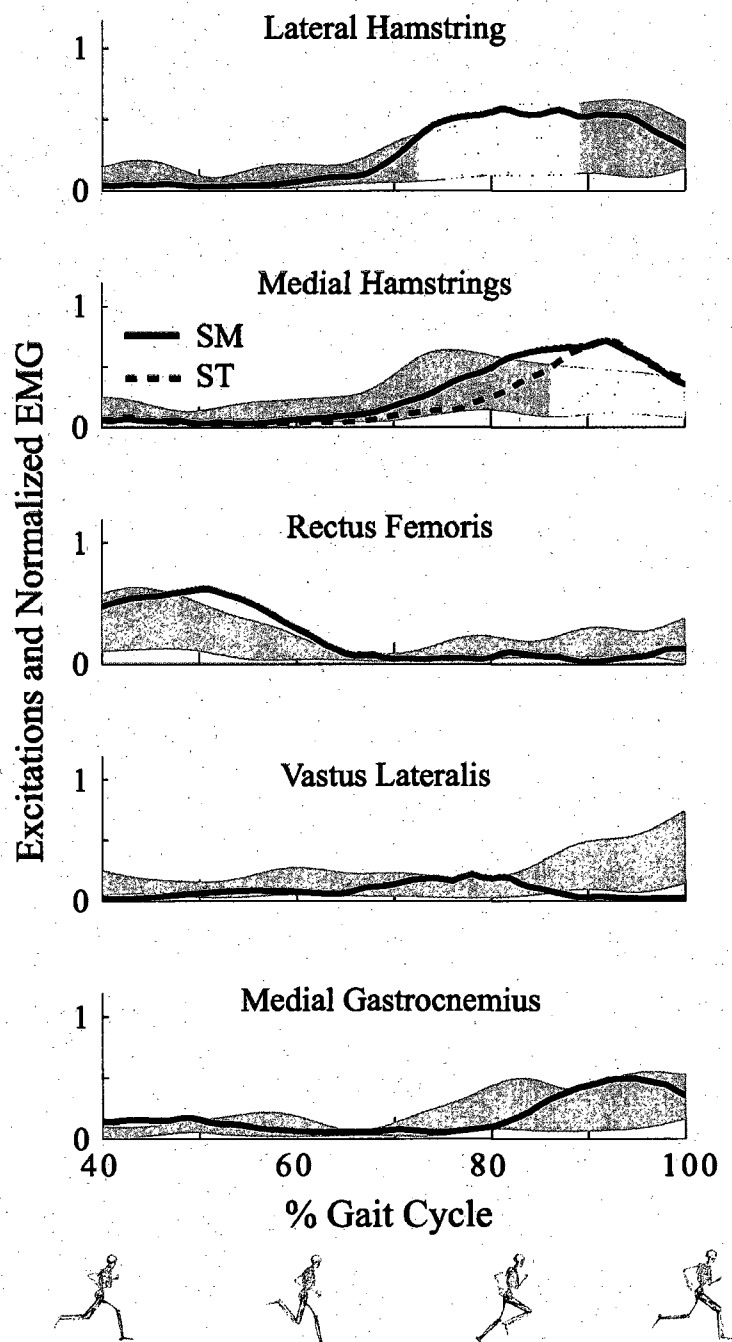
Figure 4.3. The timing of simulated muscle excitations (solid lines) and measured electromyographic (EMG) activities (shaded curves) were relatively consistent for the hamstrings, rectus femoris and gastrocnemius muscles. Vastus excitations during late swing are presumably in preparation for the subsequent stance phase, which was not simulated. Simulated excitations are the ensemble average of the predicted excitations across all subjects at the maximum sprinting speed. EMG activities are the mean (±1 s.d.) rectified, low-pass filtered activities recorded from five subjects at maximal speed.
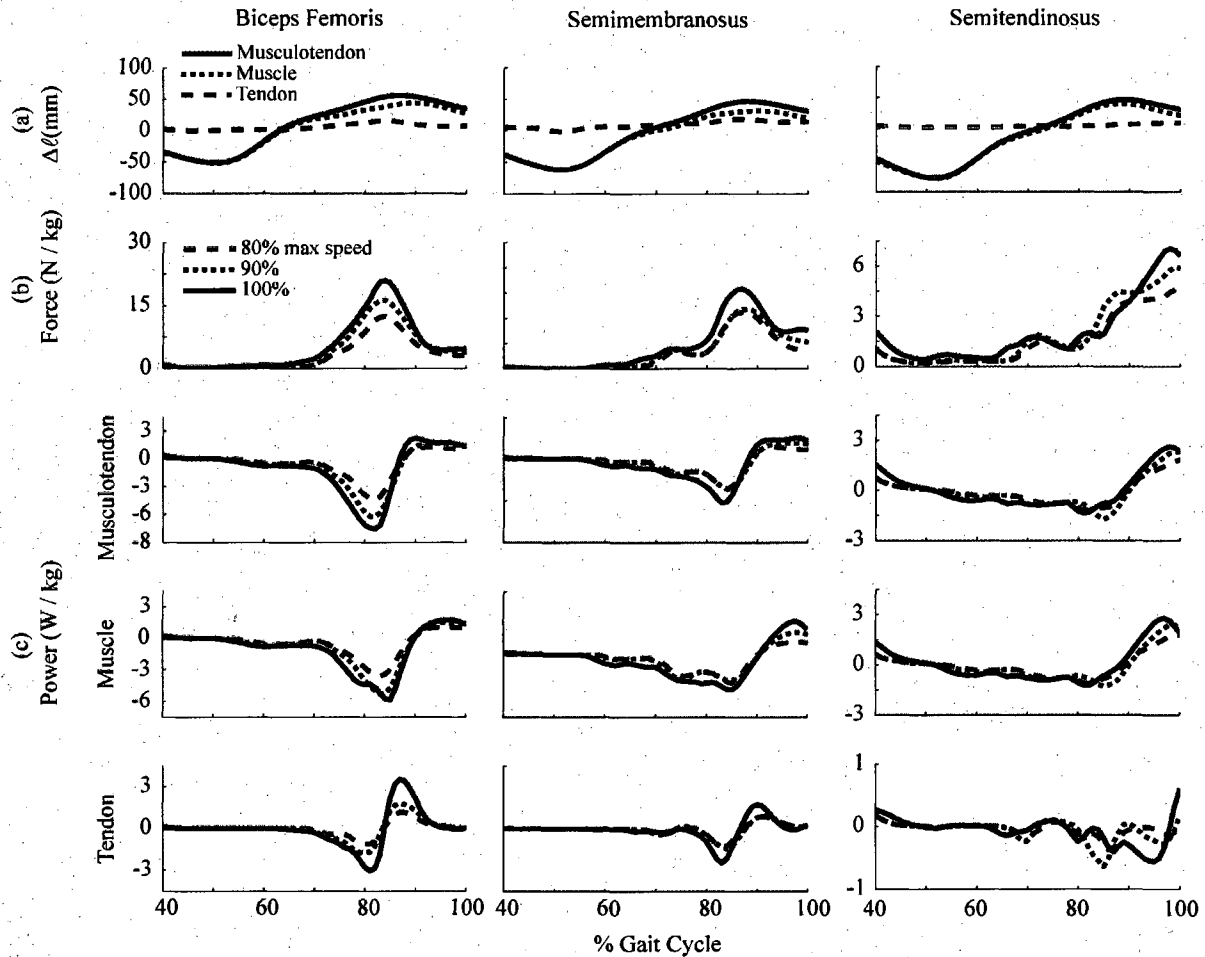
Figure 5.3. Simulated musculotendon mechanics of the hamstring muscles for one subject. (a) The change in length (ΔL) from a relaxed, upright posture of the musculotendon, muscle component and tendon at maximal sprinting speed. The musculotendon stretches more than the muscle component during late swing due to the tendon stretching as force develops (Thelen, et al., 2005a) (b) Musculotendon forces increase with speed for each of the hamstring muscles, with peak forces occurring slightly earlier in the biceps femoris and semimembranosus, compared to the semitendinosus. (c) The hamstring musculotendon units do a considerable amount of negative work up until the final 10% of the gait cycle.
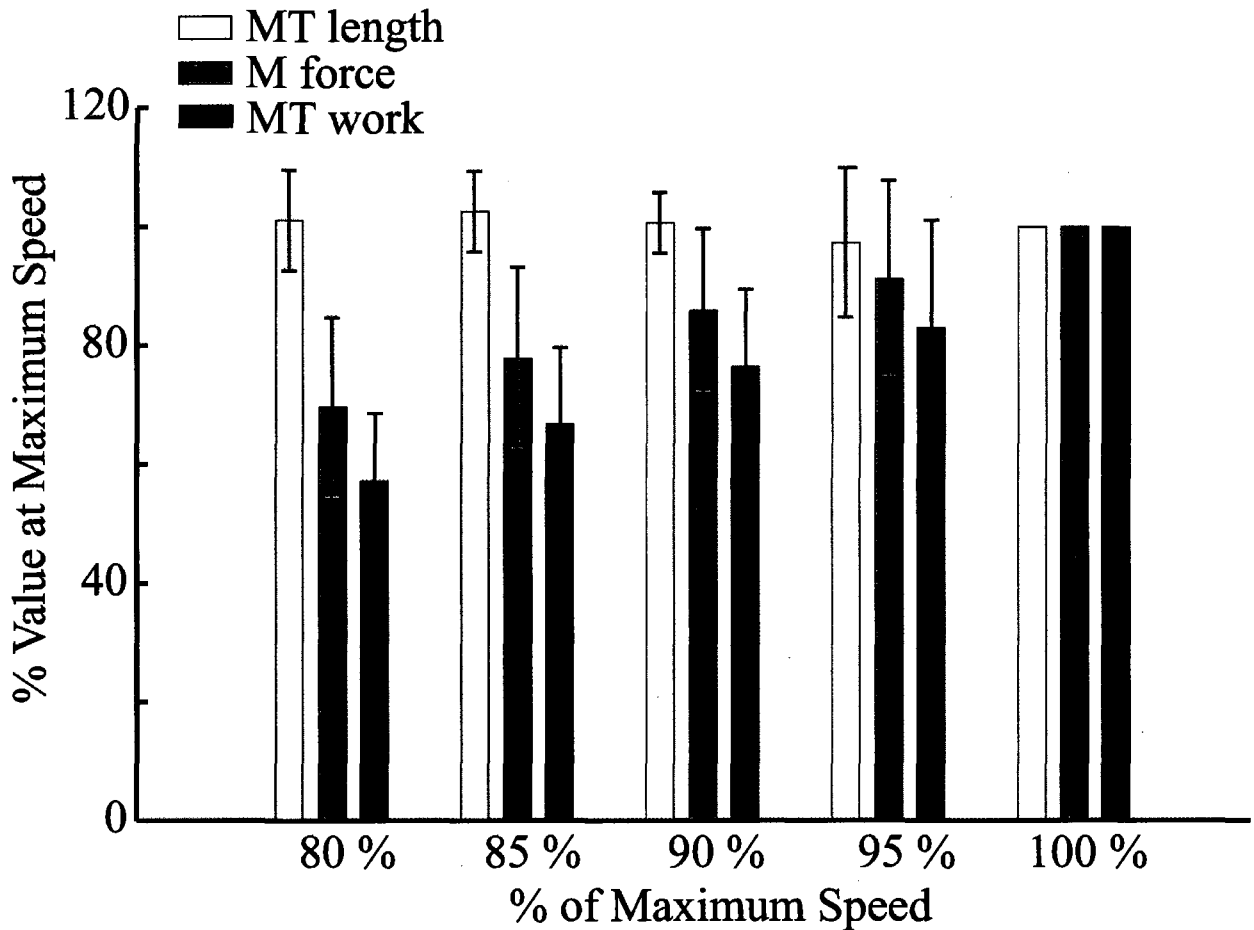
Figure 6.3. The relative (compared to 100% or maximal speed) biceps femoris musculotendon stretch, negative work, and force. Peak musculotendon stretch is invariant with sprinting speed, while force and negative work increase significantly with speed. Negative musculotendon work increased to the largest extent as sprinting speed was increased from submaximal to maximal sprinting speeds.

Table 2.3. Mean (s.d.) kinematic and kinetic measures from the hamstring muscles across all subjects. Relative to the length in a relaxed upright posture, the biceps femoris (BF) exhibited greater musculotendon stretch than the semimembranosus (SM) and semitendinosus (ST). Both the force developed and negative musculotendon work done by the hamstrings increased significantly with sprinting speed. Force and work were normalized to body weight ($\Delta \ell^{MT}$ = peak musculotendon stretch, F_{max} = peak muscle force, W_{neg}^{MT} = negative work done by the musculotendon unit).

Measure	Speed (% max)	BF		SM		ST		NET	
Kinematic measures									
$\Delta \ell^{MT}$ (mm)	80	51.4	(5.6)	43.5	(5.1)	44.7	(5.5)		
	85	52.2	(4.8)	44.1	(4.6)	45.1	(5.2)		
	90	51.4	(4.3)	42.8	(4.0)	43.4	(4.4)		
	95	49.9	(7.9)	41.2	(8.6)	41.3	(10.4)		
	100	51.2	(4.4)	42.6	(4.6)	42.9	(5.4)		
Kinetic Measures								**NET**	
[1]F_{max} (N/kg)	80	15.1	(6.3)	18.9	(6.2)	6.4	(1.3)	36.0	(12.4)
	85	16.8	(6.4)	21.4	(6.9)	6.7	(1.2)	40.5	(13.8)
	90	18.6	(6.8)	23.3	(8.6)	7.1	(1.3)	45.2	(15.4)
	95	19.8	(7.0)	25.7	(9.7)	7.4	(1.4)	49.2	(16.1)
	100	21.4	(5.4)	27.9	(7.6)	7.9	(1.8)	52.0	(13.4)
[1]W_{neg}^{MT} (J/kg)	80	0.47	(0.23)	0.50	(0.26)	0.21	(0.06)	1.40	(0.62)
	85	0.53	(0.26)	0.59	(0.31)	0.23	(0.08)	1.65	(0.73)
	90	0.61	(0.31)	0.69	(0.37)	0.25	(0.10)	1.92	(0.88)
	95	0.65	(0.31)	0.79	(0.42)	0.27	(0.13)	2.23	(0.97)
	100	0.77	(0.28)	0.99	(0.44)	0.35	(0.18)	2.61	(1.01)

[1] Significant speed effects
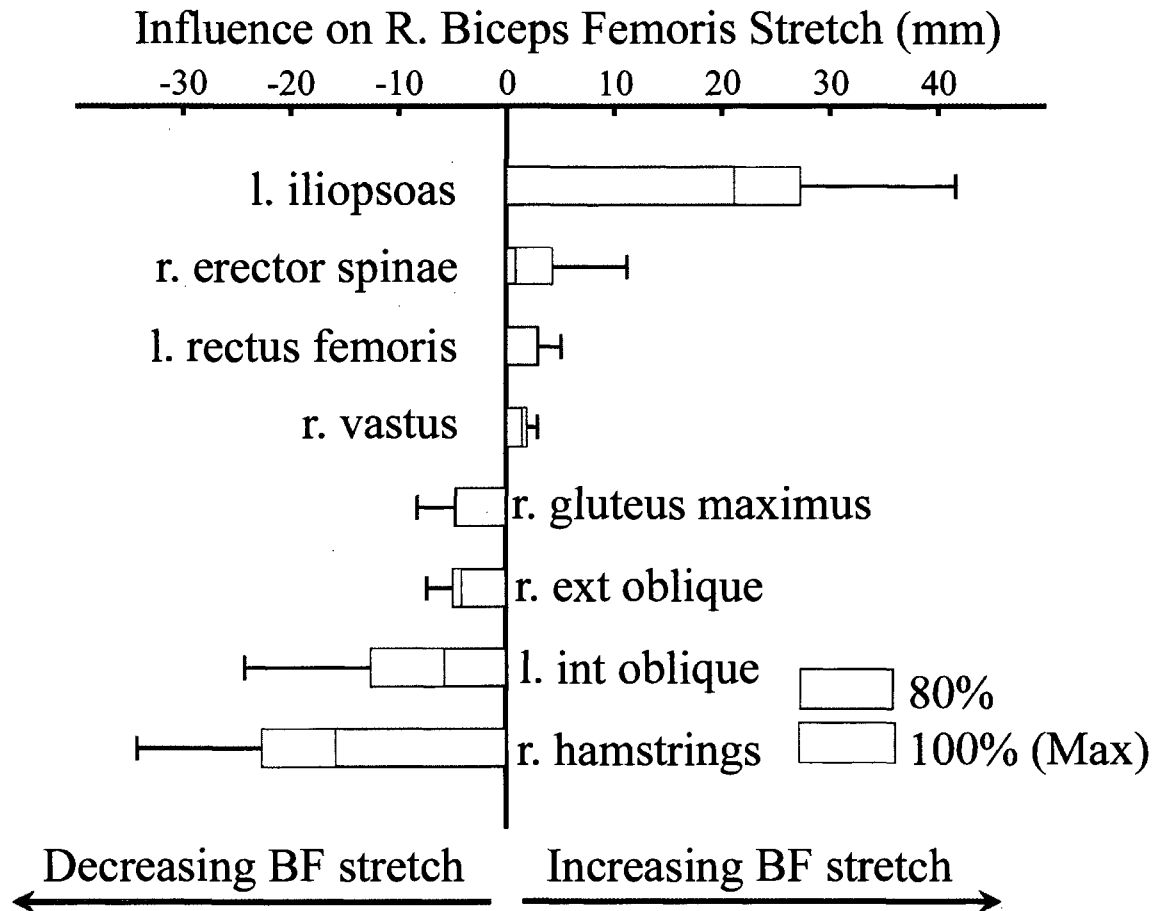
Figure 7.3. The muscles that had the greatest magnitude of influence on biceps femoris stretch during double float are shown. Note that the influence of each muscle increased as speed was increased from submaximal to maximal, reflecting the larger forces present at high speeds. When the hamstring muscles are given a positive perturbation, the hamstring force increases and contributes to a decrease in peak stretch. In contrast, the uniarticular hip flexors (iliopsoas) are simultaneously active on the opposite limb inducing a substantial increase in biceps femoris stretch.

Potential influence on R. Biceps Femoris Stretch (mm/N)
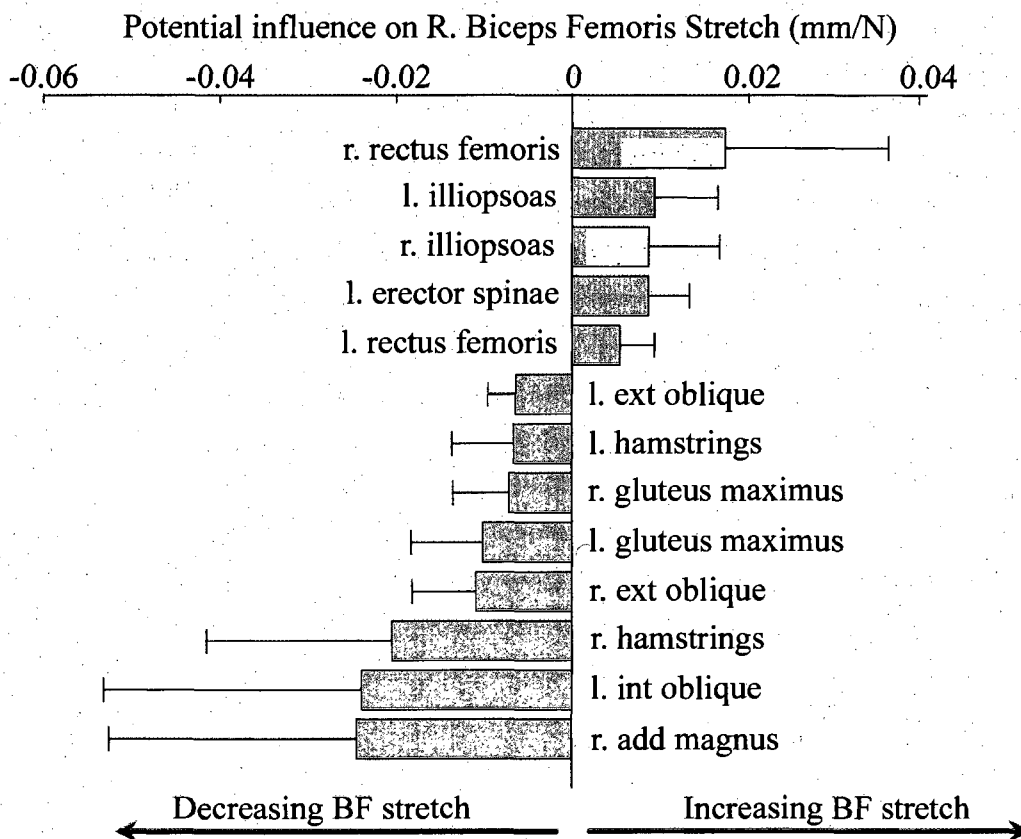
Figure 8.3. Muscles in the lumbo-pelvic region have the largest potential to influence biceps femoris stretch during double float phase. Muscles not shown (including the vasti, gastrocnemius, soleus, tibialis anterior, gluteus medius and gluteus minimus) exhibited average potential influences that were less than 0.005 mm/N.

Discussion

In this study, we used forward dynamic simulations of sprinting to investigate changes in hamstring mechanics with speed. The salient findings were that speed significantly increases the amount of negative work the hamstrings do, and magnifies the influence that individual muscles, particularly the muscles in the lumbo-pelvic region, have on hamstring stretch.

Previous studies investigating joint mechanics (Kuitunen et al. 2002; Mann 1981; Swanson and Caldwell 2000) and muscle activation patterns (Jonhagen et al. 1996; Mero and Komi 1987) during sprinting have shown that coupled hip extensor and knee flexor moments are utilized during the late swing phase of sprinting (Kuitunen et al. 2002), presumably to decelerate the limb prior to foot contact. EMG data indicate that the medial and lateral biarticular hamstrings exhibit peak activities during late swing, and increase significantly with speed (Mero and Komi 1987). The modeling approach used in this study extends these results, by providing quantitative predictions of the mechanical loading of the hamstrings during this period.

We found that the peak musculotendon stretch of the hamstrings does not vary significantly across speeds ranging from 80% to 100% of maximum, which is consistent with our results on a smaller group of subjects (Thelen 2005). Joint kinematic patterns have been shown to be relatively consistent across a range of sprinting speeds (Thelen 2005), suggesting the primary speed effect is an increase in the rate at which the joint angular excursions are traversed. Therefore, the energy associated with the limb would be expected to increase in proportion to the joint angular velocities, and equivalently

sprinting speed, squared. Such a relationship is evident in Figure 6.3, where the negative musculotendon work increases at a faster rate than peak musculotendon force.

Animal models of muscle injury have provided insights into the relationship between mechanical measures and the degree of injury. In animal models, the best indicators of injury potential are the magnitude of strain (Brooks and Faulkner 2001; Lieber and Friden 1993; Lieber and Friden 2002), or the product of force and strain (Brooks and Faulkner 2001), which may in effect be equivalent measures for maximally activated muscle (Brooks et al. 1995). In this study which involves variable activation levels, we have shown differential effects of sprinting speed on musculotendon stretch (comparable to mechanical strain) and negative work.

Our results indicate two, potentially inter-related, factors contributing to increased injury risk at high speed. One possibility is a large amount of negative work done over repeated strides may result in accumulated microdamage that predisposes the muscle to injury. This would be consistent with a recent animal model of injury, which showed that multiple stretch-shortening contractions are needed to induce injury when muscle lengths are constrained to physiological ranges (Butterfield and Herzog 2005). Secondly, fluctuations in neuromuscular control at high speed could create stride-to-stride variability in hamstring stretch, with excessive stretch in any single stride inducing an acute onset of injury. These factors could also be inter-related with microdamage due to multiple stretch-shortening cycles altering musculotendon properties, thus changing the threshold for injury over time (Butterfield and Herzog 2005), making an individual more susceptible to stride-to-stride variations in hamstring stretch.

Our perturbation analyses suggest a mechanism by which a rehabilitation program focused on core neuromuscular training (Sherry and Best 2004) could influence hamstring re-injury risk. We showed that muscles in the lumbo-pelvic regions have substantial influence on the overall stretch of the BF. For example, activation of the uniarticular hip flexors (iliopsoas) during early swing induces stretch of the hamstrings on the opposite limb. This coupling arises due to inter-segmental dynamics, in which muscles can generate substantial accelerations about joints they don't span (Zajac and Gordon 1989). In our simulations, the hip flexor muscle force induced hip flexion and a small amount of knee extension on the opposite limb which both act to increase hamstring stretch. The magnitude of this increased stretch was comparable to the shortening induced by the hamstrings themselves, demonstrating the importance of considering inter-segmental dynamics.

There are a number of assumptions in the musculotendon models that should be considered when interpreting the results. First while we scaled the lengths and moment arms of the musculotendon unit based on subject-specific segment lengths, we relied on literature-derived estimates for other important parameters such as maximum isometric force, optimum fiber length, and tendon compliance. As a result, there is a degree of uncertainty in the absolute accuracy of our force, length and work measures. For example, we have previously demonstrated that tendon compliance has substantial affects on fiber stretch and negative work done by the muscle component (Thelen 2005). For this reason, we limited our dependence on model parameters by only considering speed-dependent changes in musculotendon measures (rather than muscle and tendon component measures) to evaluate our primary hypotheses. New imaging techniques to

empirically characterize in vivo musculotendon mechanics (Fukunaga et al. 2002) may facilitate more detailed subject-specific models that are needed to enhance the accuracy of model predictions at the muscle and tendon level. Our analyses were also limited to swing phase where peak hamstring stretch occurs. However muscle activations during stance also influence kinematics during swing (Goldberg et al. 2004), and should be considered to fully understand the influence of individual muscles on injury risk.

In conclusion, our results support the idea that acute hamstring strain injury may be related to performance of large amounts of negative work over repeated strides and/or changes in neuromuscular coordination that induce excessive stretch of the hamstrings.

CHAPTER 4

Computational Techniques to use Insole Pressure Sensors for 3D Joint Kinetics

[1]Elizabeth S. Chumanov, [1]Christian D. Remy, [1]Darryl G. Thelen

[1]University of Wisconsin-Madison, Madison, WI

Abstract

This study evaluated the feasibility of using insole pressure sensors together with whole body dynamics to analyze joint kinetics while running. Local affine transformations of shoe kinematics were first used to track the position of insole sensors during locomotion. COP estimates derived from the insoles were within 10 mm of forceplate measures through much of stance, while vertical force estimates were within 15% of peak forceplate recordings. Insole data was then coupled with a least squares whole body dynamic model to obtain shear force estimates that were comparable to forceplate records during running. We demonstrate that these techniques provide for a viable approach for analyzing joint kinetics when running on uninstrumented surfaces.

Introduction

Pressure sensitive insoles are a powerful tool for assessing the loads on the feet during locomotion. For example, insole data can be used to identify high pressure spots, to locate the local center of pressure (COP) and to estimate the net vertical ground reaction force (vGRF) (Barnett et al. 2000; Chesnin et al. 2000; Forner-Cordero et al. 2006; Kernozek and Zimmer 2000; Putti et al. 2007). Such information has proven useful for designing orthotics, assessing the cause of pressure ulcers and investigating foot-floor contact models (Ahroni et al. 1998; Cavanagh and Owings 2006).

It is also appealing to consider the use of insole pressure data to assess joint kinetics during gait. Compared to fixed forceplates, insoles have the advantage of being usable outside of laboratory environments and can facilitate collection of data over multiple strides. However, insoles do not currently provide shear force measurements or the global position of the COP. As a result, it is not feasible to use insole data for segment-by-segment inverse dynamics analysis (Winter 1990), since that requires the full complement of ground reaction data to be available. An alternative is to consider the use of whole body dynamics analysis, which can accommodate missing ground reaction data (Kuo 1998; Remy and Thelen 2008; van den Bogert and Su 2008). For example, a least-squares inverse dynamics (LSID) formulation was shown to provide reasonable estimates of joint torques, even when a partial set of ground reactions (vGRF, global COP) and noisy acceleration data was used (Kuo 1998). Thus, a primary challenge of using insoles for kinetics analysis is in tracking the global COP and estimating the missing shear forces from the data that is available.

The first objective of this study was to develop and evaluate a tracking algorithm using motion capture markers affixed around the sole of a shoe to compute the global center of pressure from insole data during locomotion. To achieve this, we developed a piece-wise affine mapping approach to estimate insole sensor positions from shoe marker kinematics recorded during locomotion. The second objective was to evaluate the accuracy of using insole pressure data together with a whole body dynamics analysis to estimate shear forces during running. Both the insole tracking and shear force estimation routines were evaluated by direct comparison with fixed forceplate measures during running. Reasonable accuracy is shown such that the proposed approach can facilitate the use of insoles to characterize lower extremity joint kinetics.

Methods

Subjects. Eight volunteers participated in this study (4 Males/4 Females, 25.3±3.5 years old, 68.8±6.9kg, 173.5±5.5cm). The University of Wisconsin Institutional Review Board approved the testing protocol and all subjects provided informed consent.

Experimental protocol. Pressure sensitive insoles (Novel Inc., Munich, Germany), with 99 sensors per insole (data collection rate of 100Hz), were fitted into each subject's shoes. An eight-camera motion capture system (Motion Analysis, Santa Rosa, CA) was used to measure the three-dimensional positions at 200Hz of 56 retro-reflective markers with 18 markers located on anatomical landmarks and ten markers (10 mm diameter) affixed to the sole of the shoe (Figure 1.4). At each frame in the trials, piecewise natural cubic splines were fit through the ten shoe markers creating 100 virtual markers around the shoe (Figure 2.4). Ground reaction forces (data collection rate of 2000Hz) were

simultaneously recorded with the kinematics using three fixed, sequential forceplates (AMTI, Watertown, MA).

Each subject performed an initial upright stance trial (15 seconds) in which he/she stood on a fixed forceplate and voluntarily shifted his/her COP in the fore-aft and medio-lateral directions. Three repeated trials of three walking (slow, preferred, fast) and two running speeds (preferred, fast) were collected.
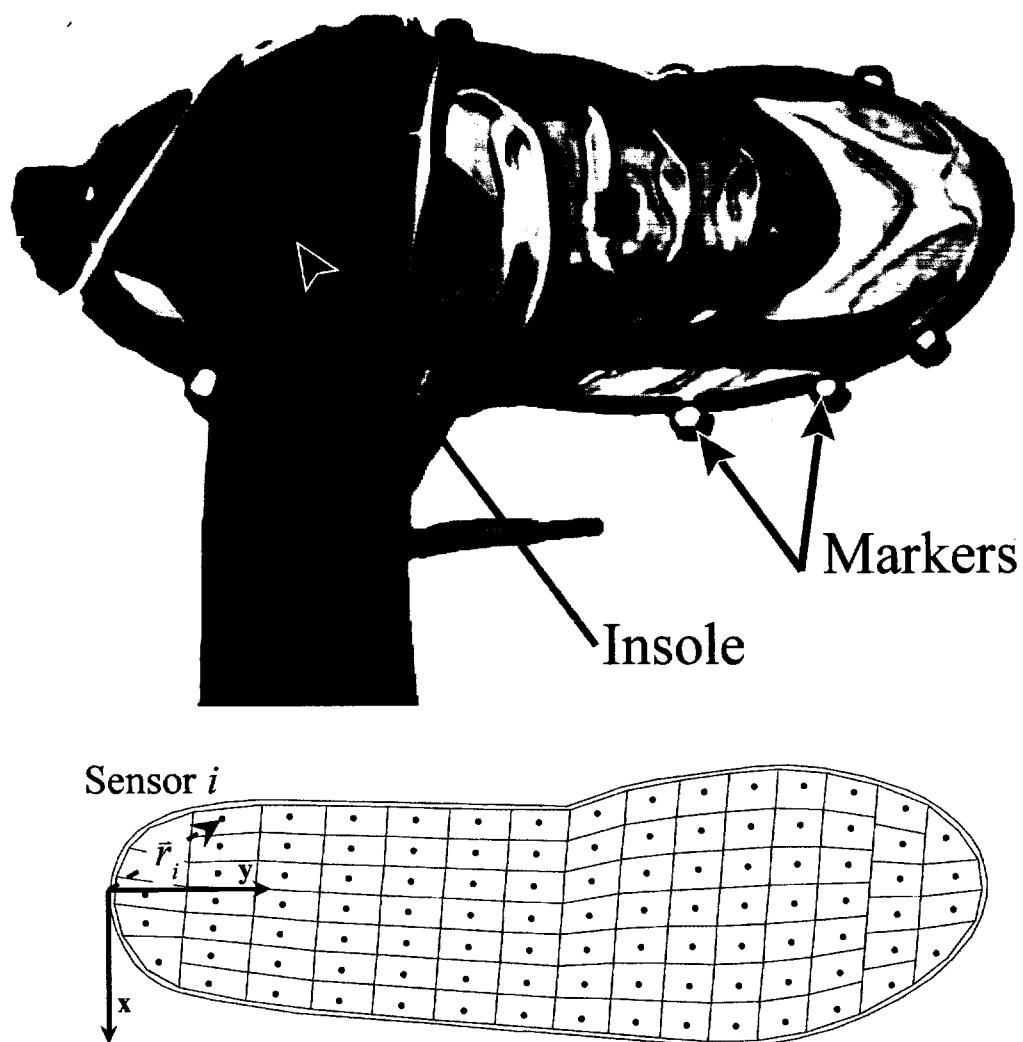
Figure 1.4. a) Ten markers (10 mm in diameter) were affixed around the periphery of each running shoe. b) The insole reference frame was positioned at the most posterior aspect of insole, with the y axis direction pointed towards the toe. The local position, $\vec{r}_i$, for each sensor was then defined as the centroid of the sensor in the insole reference frame.
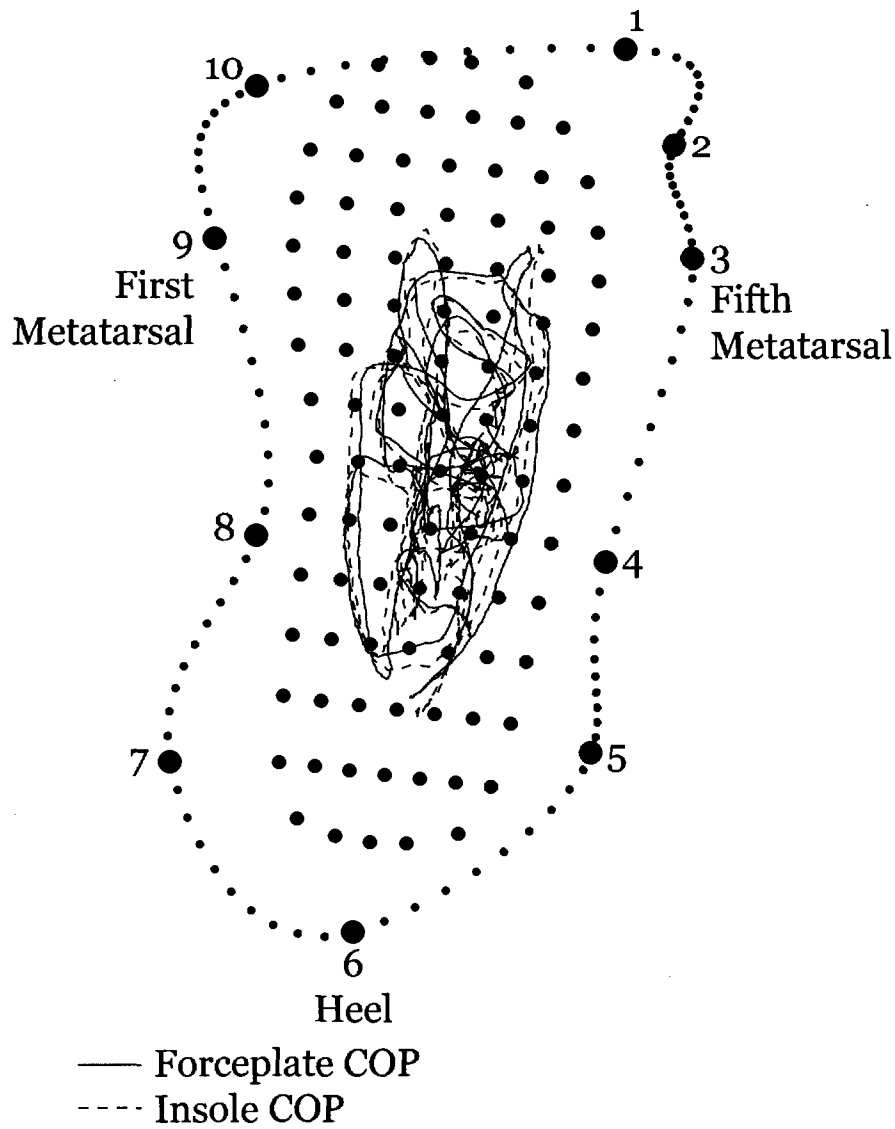
Figure 2.4. A piecewise cubic spline was used to define 100 virtual markers around the periphery of the shoe. To ensure continuity of the cubic splines, the 10 motion capture markers were always labeled consistently. An initial standing calibration trial was used to determine the sensor positions that maximized agreement between the insole and forceplate measured COP trajectories.

2.3 Insole sensor position calibration. The center of pressure information from the forceplate was used to calibrate the locations of the insole sensors in the upright stance trial. To do this, we first defined a local, undeformed insole reference frame (Figure 1.4). The centroid of each sensor, r_i, in the insole reference frame was then found using a scaled drawing of the insole provided by Novel, Inc. This information was used to express the local COP, p, as a function of the pressure recorded by each sensor, σ_i at a time frame k in the data set::

$$p(kT) = \frac{\sum_{k=1}^{N} \sigma_i(kT) r_i}{\sum_{k=1}^{N} \sigma_i(kT)}$$

(eq. 1)

Where T was the interval between data samples. We assumed that the foot remained flat on the ground and relatively stationary throughout the upright stance trial, such that a simple rotation matrix, **R**, could be used to describe the orientation of the insole reference frame relative to the global reference frame during the upright trial.

$$\mathbf{R} = \begin{bmatrix} \cos(\theta) & -\sin(\theta) & 0 \\ \sin(\theta) & \cos(\theta) & 0 \\ 0 & 0 & 1 \end{bmatrix}$$

(eq. 2)

Where θ was the axial rotation of the foot relative to a vertical axis, z. The COP could thus be transformed from the insole to global reference frame and compared to the center of pressure, p, recorded by the forceplates. We defined a cost function, J, as the sum of the squared differences in the center of pressure as estimated by the insole and measured by the forceplate:

$$J = \sum_{k=1}^{N} \left| \mathbf{R}\rho(kT) + \mathbf{d} - p(kT) \right|^2 \qquad \text{(eq. 3)}$$

For each subject, numerical optimization (*fminsearch*, Matlab, MathWorks, Inc., Natick, MA) was used to determine the rotation angle θ and translation $\mathbf{d}$ (vector between origins of global and insole reference frames), that minimized J. Transformation parameters were then directly used to define the global positions of each insole sensor, s_i^*, in the upright stance calibration trial:

$$s_i^* = \mathbf{R}\mathbf{r}_i + \mathbf{d} \qquad \text{(eq. 4)}$$

Insole sensor tracking. Affine transformations were used to map sensor positions from the calibration trial to a frame of a motion trial. This transformation was computed separately for each sensor by using virtual markers (cubic spline interpolated) close to each sensor (Figure 3.4). The position of the virtual markers closest to the sensor on the left and right sides were defined as vectors, $\mathbf{v}_1$ and $\mathbf{v}_2$, respectively. The weighted average of the next two closest virtual markers on the left and right sides was defined as vector,$\mathbf{v}_3$. A normal vector to the plane defined by these three markers was first taken as:

$$\mathbf{n} = (\mathbf{v}_2 - \mathbf{v}_1) \times (\mathbf{v}_3 - \mathbf{v}_1) \qquad \text{(eq. 5)}$$

After identifying the three closest markers for a sensor, we computed an affine transformation that mapped the vectors $\mathbf{v}_1, \mathbf{v}_2, \mathbf{v}_3$ and $\mathbf{n}$ from their values in the upright stance (denoted by *) trial to their measured values at each frame in a motion trial:

Calibration Trial

Forceplate and Insole
COP optimization
(R^*, d^*)
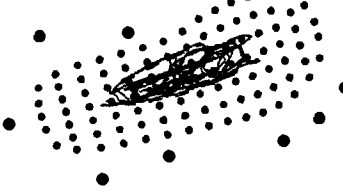
Cubic
Spline
Interp

100 Virtual Markers
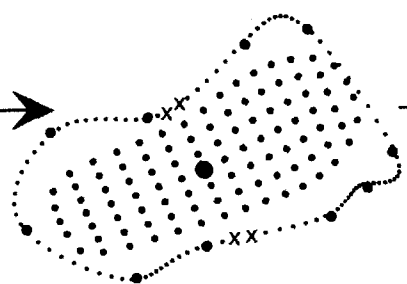
4 Closest
Virtual
Markers
(2R/2L)

Sensor i, Location relative
to 100 Virtual Markers

V_1

V_3

V_2
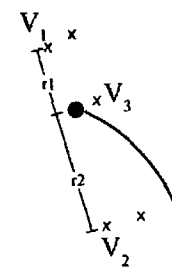
Sensors for Motion Trial
in Global Coordinates

Affine
Transformation
(A_i, d_i)
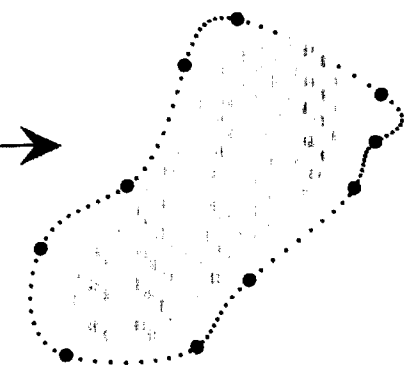
Motion Trial

10 Motion Capture
Markers
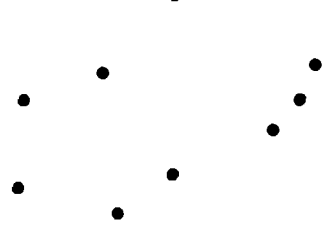
Cubic
Spline
Interp

100 Virtual Markers
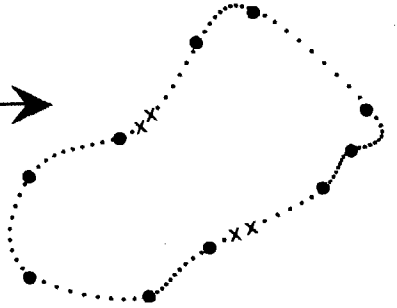
4 Virtual
Markers
from Cal

V_1

V_3

V_2
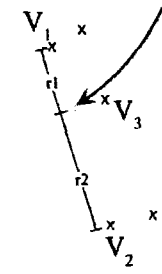
Figure 3.4. A graphical depiction of the sensor tracking algorithm is shown. Piecewise cubic spline interpolation is first used to define 100 virtual markers from the measured foot marker locations. Sensor positions in a calibration trial are first computed so as to maximize agreement between insole and forceplate center of pressure trajectories Sensor positions during locomotion are then resolved using four virtual markers in close proximity in the calibration trial: the closest markers to the sensor on the left and right sides are defined as v_1 and v_2, respectively, a weighted average of the next two closest marker is defined as v_3. These three virtual markers are then located in the frame of a locomotion trial. An affine transformation is then used to describe the translation, rotation and scaling of these three markers from the calibration trial to the current motion trial frame.

$$\mathbf{T}_i(kT) = \begin{bmatrix} \boldsymbol{v}_1 & \boldsymbol{v}_2 & \boldsymbol{v}_3 & \boldsymbol{v}_1 + \boldsymbol{n} \\ 1 & 1 & 1 & 1 \end{bmatrix}_{frame\,k} \begin{bmatrix} \boldsymbol{v}_1^* & \boldsymbol{v}_2^* & \boldsymbol{v}_3^* & \boldsymbol{v}_1^* + \boldsymbol{n}^* \\ 1 & 1 & 1 & 1 \end{bmatrix}_{calibration}^{-1} \qquad \text{(eq. 6)}$$

Where the transformation matrix $\mathbf{T}_i$ was defined as:

$$\mathbf{T}_i(kT) = \begin{bmatrix} \mathbf{A}_i(kT) & & & \mathbf{d}_i(kT) \\ 0 & 0 & 0 & 1 \end{bmatrix} \qquad \text{(eq. 7)}$$

$\mathbf{A}_i$ accounts for both scaling and rotation, and $\mathbf{d}_i$ accounts for translation. This transformation was then used to map the corresponding sensor's calibration position, s_i^*, to its global position, s_i, at a frame k in a motion trial.

$$s_i(kT) = \mathbf{A}_i(kT)s_i^* + \mathbf{d}_i(kT) \qquad \text{(eq. 8)}$$

Subsequently, the global COP was estimated from each of the sensor positions during the motion trials using the global position, s_i, and the pressure from each sensor.

$$p'(kT)_{insole} = \frac{\displaystyle\sum_{k=1}^{N} \sigma_i(kT)s_i}{\displaystyle\sum_{k=1}^{N} \sigma_i(kT)} \qquad \text{(eq. 9)}$$

Measured sensor pressures were scaled by the sensor cross-sectional areas to get the force associated with each sensor along the sensor's normal direction, $\boldsymbol{n}$. The component projected onto the vertical axis ($\boldsymbol{k}$) of this sensor force vector in the global reference frame provided an estimate of the net vertical ground reaction force, F_z', acting on the foot:

$$F_z'(kT)_{insole} = \sum_{k=1}^{N} a_i\sigma_i(kT)\boldsymbol{n} \cdot \boldsymbol{k} \qquad \text{(eq. 10)}$$

To evaluate the accuracy of the tracking algorithm, the insole-derived estimates of the COP and vertical force were compared to measures obtained from a fixed forceplate during walking and running.

Linked Segment Dynamic Model. We used a 19 segment dynamic, 31 degree of freedom (DOF) linked segment model to relate whole body kinematics to the net external forces acting on the body. The pelvis served as a 6 DOF base segment in the model. The lower limbs included a 3 DOF ball-and-socket hip, a single DOF knee in which non-sagittal rotations and translations were specified functions of the knee flexion angle (Walker et al. 1988), and a 2 DOF ankle which included the talocrural and subtalar joints (Delp et al. 1990). The upper body was attached to the pelvis by a 3 DOF ball-and-socket low-back joint at the L3-L4 level. Upper extremities included a 3 DOF ball-and-socket shoulder joints and single DOF joints for elbow flexion-extension and pronation-supination. The whole body dynamic model was created using SIMM (SIMM 4.0, Musculographics Inc.), and dynamical equations of motion were implemented using SIMM/Pipeline (v3.0) and SDFast (Parametric Technology Corporation, Waltham, MA). The whole body model was scaled to each subject based on segment lengths measured in an upright standing trial. Anthropometric properties were estimated using regression equations based on subject mass, height and segment lengths (de Leva 1996).

A global optimization inverse kinematics routine was initially used to estimate generalized coordinates (q') that optimally fit the measured marker positions (Lu and O'Connor 1999) at each frame in a trail. Generalized coordinates were subsequently low-

pass filtered at 6 Hz and then numerically differentiated to provide estimates of generalized speeds ($\dot{q}'$) and accelerations ($\ddot{q}'$).

Least Squares Forward Dynamics (LSFD). A least squares forward dynamic routine was used to compute shear forces that satisfied whole body dynamic constraints remaining optimally consistent with kinematic measures and available ground reaction data (Remy and Thelen 2008). To do this, we first formulated a set of six overall equations of motion that expressed the instantaneous relationship between external forces (F), external moments (M), and accelerations ($\ddot{q}$)

$$A(q) \begin{bmatrix} F \\ M \\ \ddot{q} \end{bmatrix} = f(q, \dot{q}) \qquad (\text{eq. 11})$$

given the current generalized coordinates (q) and generalized speeds ($\dot{q}$) of the model. In eq. (11), the matrix **A** contains information on segmental mass and geometry while **f** accounts for coriolis and centripetal effects. Direct substitution of kinematic measures ($q', \dot{q}', \ddot{q}'$) and insole-derived ground reactions ($F', M' = p' \times F'$) would not satisfy eq. (11) on account of missing shear force data and uncertainty in COP, vertical force and acceleration estimates. We thus introduced variations, δ, to the experimental measures:

$$\begin{bmatrix} F \\ M \\ \ddot{q} \end{bmatrix} = \begin{bmatrix} F' \\ M' \\ \ddot{q}' \end{bmatrix} + \begin{bmatrix} \delta F \\ \delta M \\ \delta \ddot{q} \end{bmatrix} \qquad (\text{eq. 12})$$

Substitution of (12) into (11) results in:

$$A(q) \begin{bmatrix} \delta F \\ \delta M \\ \delta \ddot{q} \end{bmatrix} = f(q, \dot{q}) - A(q) \begin{bmatrix} F' \\ M' \\ \ddot{q}' \end{bmatrix} \qquad (\text{eq. 13})$$

which can be cast as a set of underdetermined linear equations of the form:

$$\mathbf{A}\boldsymbol{\delta} = \mathbf{b} \qquad \text{(eq. 14)}$$

where $\boldsymbol{\delta}$ $(=[\delta F \quad \delta M \quad \delta \ddot{q}]^T$) is a set of variations to experimentally derived estimates of the ground reactions and accelerations that are needed to enforce dynamic consistency with the whole body dynamic model.

Eq. (14) was solved using the Moore-penrose matrix inverse, with a weighting matrix $\mathbf{W}$ to account for uncertainty in measured quantities:

$$\boldsymbol{\delta} = \mathbf{W}(\mathbf{A}\mathbf{W})^+\mathbf{b} \qquad \text{(eq. 15)}$$

In this study, we used a diagonal weighting matrix $\mathbf{W}$ and assumed standard deviations of 1-2 m·s^{-2} for translational generalized accelerations, 1-2 rad·s^{-2} for rotational generalized accelerations, 5% of the vertical force and 10 mm for the center of pressure. The unknown shear forces were given a large standard deviation (1% of the vertical force), since these quantities were not measured via the insoles. Computed accelerations were subsequently integrated forward to determine the simulated generalized coordinates and speeds over a trial, with numerical optimization used to find initial conditions that minimized the descrepancy between simulated and measured marker trajectories. LSFD was only used to process the running trials in this study. It could also be used to process the single phase of walking, but cannot decompose the left and right limb components of the shear force during double support without adding in additional assumptions.

Results

Insole Tracking. The insole tracking algorithm generated estimates for the vGRF and COP trajectories that were within 1 standard deviation of forceplate measures (Figure 4.4). Root mean square (RMS) differences in vGRF were <14% of peak vertical force (~40-80 N) for walking and <10% of peak vertical force (80-130 N) for running (Table 1.4). Medio-lateral COP RMS errors during mid-stance (between 10 and 80% of stance phase) were <8 mm during walking and running (Table 2.4). Anterio-posterior COP errors were less than 12 mm between 10 and 80% of stance phase. The largest error in the estimated COP occurred during heel contact and prior to toe off.

Table 1.4. Mean root mean squared (RMS) differences (±1 s.d.) between the forceplate vGRF and insole vGRF .

	Speed (m/s)	vGRF (N)					
		0-10 %Stance		10-80 %Stance		80-100 %Stance	
Slow Walk	1.0 (0.2)	65	(40)	40	(21)	87	(47)
Preferred Walk	1.4 (0.1)	62	(37)	38	(12)	73	(41)
Fast Walk	1.8 (0.2)	76	(46)	59	(28)	71	(34)
Preferred Run	3.1 (0.5)	95	(65)	91	(36)	101	(64)
Fast Run	5.0 (0.6)	127	(79)	92	(28)	109	(67)

vGRF (%Peak)					
0-10 %Stance		10-80 %Stance		80-100 %Stance	
9.2	(5.0)	7.0	(4.6)	13.3	(6.4)
9.0	(5.2)	5.2	(1.9)	11.3	(7.4)
8.6	(4.3)	6.8	(3.2)	8.4	(4.3)
5.8	(3.5)	5.6	(2.2)	6.4	(4.1)
7.5	(4.4)	5.4	(1.3)	6.8	(4.6)
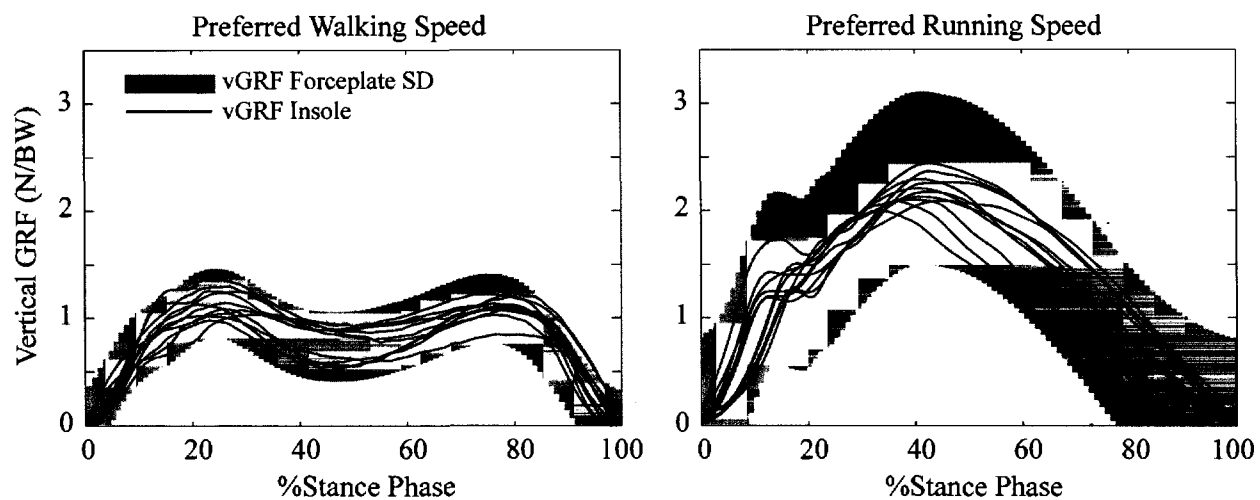
Figure 4.4. The agreement between net vertical force recorded by the insole and forceplate during a preferred walking and running trial. The shaded region is the mean ± one standard deviation of the forceplate recorded vGRF and the solid lines are the insole recorded vGRF.

Table 2.4. Mean root mean squared (RMS) differences (±1 s.d.) between the forceplate

and insole global position of the COP.

	Speed (m/s)	AP COP (mm)					
		0-10 %Stance		10-80 %Stance		80-100 %Stance	
Slow Walk	1.0 (0.2)	48.6	(12.3)	9.3	(3.9)	34.3	(11.7)
Preferred Walk	1.4 (0.1)	57.0	(14.9)	8.6	(2.5)	43.5	(21.1)
Fast Walk	1.8 (0.2)	57.0	(15.4)	11.6	(8.5)	38.0	(22.4)
Preferred Run	3.1 (0.5)	62.7	(17.6)	10.1	(5.7)	42.8	(13.4)
Fast Run	5.0 (0.6)	52.2	(25.2)	10.0	(5.4)	41.4	(9.2)

ML COP (mm)					
0-10 %Stance		10-80 %Stance		80-100 %Stance	
11.2	(3.8)	4.4	(2.5)	8.3	(4.0)
15.0	(6.1)	7.3	(7.6)	7.2	(6.0)
12.1	(3.6)	5.3	(2.8)	8.3	(4.5)
17.5	(10.7)	5.7	(5.0)	6.3	(4.2)
23.1	(8.2)	6.5	(4.2)	8.4	(4.3)

Least Squares Forward Dynamics (LSFD). Using the insole vGRF and COP estimates within the LSFD resulted in anterio-posterior shear force estimates that exhibited the characteristic braking and propulsion periods during stance (Figure 5.4). Average RMS errors for the anterior-posterior component were 52 N (8% body weight - BW) and 70 N (10% BW) for the preferred and fast running speeds, respectively. Average RMS errors for the medio-lateral force were 25 N (4% BW) and 42 N (6% BW) for these speeds (Table 3.4).
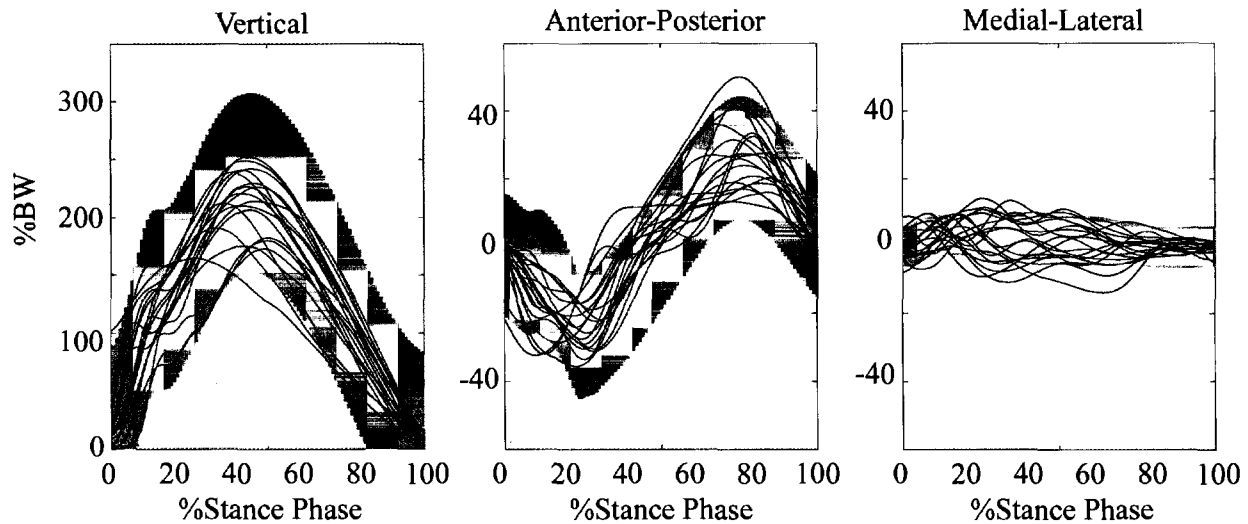
Figure 5.4. The agreement between the forceplate measured ground reactions and the computed ground reactions using the least squares forward dynamics for the preferred running trial (Note: only running was analyzed with the LSFD approach because of the lack of double support phase). The solid lines represent the LSFD computed GRFs and the shaded region is the forceplate GRFs mean ± one standard deviation (averaged over all subjects).

Table 3.4. Mean root mean squared (RMS) differences (± 1 s.d.) between the forceplate and computed ground reaction forces for the two running trials.

	Speed (m/s)	Ground Reactions (N)		
		Anterio-Posterior	Medio-Lateral	Vertical
Preferred Run	3.1 (0.5)	52.5 (25.6)	24.5 (14.5)	122.3 (63.3)
Fast Run	5.0 (0.6)	70.3 (30.8)	41.7 (16.4)	135.6 (69.4)

Discussion

We have demonstrated a novel approach for tracking insole sensors during locomotion, and then using insole pressure data together with a dynamic model, we were able to estimate shear forces. Such an approach can facilitate the use of insoles for characterizing joint kinetics during running on uninstrumented surfaces.

The use of an array of markers around the sole of the foot allowed us to track the position of insole sensors during walking. While we cannot independently verify the estimated sensor positions, the accuracy of the COP estimates derived from these data suggests that the sensor tracking was accurate. Indeed, our COP accuracy was comparable to measures made from insoles during upright standing (Fong et al. 2008; Forner-Cordero et al. 2006). A potential further use of the sensor position data is to develop and validate foot-floor contact models, which are typically represented by an array of discrete visco-elastic units distributed across the sole of the foot (Anderson and Pandy 2001; Gerritsen et al. 1995; Gilchrist and Winter 1996; Neptune et al. 2001; Neptune et al. 2000). Stiffness and damping parameters of the discrete units can be estimated from mechanical tests performed on the heel-pad and/or sole of the shoe (De Clercq et al. 1994). However, such testing is difficult and time-consuming to perform on a subject-specific basis; hence generic contact model parameters are often assumed. The methodology developed for this study could be used to systematically estimate appropriate parameters (of up to 99 separate elements) on a subject-specific basis and evaluate contact model predictions, to improve simulations of subject-specific gait dynamics.

In this study, we demonstrated that the insole data can be used within a whole body dynamics framework to estimate unmeasured components of the ground reaction forces. Whole body dynamic analysis uses whole body dynamic constraints to resolve inconsistencies between measured kinematics and ground reactions (Cahouet et al. 2002; Forner-Cordero et al. 2006; Kuo 1998; Remy and Thelen 2008; van den Bogert and Su 2008). Further, it is feasible to use least squares inverse dynamics to estimate unmeasured components of the ground reactions, with the independent estimates of the COP being important in the presence of noisy acceleration data (Kuo 1998). In this study, we used a least squares forward dynamics approach, which is more computationally intensive than LSID, but has the advantage of generating a forward dynamic simulation. LSFD also provides estimates of the joint moments, which we computed and found extremely comparable to those obtained using inverse dynamics with the forceplate data (Figure 6.4)
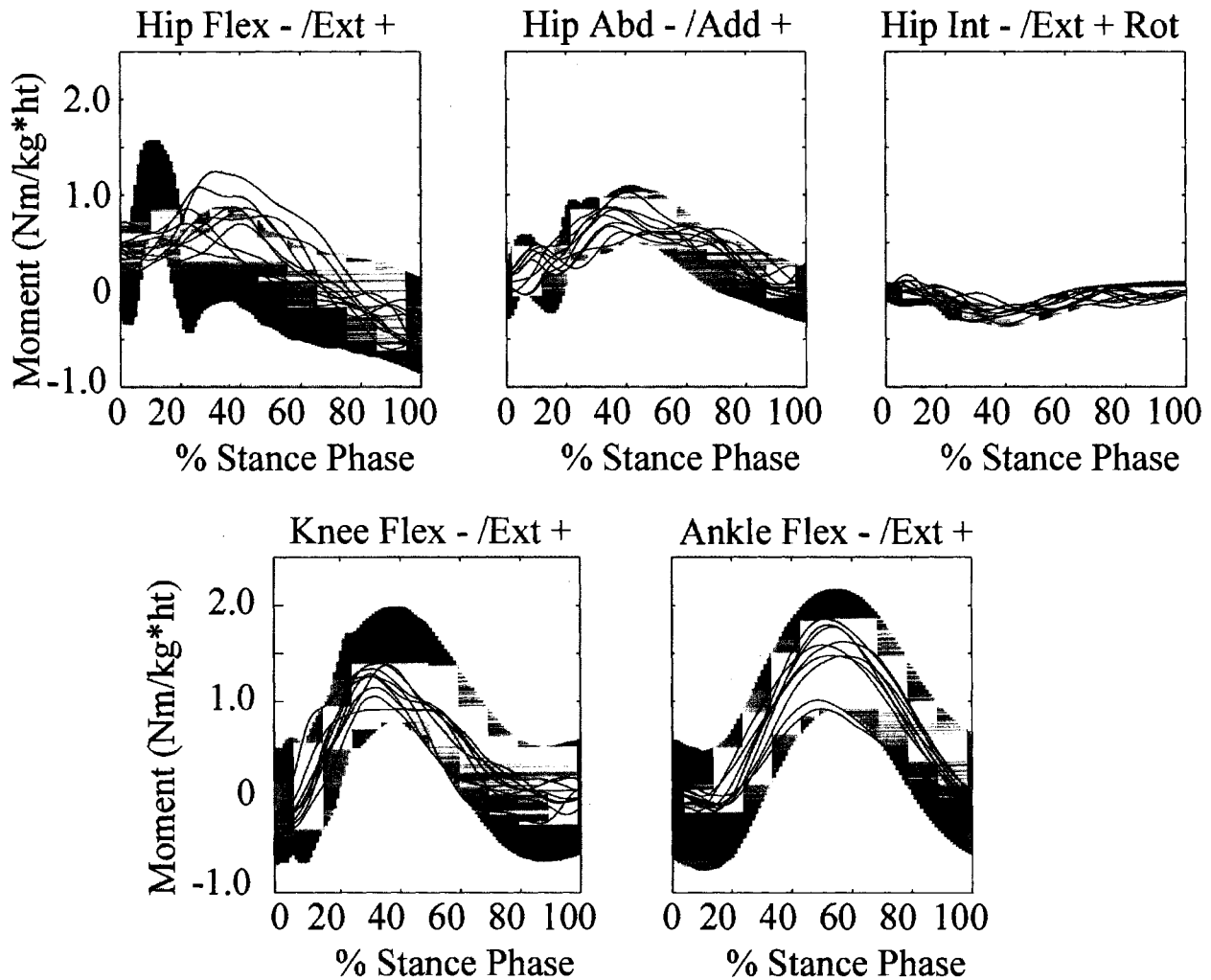
Figure 6.4. Joint moment comparison for the preferred running trial. The solid lines represent the joint moments using the LSFD computed ground reactions. The shaded region represents the mean ± one standard deviation of the joint moment (averaged over all subjects) computed from the forceplate GRF measures. The largest differences occur in the non-sagittal joint moments.

Limitations do exist when using insoles for characterizing biomechanical quantities. In particular, current insole pressure systems have substantially lower sample frequencies than forceplates. The insoles used in this study have a maximum sample frequency of 100 Hz when two insoles are sampled, however, the frequency could be doubled to 200 Hz for a single insole. In addition, the insole only records the pressure between the foot and shoe, which can differ from the pressure between the shoe and floor. This likely contributes to the lower accuracy in the COP during heel contact and prior to toe-off (Figure 7.4). Finally, we demonstrated the tracking algorithm using 10 motion capture markers around the periphery of the shoe. Additional markers could easily be added, which may improve the tracking accuracy, especially if the cubic splines on the shoe periphery near the heel and toe regions are improved (Figure 2.4). Finally, the least squares dynamics approach can only provide an estimate of the net external shear force, and thus is unable to resolve the independent components arising from the two feet during the double support phase of walking. Others have used additional assumptions to address this issue (Davis and Cavanagh 1993; Pandy and Berme 1988).

Walking

Running

100%
90%
80%
70%
60%
50%

40%

30%
20%

10%

0% Stance

100%

90%
80%
70%
60%

50%
40%

30%

20%

10%

0% Stance

━━━ Forceplate COP Trajectory
──── Insole COP Trajectory
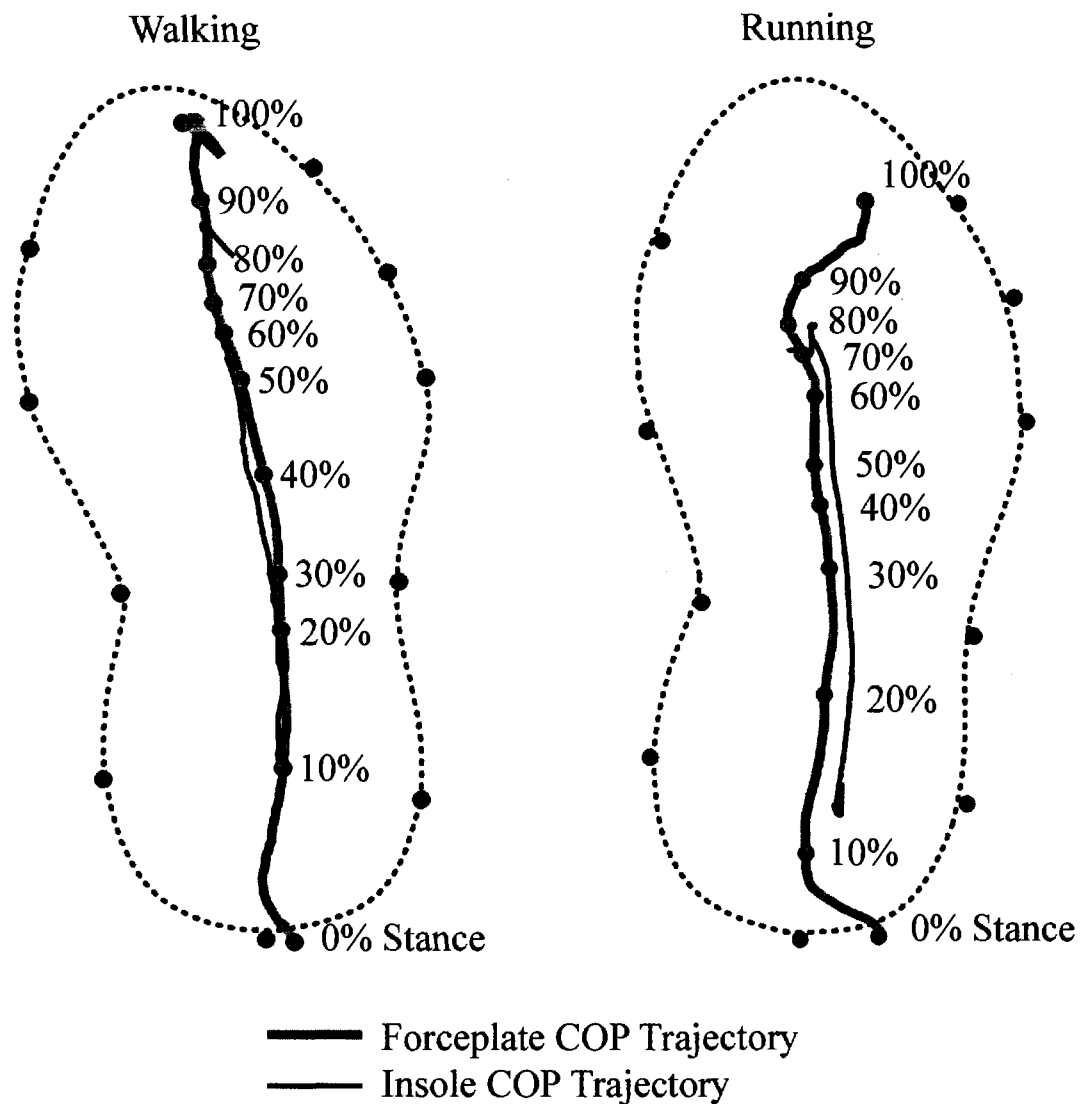
Figure 7.4. An example trial of the estimated COP trajectories for the preferred walking and running speeds. Good agreement is seen between the insole and forceplate data from 10 to 80% of the gait cycle. However, the insole COP during tends to be anterior to the forceplate COP during heel contact and then posterior to the forceplate COP approaching toe-off (the last 20% of stance).

In conclusion, we have demonstrated a simple and accurate approach for coupling motion capture with insole pressure data to dynamically track the global pressure distribution on the feet during human locomotion. This information, in conjunction with a least squares forward dynamics approach, provides for a viable approach to estimating joint kinetics when running on uninstrumented surfaces.

Acknowledgements

CHAPTER 5

Forward Dynamic Simulation of High Speed Running Gait

[1]Elizabeth S. Chumanov, [1]Bryan C. Heiderscheit, [1]Darryl G. Thelen

[1]University of Wisconsin-Madison, Madison, WI

Abstract

Hamstring strain injuries are common to sports that involve high speed running. In addition, there is disagreement whether the hamstrings are susceptible to injury during late swing phase when the hamstrings are active and lengthening or during stance when the contact loads are high, potentially overloading the hamstrings to cause injury. For this study we used forward dynamic simulations to predict hamstring musculotendon length, muscle force and negative work throughout the gait cycle. Whole body kinematics and ground reactions were collected as 11 athletes ran on a high speed treadmill at speeds ranging from 80% to maximal running speed. Fifty-two musculotendon actuators were included in the model and represented as a series of line segments connecting origin to insertion. A Hill-type model of musculotendon contraction dynamics was assumed. Computed muscle control determined the excitations necessary to drive the experimental hip and knee sagittal plane kinematics. Peak lateral hamstring force (biceps femoris) during swing phase exceeded peak stance phase forces at the fastest speed. Swing phase forces increased significantly with speed while stance phase forces remained consistent as speed increased. Net negative work was also performed solely during swing and increased significantly with speed. Other muscles such as rectus femoris and vastus lateralis did not show the same trend in forces and negative work, suggesting the hamstrings are uniquely susceptible to injury. It is our belief that the hamstrings are most likely susceptible to a strain injury during the late swing phase of high speed running.

Introduction

High speed running, i.e. sprinting, can place athletes at risk for an acute muscle strain injury (Gabbe 2005; Woods 2004). In particular, participants in track and field, football, soccer, and baseball are often troubled by hamstring strain injuries (Kujala et al. 1997; Seward et al. 1993). Clinically, hamstring strain injuries can be challenging to treat, due to the variable response of individuals to rehabilitation and the high occurrence of re-injury upon return to sport (Heiderscheit et al. in press). A better understanding of injury mechanisms could provide for a more scientific basis for designing effective rehabilitation and injury prevention strategies.

Animal models have provided insights into the relationship between mechanical measures and the degree of injury. In animal models, strain injury is associated with the magnitude of fiber strain and negative work (Brooks and Faulkner 2001; Lieber and Friden 1993; Lieber and Friden 2002), when a single maximal stretch is used to induce injury. When repeated cycles are used to induce injury, fiber strain has been shown to change over the repeated cycles possibly contributing to injury risk during a repetitive movement (Butterfield and Herzog 2005). For this study, we chose to characterize stretch and negative work during high speed running since these have been associated with injury in animal models

It has previously been shown that the hamstrings are active through late swing phase and into stance (Jonhagen et al. 1996; Swanson and Caldwell 2000; Wood 1987). However, the biarticular hamstring musculotendons are thought to lengthen only during swing and shorten throughout stance (Chumanov 2007; Thelen 2005). While hamstring

musculotendon stretch does not vary when speed is increased from 80% to 100% of maximum, (Thelen 2005), both the muscle force and negative work increase substantially during the late swing phase of the sprinting gait cycle (Chumanov 2007; van Don 1998; Wood 1987). It is plausible that these increased demands on the hamstrings place athletes at risk for a lengthening contraction injury during swing. Indeed, two studies have estimated the time of injury to be during late swing phase based upon case reports of different individuals sustaining an injury while instrumented (Heiderscheit et al. 2005; Schache et al. 2009). However, other researchers believe that contact loads during stance overload the hamstring and give rise to injury (Mann and Hagy 1980; Orchard and Best 2002). In addition, the possibility that the hamstrings may also lengthen during late stance may place the hamstrings at risk for injury at this time (Yu et al. 2008). In terms of speed, injury has been associated with maximal running speed in sports such as soccer, football and track and field (Gabbe 2005; Woods 2004).

The purpose of this study was to analyze hamstring mechanics throughout the sprinting gait cycle, in order to directly compare the stretch, loads and work between stance and swing. We hypothesized that the maximal force would occur during late swing phase and that negative work would be performed primarily during late swing. We tested the secondary hypothesis that increasing speed would increase the magnitudes of peak muscle force, as well as positive and negative musculotendon work. Finally, we also considered the relative biomechanical demands placed on major hip and knee muscles to better understand the greater propensity of strain injury to occur in the hamstrings.

Methods

Subjects. 11 athletes volunteered to participate in this study (Table 1.5). Males were required to have a maximal running speed of at least 7.6 m/s and females were required to reach 6.7 m/s to be included in this study. The average maximum speed for males was 8.0 m/s and was 7.0 m/s for females. All subjects had no prior surgical history in their lower extremity and had no lower extremity injury and/or pain in the three months prior to testing. The testing protocol was approved by the Institutional Review Boards and all subjects provided informed consent in accordance with institutional policies.

Table 1.5. Subject characteristics and maximum treadmill sprinting speed of the athletes who participated in this study.

	9Males / 2 Females
	Mean (s.d.)
Age, yrs	24.5 (4.1)
Height, cm	176.1 (5.0)
Body mass, kg	70.2 (8.8)
Max speed (m/s)	7.8 (0.5)

Experimental protocol. To record whole body kinematics, 42 reflective markers were placed on each subject; 23 of the markers were located on anatomical landmarks (Figure 1.5). In addition to the marker kinematics, subjects had electromyography (EMG) surface electrodes placed on muscles of the right lower limb: biceps femoris (BF), medial hamstrings (semitendinosus (ST) and semimembranosus (SM)), vastus lateralis, rectus femoris and gluteus medius. Each subject then ran at a preferred speed to warm up, prior

to sprinting at 80, 85, 90, 95, and 100% of his/her maximum speed, with a minimum of 5 strides (~5 seconds) collected at each speed. Two additional trials were collected: 1) a quiet standing position, to establish segment lengths, joint centers and joint coordinate systems, and 2) a hip circumduction movement (both right and left sides), to determine functional hip joint centers (Piazza et al. 2004).

Prescribed kinematics

Ground Reaction Forces

Hip / Knee kinematics

Excitations

Muscle forces

Simulated Kinematics

F^T

CE

F^T

F_0^M active passive $a=1.0$ F_0^M

ℓ_0^M $-v_{max}$ ε_0^T

$J = \sum_{i=1}^{num\ muscles} w_i \left(\dfrac{F_i^{CE}}{f_i(l_i^M)F_i^{max}} \right)$

Data collection   Computed Muscle Control   Musculotendon Dynamics   Simulation
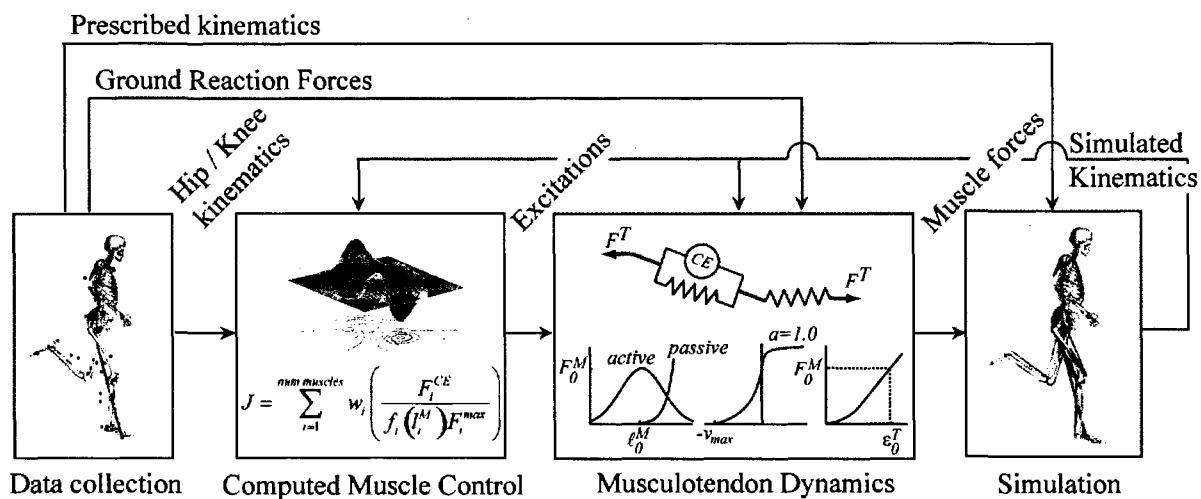
Figure 1.5. A graphical depiction of how the simulations were generated. A computed muscle control algorithm generated excitations that drove the model to closely replicate experimental kinematics. Excitations were the inputs into Hill-type models of musculotendon dynamics, which provided estimates of muscle force, length and power development. Ground reaction forces from the instrumented treadmill were used directly in the simulations, and degrees of freedom other than hip and knee flexion were prescribed to follow experimental trajectories.

Data acquisition. The three-dimensional kinematics were collected at 200 Hz using an 8-camera passive marker system (Motion Analysis Corporation, Santa Rosa, CA). Kinematic data were low pass filtered using a bidirectional, 4th order Butterworth filter with a cutoff frequency of 12 Hz.

EMG activities were recorded (synchronously with kinematics at 2000 Hz) using single differential, surface electrodes with a fixed interelectrode distance of 10 mm (DE-2.1, DelSys, Inc, Boston, MA). Each electrode pre-amplified the signal and was interfaced to an amplifier unit (Bagnoli-16, DelSys, Boston, MA; CMRR > 84 dB at 60 Hz; input impedance > 100 MΩ). The EMG signals were subsequently full-wave rectified and low pass filtered using a bidirectional, 6th order Butterworth filter with a cutoff frequency of 20 Hz.

Ground reactions were synchronously recorded at 2000 Hz using an instrumented treadmill (Bertec Corporation, Columbus, OH). Ground reactions were filtered using a bidirectional 3rd order, low pass Butterworth filter with a cutoff frequency of 25 Hz. A cutoff frequency of 25 Hz was necessary to remove low frequency oscillations present in the ground reactions recordings due to the treadmill design. Foot contact times were identified when the vertical ground reaction force exceeded 50 N.

Musculoskeletal model: The body was modeled as a 14 segment, 31 degree of freedom (DOF) articulated linkage (Figure 1.5). Anthropometric properties of body segments were scaled to each individual using the subject's height, mass, and segment lengths (de Leva 1996). The functional hip joint centers were used to scale the medio-lateral width of the pelvis. The hip joint was modeled as a ball and socket with three DOF. The knee

joint was represented as one DOF, in which the tibiofemoral translations and nonsagittal rotations were constrained functions of the knee flexion-extension angle (Walker et al. 1988). The ankle-subtalar complex was represented by two revolute joints aligned with anatomical axes (Delp et al. 1990). The low back was represented as a ball and socket joint at approximately the 3rd lumbar vertebra (Anderson and Pandy 1999). For each trial, joint angles were computed at each time step using a global optimization routine to minimize the sum of squared error between the measured and model marker positions (Lu and O'Connor 1999).

Musculotendon actuators were represented by a series of line segments connecting the origin to the insertion with wrapping about joints and other structures accounted for with wrapping surfaces (Arnold et al. 2000). The input to each musculotendon actuator was an idealized excitation level that varied between zero and one (full excitation). Muscle excitation-to-activation dynamics was represented by a first order differential equation that had a faster time constant during activation (10 ms) than deactivation (30 ms). A Hill-type lumped parameter model (Figure 1.5) of musculotendon contraction dynamics was employed, in which muscle fibers were assumed to be in series with an elastic tendon (Zajac 1989). Force produced by the musculotendon actuator was applied to the segment in which the tendon was attached. Passive joint torques (eq. 1) were included to account for uniarticular, passive-elastic structures at the hip, knee and ankle; defined as a function of the joint angle (q) and angular velocity (u) with parameters ($k_1,k_2,r_1,r_2,\phi_1,\phi_2,c$) taken from literature (Silder et al. 2007).

$$T = k_1 e^{r_1 \cdot (q - \phi_1)} + k_2 e^{r_2 \cdot (q - \phi_2)} - c \cdot u \qquad \text{(eq. 1)}$$

The equations of motion of the musculoskeletal model were derived using SDFast (Parametric Technology Corporation, Waltham, MA) and SIMM Pipeline (Musculographics Inc., Chicago, IL). Passive elastic torque parameters are given in the Appendix.

Forward dynamic simulations: We generated muscle-actuated forward dynamic simulations of sprinting to characterize hamstring stretch, force and work. A total of 52 musculotendon actuators (26 actuators on each limb) were used to actuate two DOF on each limb (hip flexion-extension, knee flexion-extension). Properties used for the musculotendon actuators can be found in the Appendix. All other DOF were prescribed to follow the measured kinematic trajectories, thereby accounting for inter-segmental dynamics (Zajac and Gordon 1989). Simulations were generated for a minimum of 5 strides for each subject and at each speed.

A computed muscle control (CMC) algorithm was used (Chumanov 2007; Thelen and Anderson 2006) to generate muscles excitations that drove the forward dynamic model to closely replicated experimental hip and knee kinematics. Muscle redundancy was resolved by using numerical optimization (eq. 2) to minimize the sum of the muscle volume-weighted normalized contractile element forces (Happee 1994).

$$J = \sum_{i=1}^{num\ muscles} w_i \left(\frac{F_i^{CE}}{f_i(l_i^M) F_i^{max}} \right) \qquad \text{(eq. 2)}$$

We added constraints on excitations during the second half of stance (no hamstring excitation from 20-40% gait cycle, and no rectus femoris excitation from 15-

35% gait cycle) to the optimization problem to ensure that hamstring and rectus femoris activity were consistent with the timing of measured EMG excitations.

Simulations were used to characterize the musculotendon stretch, force and power development of the biarticular hamstrings: BF, ST and SM. Musculotendon stretch was defined as the change in length from an upright posture. Upright musculotendon lengths were computed by setting all joint angles to zero in the subject-specific scaled model. The musculotendon power generated (absorbed) was computed as the product of the force and musculotendon velocity. The negative and positive musculotendon work was computed by integrating the respective negative and positive portions of the power curves.

Statistics: A two-way repeated measures analysis of variance was used to determine the effects of gait cycle phase and normalized speed (80, 85, 90, 95, and 100%) on the magnitude of peak force. A one-way repeated measures analysis of variance was used to determine the effect of normalized sprinting speed on musculotendon stretch along with negative and positive musculotendon work. The three biarticular hamstring works were added to obtain a measure of net negative and net positive work. Tukey's post hoc test was used to analyze significant main effects. The statistical analyses were completed using STATISTICA (version 6.0, StatSoft, Inc, Tulsa, OK, USA) with a significance level of 0.05 for all comparisons.

Results

Excitation patterns generated from the CMC algorithm were similar to measured EMG

signals (Figure 2.5) and produced simulations that closely tracked the experimental

kinematics. Root mean squared error (RMS) for the hip and knee flexion/extension

angles were 1.5 ± 0.5° for hip flexion-extension and 2.8 ± 0.8° for knee flexion-

extension when the hamstrings were active.
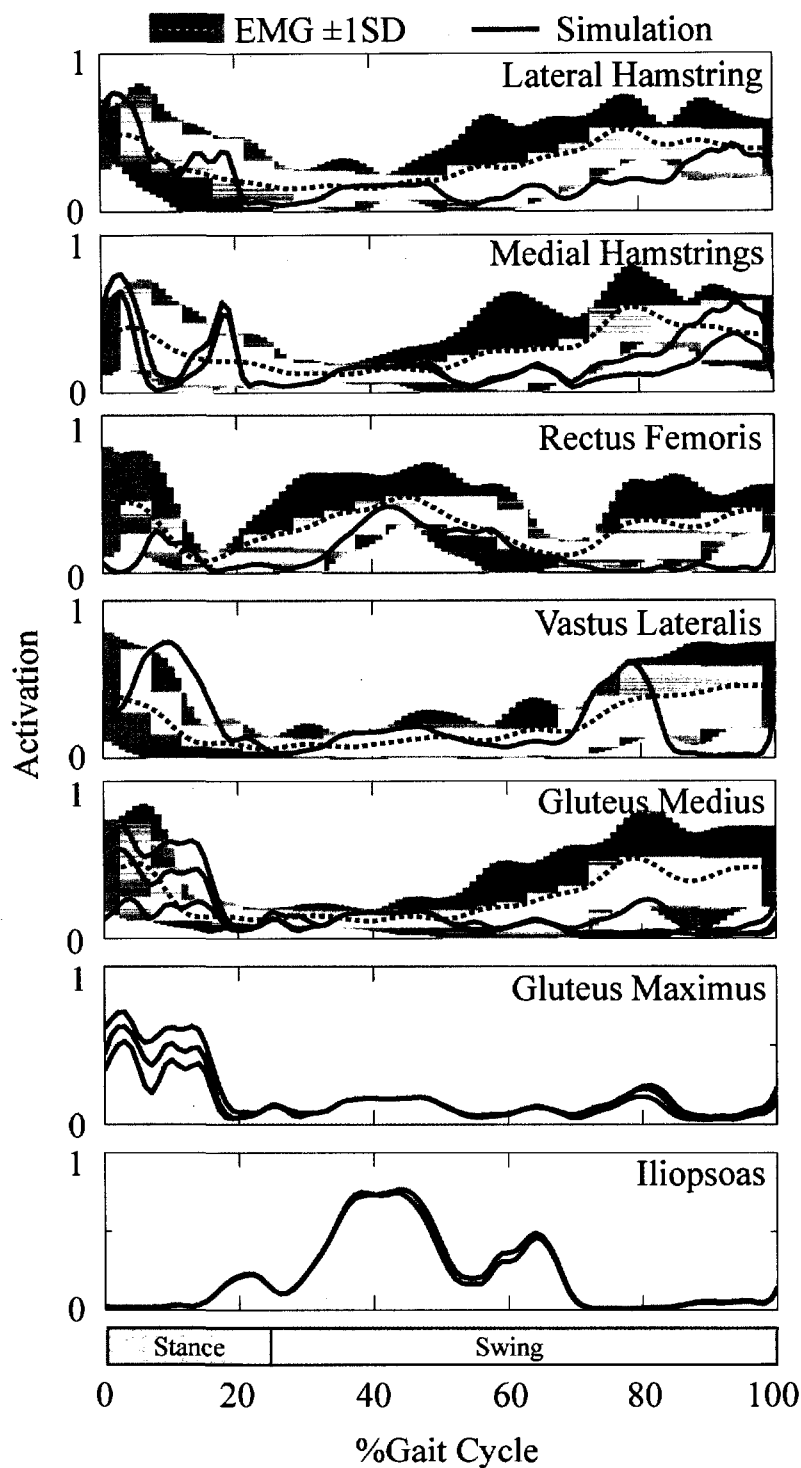
Figure 2.5. The timing of simulated muscle excitations (solid lines) and measured electromyographic (EMG) activities (shaded curves) are relatively consistent for the muscles shown. Simulated excitations are the ensemble average of the predicted excitations across all subjects at the maximum sprinting speed. EMG activities are the mean (±1 s.d.) rectified, low-pass filtered activities. Multiple simulated excitations are shown for the muscles represented by more than one line segment in the model.

The hamstring musculotendon units lengthened from approximately 50% to 90% of the gait cycle, with the negative work done primarily between 70 and 90% (Figure 3.5). Peak hamstring musculotendon stretch was independent of speed for all the hamstrings. The hamstrings shortened and did positive work from 90% of the gait cycle throughout the subsequent stance phase. A significant ($p<0.001$) speed by gait cycle phase interaction was present for work. Net negative and positive musculotendon work both increased significantly ($p<0.001$) with speed (Table 2.5); however, net negative work increased at a faster rate than positive work as speed increased (Figure 4.5).

Two distinct loading peaks were present for the hamstrings; one during late swing (between 85 and 95% of the gait cycle) and the second during early stance phase (between 0 and 15% of the gait cycle). A significant ($p<0.001$) speed by gait cycle phase interaction was present for peak hamstring force. Peak musculotendon force during swing increased significantly ($p<0.001$) with speed (Figure 3.5), while peak force during stance was independent of speed. Peak swing phase force at the fastest speed exceeded peak stance phase force for the BF long head and at all speeds the SM swing phase force exceeded the stance phase peak force. ST swing and stance peak forces were comparable in magnitude (Table 2.5; Figure 4.5).
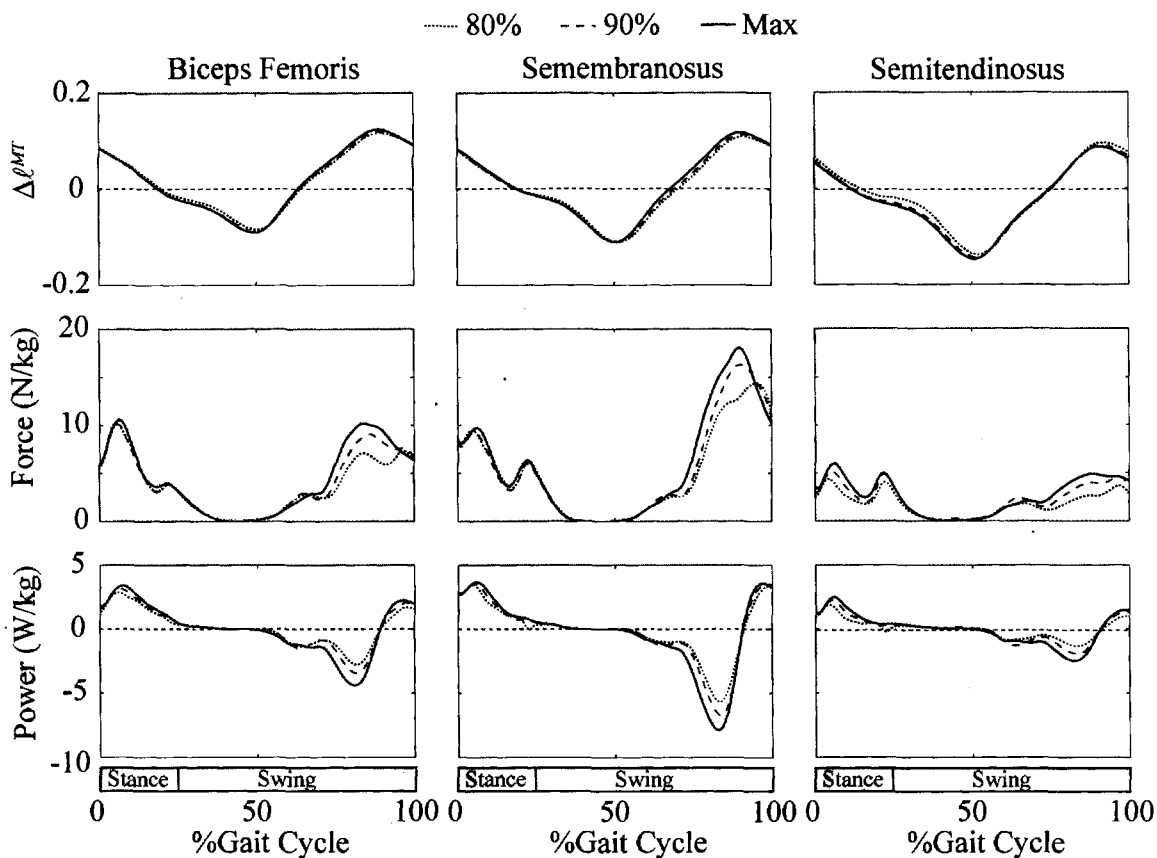
Figure 3.5. Ensemble averaged simulated musculotendon mechanics of the hamstring muscles. The musculotendon stretch is consistent across running speeds. Musculotendon lengthening is only seen during late stance phase. Peak swing phase musculotendon forces increase with speed for each of the hamstring muscles while stance phase peak forces remain consistent across a range of speeds. Negative work done by the musculotendon is confined to the swing phase. Positive work occurs during late swing and throughout stance phase.
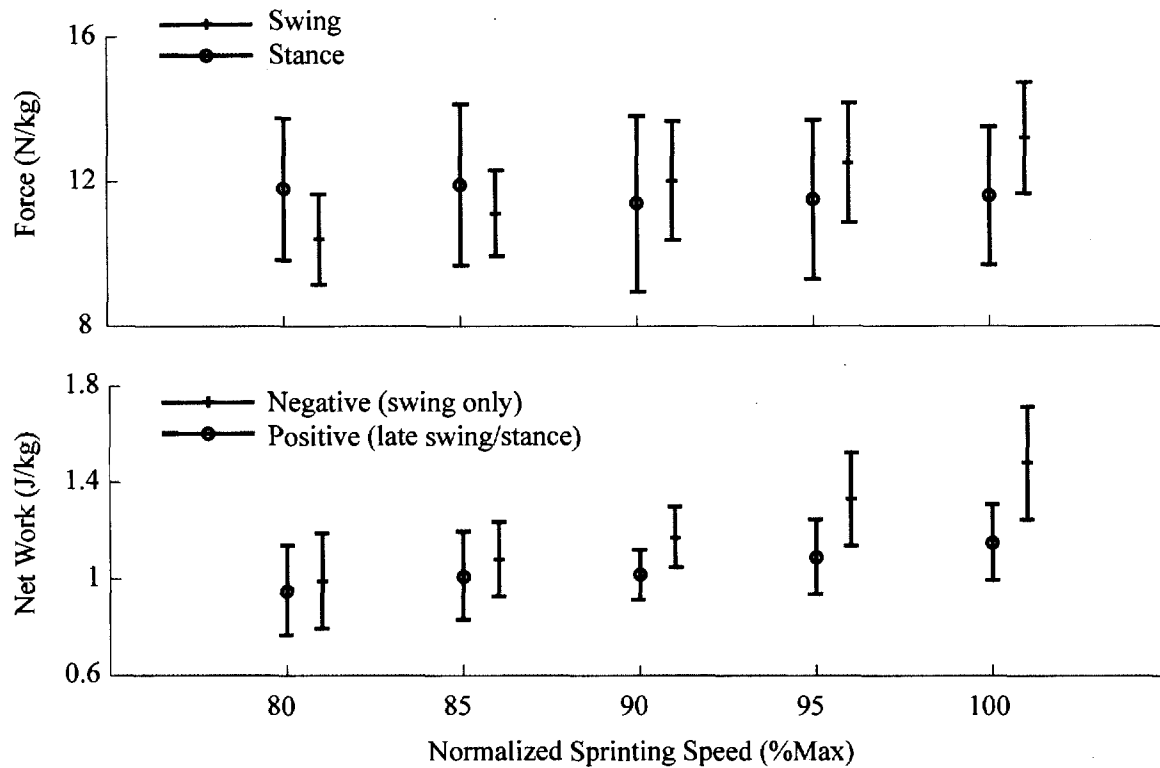
Figure 4.5. At the fastest speed, peak biceps femoris force during swing phase exceeds stance phase forces. Peak swing phase forces increase with running speed while stance phase forces remain consistent across a range of speeds. Both net negative work and positive work increase as running speed increases, with net negative work increasing at a faster rate with speed than net positive work. Net negative work is performed only during the swing phase of the gait cycle. Net work is the sum of all three biarticular hamstring work (negative and positive).

Table 2.5. Mean (s.d.) kinematic and kinetic measures from the hamstring muscles across all subjects. Peak musculotendon stretch (relative to a relaxed upright posture) remained consistent across running speeds. Peak biceps femoris (BF) length was greater than semimembranosus (SM) and semitendinosus (ST). Both the swing phase peak force and negative musculotendon work increased significantly with speed. Peak force during swing exceeded that of stance at the fastest speed for BF. The SM peak swing phase force exceeded stance phase force at all speeds, while stance and swing phase forces were comparable for the ST. $\Delta\ell^{MT}$ = peak musculotendon stretch normalized to an upright posture, F^{Max} = peak muscle force, W^{MT} = work done by the musculotendon unit.

Measure	Speed (% max)	BF		SM		ST	
Kinematic							
$\Delta \ell^{MT}$	80	1.12	(0.02)	1.11	(0.02)	1.10	(0.02)
(% upright)	85	1.12	(0.02)	1.11	(0.02)	1.10	(0.02)
	90	1.12	(0.02)	1.11	(0.02)	1.10	(0.02)
	95	1.13	(0.02)	1.11	(0.02)	1.11	(0.02)
	100	1.13	(0.02)	1.11	(0.03)	1.10	(0.03)
Stance Phase Loading							
$^2F^{Max}(N/kg)$	80	11.8	(1.9)	12.5	(3.2)	5.5	(2.1)
	85	11.9	(2.2)	12.2	(2.7)	5.7	(2.1)
	90	11.4	(2.4)	11.9	(2.4)	6.0	(2.1)
	95	11.5	(2.2)	11.9	(2.3)	5.8	(1.9)
	100	11.6	(1.9)	12.1	(2.4)	6.2	(2.2)
Swing Phase Loading							
$^{1,2}F^{Max}(N/kg)$	80	10.4	(1.2)	18.6	(2.2)	4.8	(1.3)
	85	11.1	(1.2)	19.9	(2.8)	5.2	(1.6)
	90	12.0	(1.6)	21.8	(3.6)	5.3	(1.5)
	95	12.5	(1.6)	23.0	(3.8)	5.3	(1.4)
	100	13.2	(1.5)	23.9	(3.5)	5.9	(1.9)
Positive Work							
$^1W^{MT}(J/kg)$	80	0.36	(0.06)	0.42	(0.08)	0.18	(0.05)
	85	0.37	(0.06)	0.43	(0.08)	0.21	(0.05)
	90	0.38	(0.05)	0.43	(0.05)	0.22	(0.03)
	95	0.40	(0.06)	0.45	(0.07)	0.24	(0.05)
	100	0.43	(0.06)	0.47	(0.08)	0.26	(0.04)
Negative Work							
$^1W^{MT}(J/kg)$	80	0.31	(0.09)	0.48	(0.09)	0.19	(0.04)
	85	0.33	(0.07)	0.51	(0.05)	0.23	(0.06)
	90	0.36	(0.05)	0.56	(0.05)	0.25	(0.05)
	95	0.41	(0.07)	0.63	(0.10)	0.28	(0.05)
	100	0.46	(0.09)	0.69	(0.10)	0.35	(0.06)

[1] Significant speed effects

[2] Significant speed by gait cycle interaction

Discussion

In this study, we extended our prior analysis of sprinting hamstring mechanics during swing (Chumanov 2007; Thelen 2005; Thelen 2006) to stance phase, thereby providing insights into when the hamstrings seem most susceptible to injury. We show that hamstring loading increases with speed during swing but not stance, and further that peak stretch and negative work demands occur exclusively during swing. These data lend further evidence to the belief that the inertial loads associated with high speed sprinting put the hamstrings at risk for injury (Chumanov 2007; Heiderscheit et al. 2005; Schache et al. 2009).

Characterizing injury risk using joint level analysis (Kuitunen et al. 2002; Mann 1981; Swanson and Caldwell 2000) is challenging due to the biarticular nature of the hamstrings For instance hip and knee angles change significantly with speed at the time of peak hamstring stretch (Kuitunen et al. 2002; Thelen 2005), while peak hamstring stretch is actually independent of speed. Joint moments and powers during late swing phase also increase with speed (Kuitunen et al. 2002) but how the hip and knee moments and powers combine, and their relationship to hamstrings force and power, is not straightforward (Figure 5.5).
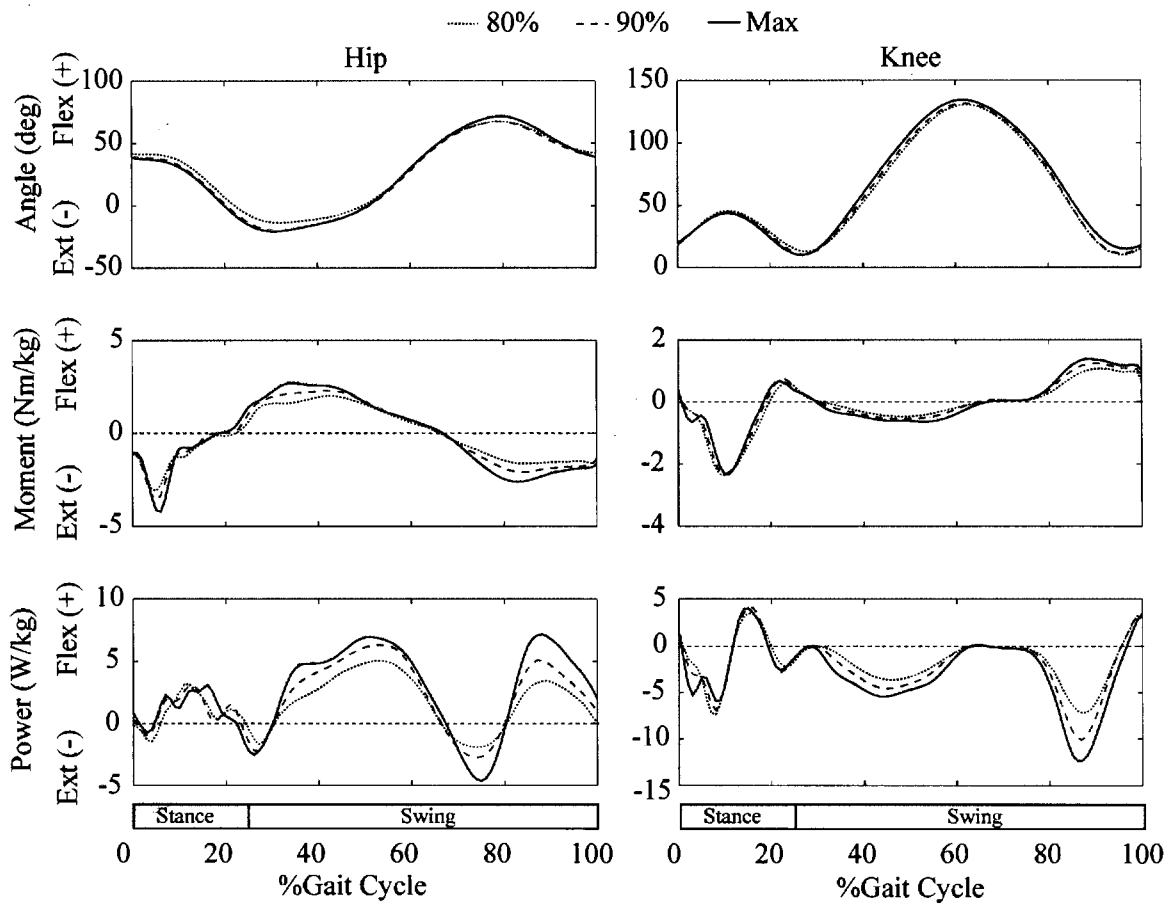
Figure 5.5. Hip and knee joint angles, moments and powers throughout the sprinting gait cycle.

Our results suggest that the hamstring musculotendons are substantially loaded during both the stance and swing phases of high speed running. However, we only found that the hamstrings undergo a lengthening contraction during late swing phase and thus negative work is constrained only to this phase. In contrast to Yu, et al. (2008) we did not find that the hamstrings underwent a lengthening contraction during the late stance phase at the musculotendon level. We do note that it is possible that the muscle fibers can lengthen while the musculotendon unit is shortening (Fukunaga et al. 2002). Such a scenario could occur during late stance if the tendon shortening were to exceed the musculotendon shortening, which would result in the muscle fibers lengthening. However from our simulations we also have estimates for tendon and muscle lengths and did not observe the muscle fiber component to be lengthening during stance.

In animal models of muscle injury, active lengthening contractions are linked with injury (Lieber and Friden 2002) and the degree of injury is associated with the magnitude of negative work done by a maximally activated muscle (Brooks and Faulkner 2001). At maximal running speed we find that both the loading of the hamstrings and the negative work done by the muscle has increased, thus it is plausible that the hamstrings are susceptible to an acute muscle strain injury at this time. When a physiological range of motion is used to induce injury in animal models repeated stretch shortening cycles are needed to cause injury (Butterfield and Herzog 2005). It is possible that not only maximal speed places individuals at risk for injury, but also repeated strides at this high level of force and negative work.

It is interesting to use the simulations to consider why the hamstrings are uniquely susceptible to injury relative to other muscles about the hip and knee. For example in Australian rules football, hamstring strains were shown to outnumber quadriceps strains almost five to one (Orchard 2001). In our simulations (Figure 6.5), the vastus lateralis are loaded and do a significant amount of negative work during stance, though the stretch incurred by this muscle during stance is much less than is seen during swing. The iliopsoas does substantial negative work during late stance through early swing, but peak loading seems to occur after the muscle has started to shorten. The rectus femoris exhibits biomechanical patterns that are somewhat reciprocal to the hamstrings, with high load, negative work and peak stretch all peaking at ~50% of the gait cycle. However unlike the hamstrings, the negative rectus femoris work does not exhibit as much speed dependence. Hence, our biomechanical analyses suggest that the hamstrings are more predisposed to injury due to unique mechanical demands placed on them at maximal running speeds.
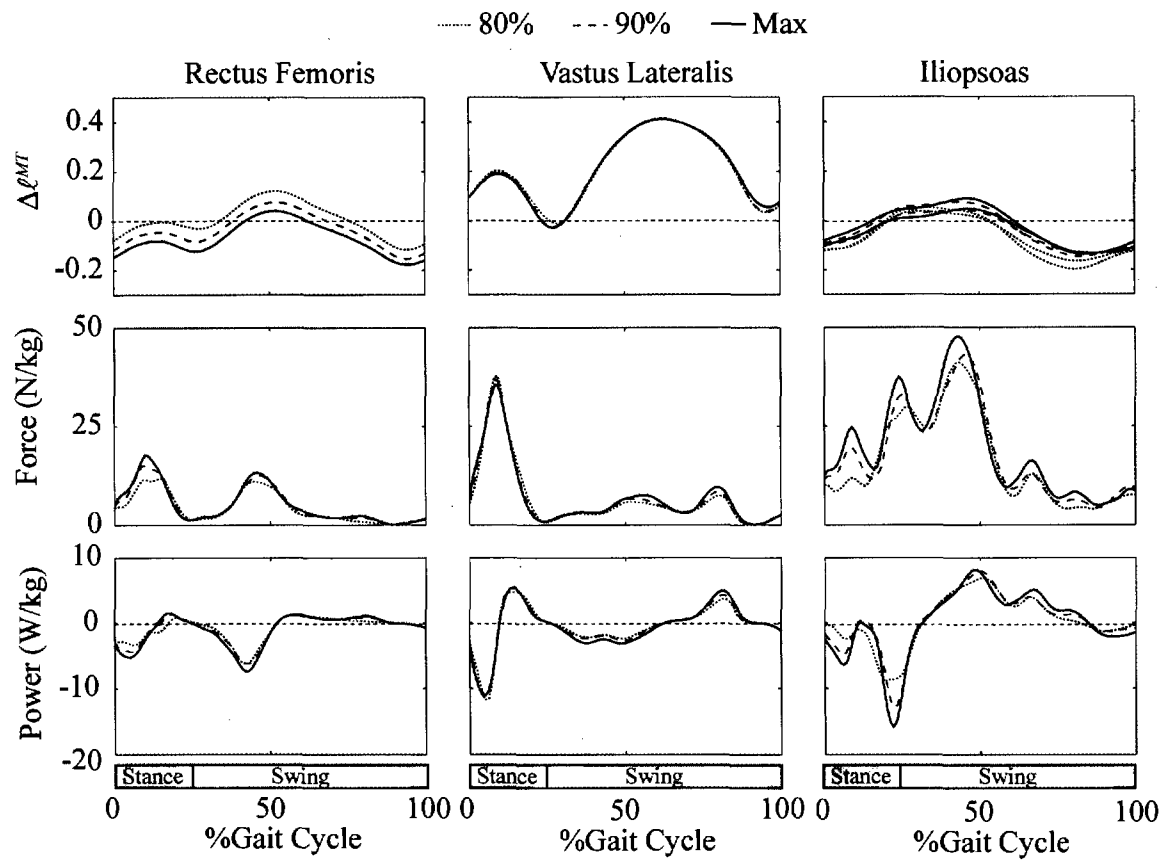
Figure 6.5. Ensemble averaged simulated musculotendon mechanics of rectus femoris, vastus lateralis and the iliopsoas.

When using musculoskeletal forward dynamic models, there are a number of assumptions that are important when interpreting the results. First, we relied on literature-derived estimates for parameters such as maximum isometric force, optimum fiber length, and tendon compliance (Appendix). As a result, there is a degree of uncertainty in the absolute accuracy of our force, length and work measures. For this reason, we chose to limit our dependence on model parameters by only considering speed and gait cycle-dependent changes in musculotendon measures (rather than individual muscle and tendon component measures) to evaluate our primary hypotheses. In addition, our distribution of power between the hamstrings muscles may be inaccurate, thus we have chosen to report the combined work to use in the analyses, even though individual negative work quantities for each muscle show similar results. As imaging technology improves (Fukunaga et al. 2002), it may be possible to eventually incorporate subject specific musculotendon mechanics (e.g. tendon stiffness) into our model thus improving the accuracy of our measures.

In conclusion, we believe that the hamstrings are at greatest risk for injury during the late swing phase of sprinting since the biomechanical demands placed on the hamstrings are consistent with acute musculotendon injury mechanisms.

Acknowledgements

CHAPTER 6: CONCLUSIONS AND RECOMENDATIONS

The aims for this thesis were to 1) Investigate how hamstring musculotendon mechanics during swing phase vary with treadmill sprinting speed. 2) Investigate how individual muscles, particularly those surrounding the pelvis and back (i.e. the "core"), could influence hamstring stretch during sprinting. 3) Develop a least squares forward dynamics methodology for analyzing joint kinetics during running on an un-instrumented treadmill. 4) Systematically compare biomechanical demands between stance and swing phase of the sprinting gait cycle to better understand potential injury mechanisms.

Contributions. Three major advances were made in the area of biomechanical analysis methods when completing the research for this thesis. The first major advance was that a tracking algorithm in conjunction with a least squares approach enables the use of pressure sensitive insoles on un-instrumented surfaces to obtain ground reaction force information. Secondly, forward dynamic simulations were implemented to estimate musculotendon dynamics during a high-speed dynamic movement. Information on musculotendon dynamics was then used to infer injury risk and this approach could conceivably be used to characterize other patterns of movement and investigate other types of muscle injury mechanisms. Lastly, the influence of neuromuscular coordination muscle stretch was assessed. Through the understanding of the neuromuscular coordination of multi-joint movement this study adds to the knowledge of why specific rehabilitation programs maybe successful at reducing hamstring re-injury risk (Sherry and Best 2004).

Insights into hamstring injury mechanisms. In terms of injury, swing phase appears to be the most likely time for injury to occur for several reasons. Firstly the hamstrings are active and undergoing a lengthening contraction (Chumanov 2007; Jonhagen et al. 1996; Swanson and Caldwell 2000; Thelen 2005; Wood 1987) and lengthening contractions in animal models have been shown to cause muscle damage (Lieber 1992). Secondly, force in swing is increased as gait speed is increased, while stance phase forces tend to remain consistent across a range of speeds. Negative work (i.e. the muscle is acting to absorb energy) also increases significantly during swing phase, which has also been linked with injury in animal models (Brooks and Faulkner 1996). Additional support for the assertion that swing phase is the likely of time of injury also comes from two recent studies (Heiderscheit et al. 2005; Schache et al. 2009) that happened to be collecting data while an athlete (fully instrumented) sustained an injury to their hamstrings both pointing to late swing phase as the likely time for injury.

The most frequently injured hamstring is the biceps femoris; (De Smet and Best 2000; Garrett et al. 1989; Koulouris and Connell 2003) and it was found that the biceps femoris long head was stretched more than the semitendinosus and the semimembranosus which is consistent with the injury rate discrepancy between the hamstrings. It is important to note that this results from subtleties in knee moment arm differences between the three biarticular hamstrings and could not be predicted from a two dimensional model or joint level analyses alone.

Neuromuscular coordination also plays a crucial role in hamstring injury risk since it was found that the lumbo-pelvic muscles exhibited a large influence on hamstring

stretch, especially the contralateral iliopsoas. Muscles surrounding the pelvis and low back that act to increase anterior pelvic tilt tend to cause additional hamstring stretch, since the hamstring originate at the ischial tuberosity.

In addition to neuromuscular coordination, this study also examined why the hamstrings are uniquely predisposed to injury during running. In contrast, to other muscles (i.e. rectus femoris) which are also susceptible to acute strain injuries, albeit to a lesser extent (Orchard 2001), the hamstrings show a distinct speed dependence on negative work. This negative work is also performed when loading reaches a peak and the hamstrings are lengthened. Since injury most often occurs at maximal running speeds (Gabbe 2005; Woods 2004) all these factors combined put the hamstrings at additional risk during high speed running when compared to the other musculature of the lower extremity.

Implications for muscle injury prevention and rehabilitation. Hamstring re-injuries still remain problematic despite recent evidence that rehabilitation programs aimed at early movement and neuromuscular control show dramatic reduction in re-injury rates (Sherry and Best 2004). The finding that the lumbo-pelvic muscles have substantial influence on hamstring stretch lends support that neuromuscular coordination is crucial in re-injury reduction. Other studies have suggested that after an initial injury there is a change in optimal length for force production of the hamstrings (Brockett et al. 2004; Proske et al. 2004) and thus have promoted the use of lengthening contractions to reduce re-injury rates (Proske et al. 2004). Using this type of research to understand the basic hamstring

mechanics during running gait imparts credibility to the development of rehabilitation or prevention programs that target specific aspects of hamstring mechanical behavior. In the future, training regimes with an intense focus on improving hamstring function by utilizing lengthening contractions and neuromuscular coordination may dramatically reduce re-injury rates. With the development of subject-specific modeling it may one day be possible to develop tailored rehabilitation programs that address each individual's maladaptive mechanics.

Future research. As imaging technology improves it may be possible to incorporate subject-specific parameters into the model rather than relying on literature derived estimates for muscle parameters such as maximum isometric force, optimal fiber length, tendon compliance, etc. Developing subject-specific models is important because it increases the absolute accuracy of the results (i.e. the simulation closer represents the physiology) by incorporating individual biological variation. For instance, age has been associated with an increase in hamstring injury risk (Orchard 2001), it may be possible that age-related changes in tendon compliance (Blevins et al. 1994; Lewis and Shaw 1997) may place the hamstrings at additional risk. A subject-specific model could also be of great benefit to a therapist since they would be able to get information that would not be readily available by simply examining the patient as they perform a task.

The musculotendon actuators present in the model, currently only actuate a limited number of degrees of freedom. As the three dimensional imaging of muscle improves along with computational processing speed, the way individual muscles are

modeled can eventually move away from the current approach of a line connecting origin to insertion. Additional degrees of freedom that are muscle actuated can then be added with greater confidence to answer questions such as how gender differences in non-sagittal kinematics might arise (Chumanov et al. 2008).

Exactly how these results translate to an athlete performing high speed running overground is unclear, but it is important to considered when interpreting the results. It is likely that the same trends in force and negative work are present; however, the subjects in this study were not fatigued. It is likely that fatigue may play a substantial role in hamstring injury risk because neuromuscular coordination may be compromised (Derrick et al. 2002; Miller et al. 2007) and fatigue has been linked with running related injuries (Bradley et al. 2002; Gabbett 2004). For future research, it may be relevant to investigate how fatigue plays a role in neuromuscular coordination and subsequently hamstring injury risk.

In conclusion, this thesis used a modeling approach to gain insights into how muscles behave during dynamic movement. As technology continually improves it may be possible one day to fully instrument a runner and obtain real time measures of muscle forces and powers, *in vivo*, without the need for modeling. However until then, the insights gained from this type of research can serve as a guide for developing evidenced-based rehabilitation programs and targeted injury prevention strategies.

REFERENCES

1. Ahroni, J. H., E. J. Boyko, et al. (1998). "Reliability of F-Scan in-shoe measurement of plantar pressure." *Foot and Ankle International* 19(10): 668-673.

2. Anderson, F. C. and M. G. Pandy (1999). "A dynamic optimization solution for vertical jumping in three dimensions." *Computer Methods in Biomechanics and Biomedical Engineering* 2: 201-231.

3. Anderson, F. C. and M. G. Pandy (2001). "Dynamic optimization of human walking." *Journal of Biomechanical Engineering* 123: 381-390.

4. Arnold, A. S., S. Salinas, et al. (2000). "Accuracy of muscle moment arms estimated from MRI-based musculoskeletal models of the lower extremity." *Computer Aided Surgery* 5(2): 108-19.

5. Asakawa, D. S., G. P. Pappas, et al. (2003). "Cine phase-contrast magnetic resonance imaging as a tool for quantification of skeletal muscle motion." *Seminars in Musculoskeletal Radiology* 7(4): 287-95.

6. Barnett, S., J. L. Cunningham, et al. (2000). "A Comparison of vertical force and temporal parameters produced by an in-shoe pressure measuring system and a force platform." *Clinical Biomechanics* 15: 781-785.

7. Best, T., J. McElhaney, et al. (1995). "Axial strain measurements in skeletal muscle at various strain rates." *Journal of Biomechanical Engineering* 117(3): 262-265.

8. Blevins, F., A. Hecker, et al. (1994). "The effects of donor age ans strain rate on the biomechanical properties of bone-patellar tendon-bone allografts." *American Journal of Sports Medicine* 22: 328-333.

9. Bradley, J. P., J. J. Klimkiewicz, et al. (2002). "Anterior cruciate ligament injuries in the National Football League: epidemiology and current treatment trends among team physicians." *Arthroscopy* 18: 502-509.

10. Brockett, C. L., D. L. Morgan, et al. (2004). "Predicting hamstring strain injury in elite athletes." *Medicine and Science in Sports and Exercise* 36(3): 379-87.

11. Brooks, S. V. and J. A. Faulkner (1996). "The magnitude of the initial injury induced by stretches of maximally activated muscle fibres of mice and rats increases in old age." *Journal of Physiology* 497 (Pt 2): 573-80.

12. Brooks, S. V. and J. A. Faulkner (2001). "Severity of contraction-induced injury is affected by velocity only during stretches of large strain." *Journal of Applied Physiology* 91(2): 661-6.

13. Brooks, S. V., E. Zerba, et al. (1995). "Injury to muscle fibres after single stretches of passive and maximally stimulated muscles in mice." *Journal of Physiology* 488: 459-69.

14. Buford, W., F. Martey Ivey, et al. (1997). "Muscle balance at the knee - moment arms for the normal knee and the ACL-minus knee." *IEEE Transactions on Rehabilitation Engineering* 5: 367-379.

15. Butterfield, T. A. and W. Herzog (2005). "Quantification of muscle fiber strain during in-vivo repetitive stretch-shortening cycles." *Journal of Applied Physiology* 99: 593-602.

16. Cahouet, V., M. Luc, et al. (2002). "Static optimal estimation of joint accelerations for inverse dynamics problem solution." *Journal of Biomechanics* 35(11): 1507-1513.

17. Cavanagh, P. R. and T. M. Owings (2006). "Nonsurgical strategies for healing and preventing recurrence of diabetic foot ulcers." *Foot and Ankle International* 11: 735-743.

18. Chapman, A. and G. Caldwell (1983). "Kinetic limitations of maximal sprinting speed." *Journal of Biomechanics* 16(1): 79-83.

19. Chesnin, K. J., L. Selby-Silverstein, et al. (2000). "Comparison of an in-shoe pressure measurement device to a force plate: concurrent validity of center of pressure measurements." *Gait and Posture* 12: 128-133.

20. Chumanov, E., C. Wall-Scheffler, et al. (2008). "Gender differences in walking and running on level and incline surfaces." *Clinical Biomechanics* 23(10): 1260-1268.

21. Chumanov, E. S., B. C. Heiderscheit, D. G. Thelen (2007). "The effect of speed and influence of individual muscles on hamstring mechanics during the swing phase of sprinting." *Journal of Biomechanics* 40: 3555-3562.

22. Connell, D. A., M. E. Schneider-Kolsky, et al. (2004). "Longitudinal study comparing sonographic and MRI assessments of acute and healing hamstring injuries." *American Journal of Roentgenology* 183(4): 975-84.

23. Davis, B. L. and P. R. Cavanagh (1993). "Decomposition of superimposed ground reaction forces into left and right force profiles." *Journal of Biomechanics* 26(4-5).

24. De Clercq, D., P. Aerts, et al. (1994). "The mechanical characteristics of the human heel pad during foot strike in running: an in vivo cineradiographic study." *Journal of Biomechanics* 27(10): 1213-1222.

25. de Leva, P. (1996). "Adjustments to Zatsiorsky-Seluyanov's segment inertia parameters." *Journal of Biomechanics* 29(9): 1223-30.

26. De Smet, A. A. and T. Best (2000). "MR imaging of the distribution and location of acute hamstring injuries in athletes." *American Journal of Roentgenology* 174: 393-399.

27. Delp, S., F. Anderson, et al. (2007). "OpenSim: open-source software to create and analyze dynamic simulations of movement." *IEEE Transactions in Biomedical Engineering* 54(11): 1940-1950.

28. Delp, S. L., A. E. Grierson, et al. (1996). "Maximum isometric moments generated by the wrist muscles in flexion-extension and radial-ulnar deviation." *Journal of Biomechanics* 29(10): 1371-5.

29. Delp, S. L., J. P. Loan, et al. (1990). "An interactive graphics-based model of the lower extremity to study orthopaedic surgical procedures." *IEEE Transactions on Biomedical Engineering* 37(8): 757-67.

30. Derrick, T. R., D. Dereu, et al. (2002). "Impacts and kinematic adjustments during an exhaustive run." *Medicine and Science in Sports and Exercise* 34(6): 998-1002.

31. Fong, D. T. P., Y. Y. Chan, et al. (2008). "Estimating the complete ground reaction forces with pressure insoles in walking." *Journal of Biomechanics* 41(11): 2597-2601.

32. Forner-Cordero, A., H. J. F. M. Koopman, et al. (2006). "Inverse dynamics calculations during gait with restricted ground reaction force information from pressure insoles." *Gait and Posture* 23: 189-199.

33. Fukunaga, T., Y. Kawakami, et al. (2002). "Muscle and tendon interaction during human movements." *Exercise Sport Science Reviews* 30(3): 106-10.

34. Fukunaga, T., K. Kubo, et al. (2001). "In vivo behaviour of human muscle tendon during walking." *Proceedings of the Royal Society of London Series B Biolgical Sciences* 268(1464): 229-33.

35. Gabbe, B. J., C F Finch, K L Bennel, H Wajswelner (2005). "Risk factors for hamstring injuries in community level Australian football." *British Journal of Sports Medicine* 39: 106-110.

36. Gabbett, T. J. (2004). "Influence of training and match intensity on injuries in rugby league." *Journal of Sports Science* 22: 409-417.

37. Garrett, W., F. Rich, et al. (1989). "Computed tomography of hamstring muscle strains." *Medicine and Science in Sports and Exercise* 21: 506-514.

38. Garrett, W. E., Jr. (1996). "Muscle strain injuries." *American Journal of Sports Medicine* 24(6 Suppl): S2-8.

39. Garrett, W. E., Jr., F. R. Rich, et al. (1989). "Computed tomography of hamstring muscle strains." *Medicine and Science in Sports and Exercise* 21(5): 506-14.

40. Gerritsen, K., A. J. van den Bogert, et al. (1995). "Direct dynamics simulation of the impact phase in heel-toe running." *Journal of Biomechanics* 28: 661-668.

41. Gilchrist, L. A. and D. A. Winter (1996). "A two-part, viscoelastic foot model for use in gait simulations." *Journal of Biomechanics* 29(6): 795-798.

42. Goldberg, S. R., F. C. Anderson, et al. (2004). "Muscles that influence knee flexion velocity in double support: implications for stiff-knee gait." *Journal of Biomechanics* 37(8): 1189-96.

43. Happee, R. (1994). "Inverse dynamic optimization including muscular dynamics, a new simulation method applied to goal directed movements." *Journal of Biomechanics* 27(7): 953-60.

44. Heiderscheit, B., M. Sherry, et al. (in press). "Acute Hamstring Injuries: Recommendations for Diagnosis Rehabilitation and Injury Prevention." *Journal of Orthopedic Sports Physical Therapy*.

45. Heiderscheit, B. C., D. M. Hoerth, et al. (2005). "Identifying the time of occurrence of a hamstring strain injuring during treadmill running: a case study." *Clinical Biomechanics* 20(10): 1072-1078.

46. Jacobs, R. and G. Vvan Ingen Schenau (1992). "Intermuscular coordination in a sprint push-off." *Journal of Biomechanics* 25(9): 953-965.

47. Jonhagen, S., M. O. Ericson, et al. (1996). "Amplitude and timing of electromyographic activity during sprinting." *Scandinavian Journal of Medicine and Science in Sports* 6: 15-21.

48. Kaariainen, M., T. Jarvinen, et al. (2000). "Relation between myofibers and connective tissue during muscle injury repair." *Scandinavian Journal of Medicine and Science in Sports* 10(6): 332-7.

49. Kernozek, T. W. and K. A. Zimmer (2000). "Reliability and running speed effects of in-shoe loading measurements during slow treadmill running." *Foot and Ankle International* 21(9): 749-752.

50. Koulouris, G. and D. Connell (2003). "Evaluation of the hamstring muscle complex following acute injury." *Skeletal Radiology* 32(10): 582-9.

51. Kuitunen, S., P. V. Komi, et al. (2002). "Knee and ankle joint stiffness in sprint running." *Medicine and Science in Sports and Exercise* 34(1): 166-73.

52. Kujala, U. M., S. Orava, et al. (1997). "Hamstring injuries: current trends in treatment and prevention." *Sports Medicine* 23(6): 397-404.

53. Kuo, A. D. (1998). "A Least-Squares Estimation Approach to Improving the Precision of Inverse Dynamics Computations." *Journal of Biomechanical Engineering* 120: 148-159.

54. Lewis, F. L. and K. Shaw (1997). "Tensile properties of human tendo achilis: effect of donor age and strain rate." *Journal of Foot and Ankle Surgery* 36: 435-445.

55. Lieber, R. (1992). *Skeletal Muscle Structure and Function: Implications for Rehabilitation and Sports Medicine.* Baltimore, Williams & Wilkins.

56. Lieber, R. L. and J. Friden (1993). "Muscle damage is not a function of muscle force but active muscle strain." *Journal of Applied Physiology* 74(2): 520-6.

57. Lieber, R. L. and J. Friden (2002). "Mechanisms of muscle injury gleaned from animal models." *American Journal of Physical Medicine and Rehabilitation* 81(11 Suppl): S70-9.

58. Loram, I. D., C. N. Maganaris, et al. (2006). "Use of ultrasound to make noninvasive in vivo measurement of continuous changes in human muscle contractile length." *J Appl Physiol* 100(4): 1311-23.

59. Lu, T. W. and J. J. O'Connor (1999). "Bone position estimation from skin marker co-ordinates using global optimisation with joint constraints." *Journal of Biomechanics* 32(2): 129-34.

60. Mann, R. and J. Hagy (1980). "Biomechanics of walking, running, and sprinting." *American Journal of Sports Medicine* 8(5): 345-350.

61. Mann, R. V. (1981). "A kinetic analysis of sprinting." *Medicine and Science in Sports and Exercise* 13(5): 325-328.

62. Mann, R. V. and P. Sprague (1980). "A kinetic analysis of the ground leg during sprint running." *Research Quarterly for Exercise and Sport* 51(2): 334-348.

63. Mero, A. and P. V. Komi (1987). "Electromyographic activity in sprinting at speeds ranging from sub-maximal to supra-maximal." *Medicine and Science in Sports and Exercise* 19(3): 266-74.

64. Miller, R. H., J. L. Lowry, et al. (2007). "Lower extremity mechanics of iliotibial band syndrome during an exhaustive run." *Gait and Posture* 26(3): 407-13.

65. Neptune, R. R., S. A. Kautz, et al. (2001). "Contributions of the individual ankle plantar flexors to support, forward progression and swing initiation during walking." *Journal of Biomechanics* 34: 1387-1398.

66. Neptune, R. R., I. C. Wright, et al. (2000). "A method for numerical simulation of single limb ground contact events: application to heel-toe running." *Compative Methods of Biomechanical and Biomedical Engineering* 3(4): 321-334.

67. Orchard, J. (2002). "Biomechanics of muscle strain injury." *New Zealand Journal of Sports Medicine* 30(4): 92-98.

68. Orchard, J. and T. M. Best (2002). "The management of muscle strain injuries: an early return versus the risk of recurrence." *Clinical Journal of Sport Medicine* 12(1): 3-5.

69. Orchard, J. W. (2001). "Intrinsic and extrinsic risk factors for muscle strains in Australian football." *American Journal of Sports Medicine* 29(3): 300-3.

70. Pandy, M. G. and N. Berme (1988). "A numerical method for simulating the dynamics of human walking." *Journal of Biomechanics* 21(12): 1043-1051.

71. Piazza, S. J., A. Erdemir, et al. (2004). "Assessment of the functional method of hip joint center location subject to reduced range of hip motion." *Journal of Biomechanics* 37: 349-356.

72. Proske, U., D. L. Morgan, et al. (2004). "Identifying athletes at risk of hamstring strains and how to protect them." *Clinical and Experimental Pharmacology and Physiology* 31(8): 546-50.

73. Putti, A. B., G. P. Arnold, et al. (2007). "The pedar in-shoe system: repeatability and normal pressure values." *Gait and Posture* 25: 401-405.

74. Remy, C. D. and D. G. Thelen (2008). "Optimal estimation of dynamically consistent kinematics and kinetics for forward dynamic simulations of gait." *Journal of Biomechanical Engineering* 131(3): 031005.

75. Schache, A., T. Wrigley, et al. (2009). "Biomechanical response to hamstring muscle strain injury." *Gait and Posture* 29(2): 332-338.

76. Seward, H., J. Orchard, et al. (1993). "Football injuries in Australia at the elite level." *Medical Journal of Australia* 159: 298-301.

77. Sherry, M. and T. Best (2004). "A comparison of two rehabilitation programs in the treatment of acute hamstring strains." *Journal of Orthopaedic and Sports Physical Therapy* 34(3): 116-125.

78. Silder, A., B. Whittington, et al. (2007). "Identification of passive elastic joint moment-angle relationships in the lower extremity." *Journal of Biomechanics* 40(12): 2628-2635.

79. Simonsen, E. B., L. Thomsen, et al. (1985). "Activity of mono- and biarticular leg muscles during sprint running." *European Journal of Applied Physiolology and Occupational Physiology* 54(5): 524-32.

80. Swanson, S. and G. Caldwell (2000). "An integrated biomechanical analysis of high speed incline and level treadmill running." *Medicine and Science in Sports and Exercise* 32: 1146-1155.

81. Thelen, D. G. and F. C. Anderson (2006). "Using computed muscle control to generate forward dynamic simulations of human walking from experimental data." *Journal of Biomechanics* 39: 1107-1115.

82. Thelen, D. G., F. C. Anderson, et al. (2003). "Generating dynamic simulations of movement using computed muscle control." *Journal of Biomechanics* 36(3): 321-328.

83. Thelen, D. G., Chumanov E.S., Sherry M., and Heiderscheit, B.C. (2006). "Neuromusculoskeletal models provide insights into the mechanisms and rehabilitation of hamstring strains." *Exercise Sport Science Reviews* 34(3): 135-141.

84. Thelen, D. G., Chumanov, Elizabeth S., Best, Thomas M., Swanson, Stephen C., Heiderscheit, Bryan C. (2005). "Simulation of biceps femoris musculotendon mechanics during the swing phase of sprinting." *Medicine and Science in Sports and Exercise* 37: 1931-1938.

85. Thelen, D. G., Chumanov, Elizabeth S., Hoerth, Dina M., Best, Thomas M., Swanson, Stephen C., Li, Li, Young, Michael, Heiderscheit, Bryan C. (2005). "Hamstring muscle kinematics during treadmill sprinting." *Medicine and Science in Sports and Exercise* 37(1): 108-114.

86. van den Bogert, A. and A. Su (2008). "A weighted least squares method for inverse dynamic analysis." *Computer Methods in Biomechanics and Biomedical Engineering* 11(1): 3-9.

87. van Don, B. J. (1998). Hamstring injuries in sprinting. Exercise Science. Iowa City, The University of Iowa: 187.

88. Walker, P. S., J. S. Rovick, et al. (1988). "The effects of knee brace hinge design and placement on joint mechanics." *Journal of Biomechanics* 21(11): 965-74.

89. Whiting, W. and R. Zernicke (1998). *Biomechanics of Musculoskeletal Injury.* Champaign, IL, Human Kinetics.

90. Winter, D. A. (1990). *Biomechanics and motor control of human movement.* New York, NY, Wiley.

91. Wood, G. (1987). "Biomechanical limitations to sprint running." *Medicine and Science in Sports and Exercise* 25: 58-71.

92. Woods, C., R.D. Hawkins, S. Maltby, M. Hulse, A. Thomas, and A. Hodson (2004). "The football association medical research programme: an audit of injuries in professional football - analysis of hamstring injuries." *British Journal of Sports Medicine* 38: 36-41.

93. Yamamoto, T. (1993). "Relationship between hamstring strains and leg muscle strength: a follow-up study of collegiate track and field athletes." *Journal of Medicine in Sports and Physical Fitness* 33(2): 194-199.

94. Yu, B., R. Queen, et al. (2008). "Hamstring muscle kinematics and activation during overground sprinting." *Journal of Biomechanics* 41(15): 3121-3126.

95. Zajac, F. E. (1989). "Muscle and tendon: properties, models, scaling and application to biomechanics and motor control." *Critical Reviews in Biomedical Engineering* 17: 359-411.

96. Zajac, F. E. and M. E. Gordon (1989). "Determining muscle's force and action in multi-articular movement." *Exercise and Sport Sciences Reviews* 17: 187-230.

APPENDICES

EQUATIONS

Activation/Deactivation

$$\frac{da}{d\tau} = \frac{u-a}{\tau_a(a,u)}$$

(eq. A1)

$$\tau_a(a,u) = \begin{cases} \tau_{act}(0.5+1.5a); & u > a \\ \tau_{deact}/(0.5+1.5a); & u \le a \end{cases}$$

(eq. A2)

Passive Muscle Force

$$\bar{F}^{PE} = \frac{e^{k^{PE}(\bar{L}^M-1)/\varepsilon_o^M} - 1}{e^{k^{PE}} - 1}$$

(eq. A3)

Active Force-Length Gaussian Function

$$f_1 = e^{-(\bar{L}^M-1)^2/\gamma}$$

(eq. A4)

Force-Strain Relationship for Tendon

$$\bar{F}^T = \begin{cases} \dfrac{\bar{F}_{toe}^T}{e^{k_{toe}}-1}(e^{k_{toe}\varepsilon^T/\varepsilon_{toe}^T}-1); & \varepsilon^T \le \varepsilon_{toe}^T \\ k_{lin}(\varepsilon^T - \varepsilon_{toe}^T) + \bar{F}_{toe}^T; & \varepsilon^T > \varepsilon_{toe}^T \end{cases}$$

(eq. A5)

Force-Velocity Relationship

$$V^M = (0.25 + 0.75a)V_{max}^M \frac{\bar{F}^M - af_1}{b}$$

(eq. A6)

$$b = \begin{cases} af_1 + \bar{F}^M/A_f; & \bar{F}^M \le af_1 \\ \dfrac{(2+2/A_f)(af_1\bar{F}_{len}^M - \bar{F}^M)}{(\bar{F}_{len}^M - 1)}; & \bar{F}^M > af_1 \end{cases}$$

(eq. A7)

Normalized Tendon Length

$$\bar{L}^T = \bar{L}^{MT} - \bar{L}^M \cos\alpha$$

(eq. A8)

F^T

CE

F^T

$L^M cos\alpha$

α

L^T

L^{MT}

Force

F_0^M

active

passive

$a=1.0$

$a=0.5$

F_0^M

L_0^M $(1+\varepsilon_0^M)L_0^M$ $-v_{max}$

ε_0^T

Muscle Fiber Length   Muscle Fiber Velocity   Tendon Strain
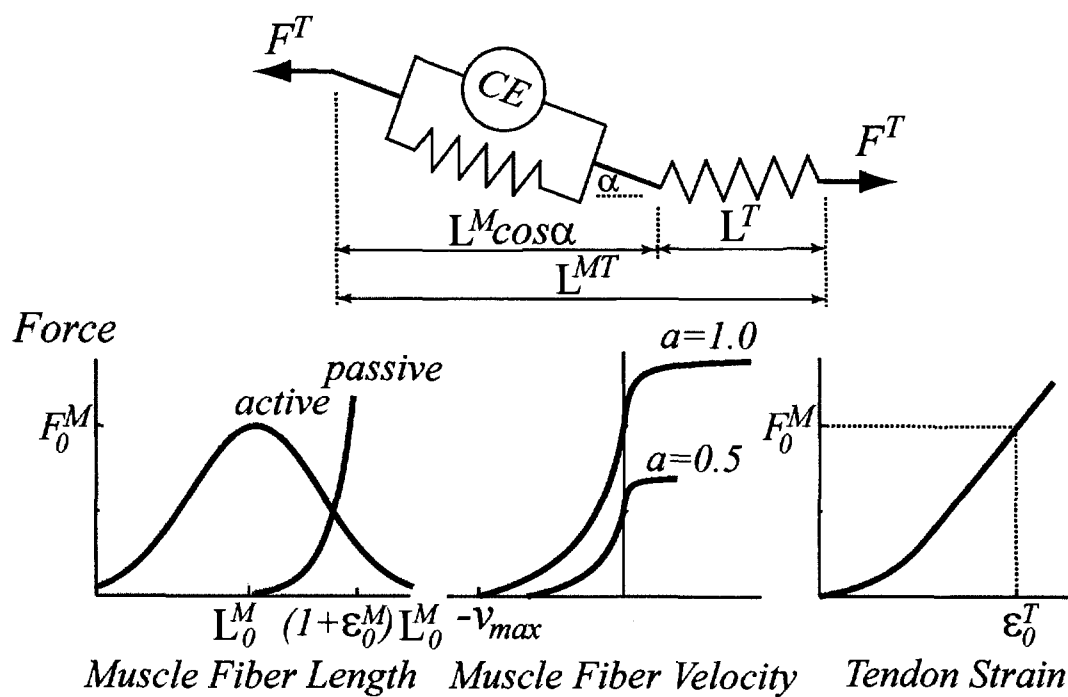
Figure A1. Hill-type model of musculotendon contraction dynamics.

Table A1. Muscle properties used in the model.

Muscle	F_o^M (N) Max muscle force	ℓ_o^M (m) Optimal fiber length	ℓ_s^T (m) Tendon slack length	α (deg) Pennation angle
Biarticular Hamstrings				
Biceps Femoris Long Head	896	0.1090	0.341	0.0
Semimembranosus	1288	0.0800	0.359	15.0
Semitendinosus	410	0.2010	0.262	5.0
Quadriceps				
Rectus Femoris	1169	0.1140	0.325	5.0
Vastus Lateralis	1871	0.0840	0.175	5.0
Vastus Intermedius	1365	0.0870	0.155	3.0
Vastus Medialis	1294	0.0890	0.145	5.0
Adductors				
Adductor Longus	627	0.1380	0.100	6.0
Adductor Brevis	429	0.1330	0.020	0.0
Adductor Magnus (3 separate components)	381	0.0870	0.060	5.0
Uniarticular Hip Extensors				
Gluteus Maximus (3 separate components)	573	0.1420	0.100	5.00
Gluteus Medius (3 separate components)	819	0.0535	0.078	8.0
Gluteus Minimus (3 separate components)	270	0.0680	0.016	10.0
Uniarticular Hip Flexors				
Psoas	2000	0.1000	0.130	8.0
Iliacus	2000	0.1000	0.100	7.0
Other Knee Flexors				
Medial Gastrocnemius	1558	0.0600	0.375	17.0
Lateral Gastrocnemius	683	0.0640	0.365	8.0
Biceps Femoris Short Head	804	0.1730	0.090	23.0

Other generic properties included:

$u = 0.01$ Ns (Damping)

$\tau_{act} = 0.01$ s (Activation time constant)

$\tau_{deact} = 0.03$ s (Deactivation time constant)

$k_{toe} = 2.0$ (Exponential shape factor for tendon)

$\varepsilon_o^T = 0.05$ (Tendon strain due to max isometric force)

$k_{lin} = 1.712 / \varepsilon_o^T$ (Linear shape factor for tendon strain curve)

$\varepsilon_{toe}^T = 0.333$ (Tendon strain above which tendon exhibits linear behavior)

$\varepsilon_o^M = 0.6$ (Passive muscle strain due to max isometric force)

$\gamma = 0.4$ (Shape factor for force length curve of individual sarcomeres)

$k^{PE} = 4.0$ (Exponential shape factor for passive muscle force)

$V_{max}^M = 15.0$ (L_o^M / s) (Maximum contraction velocity)

$V_o^M = 5.0$ (L_o^M / s) (Contraction velocity at maximum isometric force)

$\bar{F}_{len}^M = 1.5$ (Maximum normalized muscle force when fiber is lengthening

$A_f = 0.3$ (Force-velocity shape factor)

Muscle Density = 1056 kgm^{-3}

Max isometric stress = 350000 Nm-^{2}

Muscle Force

$F(t)$

Muscle
Contraction
Dynamics

$a(t)$

Muscle
Activation

Muscle
Activation
Dynamics

$u(t)$

Muscle
Excitation

Muscle Contraction Dynamics

Tendon Force

$$F^T = f_T(\varepsilon^T) * F_o^M$$

F^T

ε^T

Tendon Strain

$$\varepsilon^T = \frac{L^T - \ell_s^T}{\ell_s^T}$$

L^T

Tendon Length

$$L^T = L^{MT} - L^M \cos\alpha$$

α

L^{MT}

Pennation

$$w = \ell_o^M \sin\alpha_o$$
$$\alpha = \sin^{-1}(w/L^M)$$

L^M

CE Muscle Velocity

$$V_{CE}^M = f_v^{-1}\left(\frac{F_{CE}^M}{a * f_? * F_o^M}, a\right)$$

V_{CE}

$$\begin{cases} F_{CE}^M < a * f_? * F_o^M \quad shortening \\ F_{CE}^M > a * f_? * F_o^M \quad lengthening \end{cases}$$

a

F_{CE}^M

CE Muscle Force

$$F_{CE}^M = \frac{F^T}{\cos\alpha} - F_{PE}^M$$

F_{PE}^M

Passive Muscle Force

$$F_{PE}^M = F_o^M f_{PE}(L^M)$$

L^M

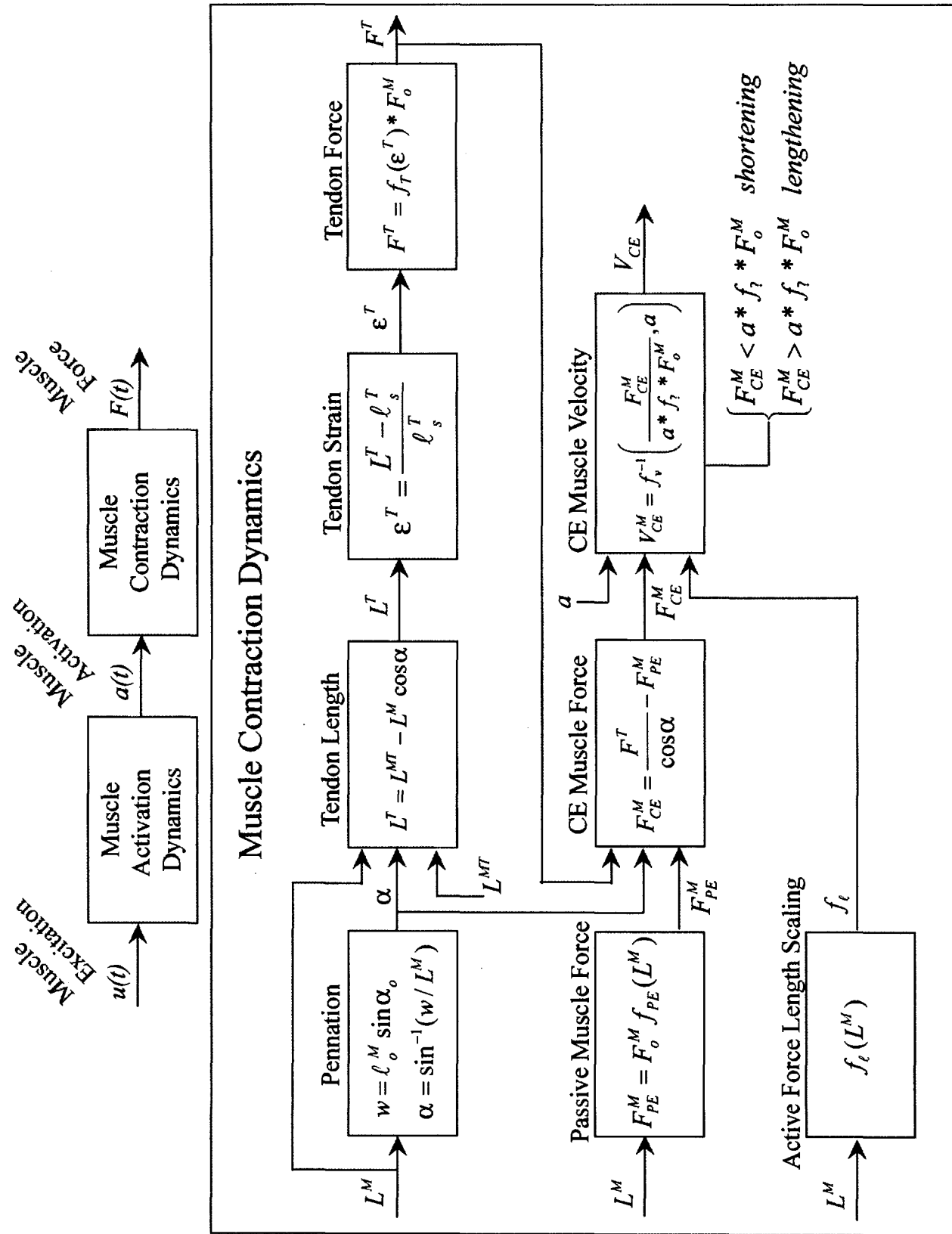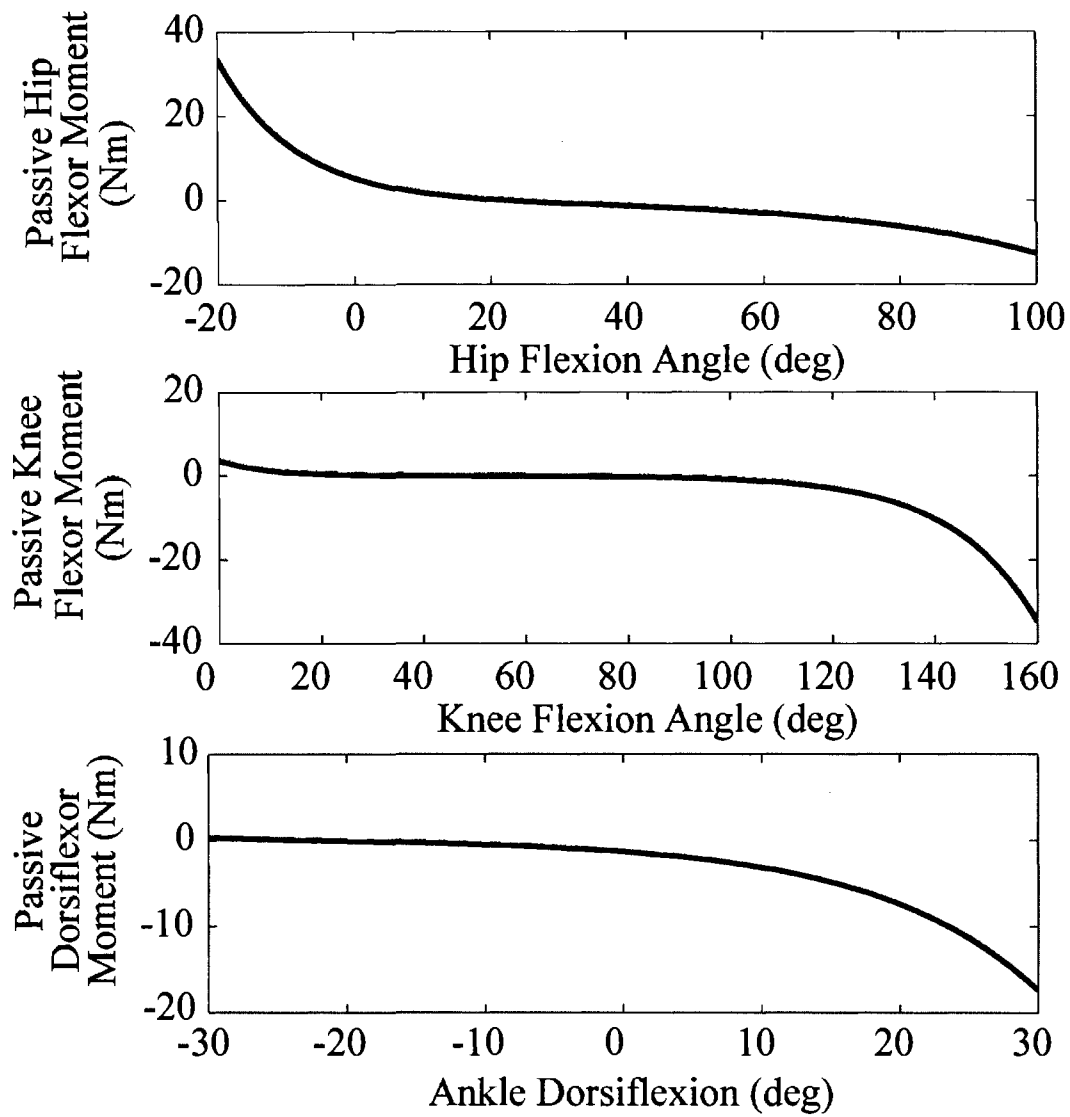**Active Force Length Scaling**

$$f_\ell(L^M)$$

f_ℓ

L^M

Figure A2. Block diagram of how musculotendon dynamics are computed

$$T = k_1 e^{r_1 \cdot (q - \phi_1)} + k_2 e^{r_2 \cdot (q - \phi_2)} - c \cdot u \qquad \text{(eq. A9)}$$

Table A2. Passive joint torque constants.

	Hip flexion	Knee flexion	Ankle flexion
k_1(Nm)	-1.0	-1.0	-1.0
k_2(Nm)	1.0	1.0	1.0
r_1	2.0	3.5	4.9
r_2	-5.1	-5.8	-4.9
ϕ_1(rad)	0.4765	1.778	-0.0593
ϕ_2(rad)	0.34	0.2234	-0.70
C (Ns)	0.10	0.10	0.10

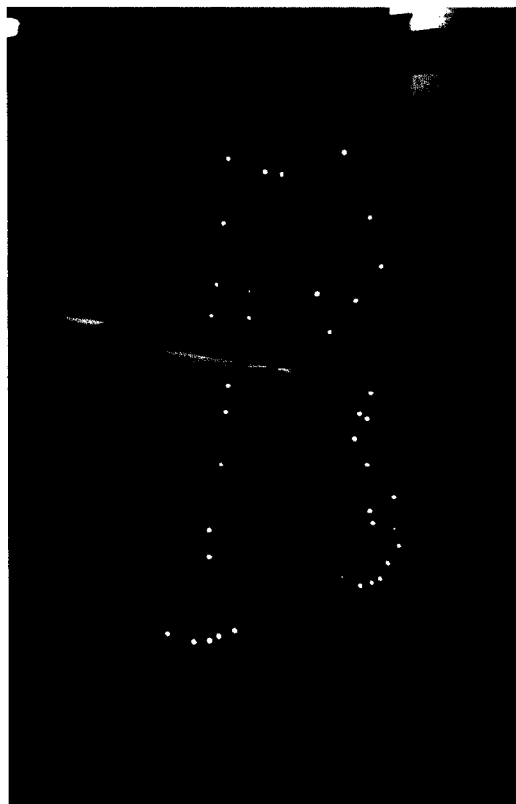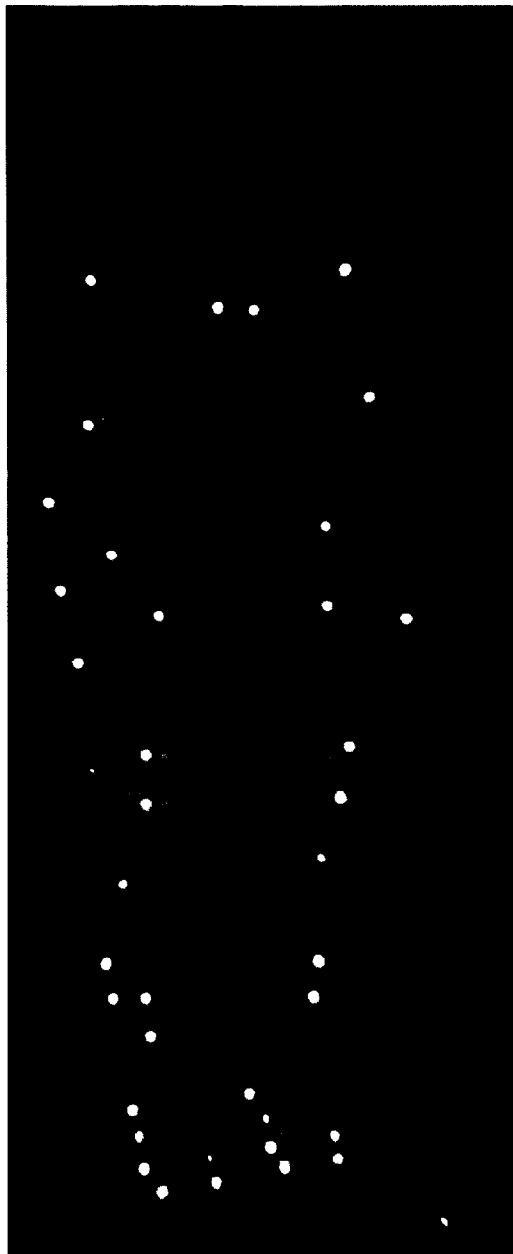**Figure A3.** Passive joint moments included in the model.

Photographs of experiments

Insole Setup (Tracking algorithm and LSFD):

High speed running on a treadmill: